

Harnessing T Cell Generation and Metabolism to Modulate T Cell Recovery
Following Radiation Exposure and Bone Marrow Transplantation

by

Yujing Zou

Department of Pathology
Duke University

Date: _____

Approved:

Nelson Chao, Supervisor

Benny Chen

Xiaofan Wang

Soman Abraham

Dissertation submitted in partial fulfillment of
the requirements for the degree of Doctor
of Philosophy in the Department of
Pathology in the Graduate School
of Duke University

2022

ABSTRACT

Harnessing T Cell Generation and Metabolism to Modulate T Cell Recovery
Following Radiation Exposure and Bone Marrow Transplantation

by

Yujing Zou

Department of Pathology
Duke University

Date: _____

Approved:

Nelson Chao, Supervisor

Benny Chen

Xiaofan Wang

Soman Abraham

An abstract of a dissertation submitted in partial
fulfillment of the requirements for the degree
of Doctor of Philosophy in the Department of
Pathology in the Graduate School of
Duke University

2022

Copyright by
Yujing Zou
2022

Abstract

Total body irradiation (TBI) causes profound suppression of hematopoiesis and T cell depletion, increasing chances of morbidity associated with opportunistic infections in the lymphopenic condition. Currently, therapeutic options for improving recovery of the T cell compartment following radiation exposure are not available. Although mouse and nonhuman primate studies have demonstrated prolonged effects of TBI on T cell reconstitution, there is a lack of understanding in the kinetics and metabolic signatures of radioresistant T cells actively undergoing homeostatic proliferation. Furthermore, whether kinetics of systemic T cell recovery recapitulates T cell recovery in circulation remains unknown. In the current study, we performed comprehensive immunophenotyping and single-cell sequencing analyses of radioresistant T cells, as well as imaging of T cell recovery in vivo, to determine preferentially upregulated pathways during T cell recovery. We identified T cell populations unique to TBI treatment that upregulate components essential to support oxidative phosphorylation, a mitochondria-dependent metabolic process. We further investigated mechanisms of recovery in donor T cells following TBI exposure in the bone marrow transplant setting. We demonstrated that recovery of alloreactive donor T cells was highly dependent on aerobic glycolysis, which can be manipulated to reduce graft-versus-host-disease and preserve the functional recovery of non-alloreactive donor T cells. We then examined the effect of NT-I7, a long-acting recombinant human IL-7, in mediating T cell reconstitution due to its role in integrating metabolic requirements with pathways critical for T cell survival and growth. We found that NT-I7 led to accelerated T cell recovery following TBI through both thymic-dependent and independent pathways. More importantly, NT-I7 promoted functional T cell recovery. Taken together, these findings reveal unique kinetics and mechanisms of T cell recovery in response to radiation. The study also identified NT-I7 as a potential

therapeutic treatment during T cell lymphopenia by supporting critical mechanisms utilized in T cell recovery.

Contents

Abstract	iv
List of Figures	xii
Acknowledgements	xviii
1. Introduction	1
1.1 T cell reconstitution following total body irradiation.....	1
1.1.1 Background of total body irradiation exposure	1
1.1.2 TBI leads to profound T cell depletion and increased risk of infections.....	2
1.1.3 The recovery of various T cell subsets post-TBI.....	3
1.1.4 Thymic-dependent and independent pathways of T cell recovery after TBI	4
1.2 T cell reconstitution following bone marrow transplantation	5
1.2.1 Recovery of pathogenic versus beneficial donor T cells following bone marrow transplantation	6
1.2.2 Recovery of alloreactive donor T cells enables the development of GVHD	7
1.2.3 Alloreactive donor T cell recovery and pathogenicity are associated with T cell metabolic reprogramming	8
1.2.4 Recovery of non-alloreactive donor T cells promotes GVL and protects against opportunistic infections	9
1.2.5 Anti-tumor capacity and memory T cell persistence are dependent on different metabolic pathways compared to activated alloreactive T cells.....	10
1.3 IL-7 integrates T cell generation mechanisms and metabolic demands to support T cell recovery	11
1.3.1 IL-7 is critical for de novo T cell generation and homeostatic proliferation of mature T cells	11
1.3.2 IL-7 supports T cell persistence and growth through regulation of distinct metabolic processes via PI3K/Akt axis and STAT5 activation	13

1.3.3 NT-I7, a long-acting recombinant human IL-7 that boosts T cell recovery in various disease states in clinical trials, potentially supports T cell recovery post-TBI.....	13
1.4 Significance and study objective	14
1.4.1 Characterizing the phenotypic, differentiation, and metabolic profile of T cell recovery following total body irradiation.....	14
1.4.2 Harnessing T cell metabolism to prevent the recovery of alloreactive donor T cells and promote the recovery of donor T cells against tumor development following bone marrow transplantation	16
1.4.3 Enhancing T cell reconstitution using long-acting recombinant human IL-7, which integrates T cell generation mechanisms and metabolic demands during T cell recovery. ..	18
2. Methods.....	20
2.1 T cell recovery following Total body irradiation	20
2.1.1 Mice.....	20
2.1.2 TBI model	20
2.1.3 Bioluminescent imaging.....	21
2.1.4 TCR sequencing	21
2.1.5 TCR repertoire analyses	22
2.1.6 Single-cell sequencing library preparation.....	22
2.1.7 Single-cell sequencing sequencing data processing and analyses.....	23
2.1.8 Gene ontology enrichment analysis	24
2.1.9 Trajectory analyses.....	25
2.1.10 Metabolic assays	25
2.1.11 Murine cell preparation and T cell stimulation	26
2.1.12 Flow cytometry	26
2.1.13 Statistics	27

2.2. T cell recovery in Bone marrow transplantation	27
2.2.1 Mice.....	27
2.2.2 Murine cell preparation and T cell stimulation	28
2.2.3 Human cell preparation and T cell stimulation	29
2.2.4 GVHD model	30
2.2.5 GVL model.....	30
2.2.6 Tumor cell lines.....	31
2.2.7 Bioluminescent imaging.....	32
2.2.8 Mixed lymphocyte reaction.....	32
2.2.9 Metabolic assays	32
2.2.10 Enzyme-linked immunosorbent assay	33
2.2.11 Flow cytometry	33
2.2.12 Western blotting	34
2.2.13 Histology	35
2.2.14 Statistics	36
2.3. Role of NT-I7 in T cell recovery	36
2.3.1 Mice.....	36
2.3.2 CBC.....	37
2.3.3 Murine cell preparation and T cell stimulation	37
2.3.4 Bioluminescent imaging.....	37
2.3.5 Flow cytometry	37
2.3.6 Statistical analysis	38

3. Results.....	39
3.1 Characterizing phenotypic, differentiation, and metabolic profile of T cell recovery following total body irradiation.....	39
3.1.1. Investigating kinetics of T cell recovery in the peripheral blood (nadir, window of susceptibility, radiation dose-dependent)	39
3.1.2. Establishing an imaging system to track T cell recovery in vivo.....	41
3.1.3. Investigating kinetics and mechanisms of systemic T cell recovery following TBI.....	46
3.1.4. Role of TBI in thymic development during T cell recovery	49
3.1.5. TCR repertoire diversity is largely preserved following various doses of TBI exposure.....	51
3.1.6. Single-cell RNA-sequencing reveals distinct T cell populations unique to TBI treatment.....	53
3.1.7. Trajectory analyses reveal thymic-independent generation of radioresistant T cells, which involves the acquisition of effector memory phenotype during recovery	57
3.1.8. Radioresistant T cells demonstrate a preferential upregulation of mitochondrial activity and oxidative phosphorylation during the recovery process	60
3.1.9. During recovery, subsets of radioresistant T cells acquire increased proliferation capacity in response to different sources of stimuli in vitro	66
3.2. Manipulating donor T cell recovery following bone marrow transplantation	68
3.2.1. Donor T cell pathogenicity is fueled by glycolysis upon recognition of alloantigens, a thymic-independent process during donor T cell recovery.....	68
3.2.2. Glut1 is required for the metabolic reprogramming and expansion of donor alloreactive T cells	71
3.2.3. Glut1 is required for the survival of alloreactive donor T cells	74

3.2.4. Glut1 deficiency in donor T cells ameliorates GVHD while preserving GVL effects.....	78
3.2.5. Inhibition of glycolysis by 2-DG selectively targets murine and human alloreactive T cells in vitro and preserves T cells with irrelevant specificities	82
3.2.6. 2-DG-mediated inhibition of glycolysis ex vivo significantly reduces donor T cell-mediated GVHD while sparing T cells mediating GVL, demonstrating functional recovery of donor anti-tumor T cells	86
3.3. NT-I7 is a promising therapeutic agent that integrates requirements for various T cell recovery pathways	89
3.3.1. NT-I7 promotes peripheral blood T cell reconstitution following TBI.....	90
3.3.2. NT-I7 promotes systemic T cell recovery.....	94
3.3.3. NT-I7 enhances T cell reconstitution through both thymic-dependent and independent mechanisms	99
3.3.4. NT-I7 alters DN-to-DP transition and enforces commitment to cytotoxic-lineage T cells.....	103
3.3.5. NT-I7 alters the frequency and number of HSC and progenitors after TBI...	107
3.3.6. NT-I7 treatment preserves T cell effector function and proliferation in response to TCR stimulation.....	110
4. Discussion.....	114
4.1 Characterizing T cell constitution following TBI.....	114
4.2. Manipulating T cell reconstitution following bone marrow transplantation	121
4.3. Improving T cell reconstitution using NT-I7.....	130
5. Conclusions and implications	141
5.1 Overall conclusions	141
5.2. Implications and future directions.....	142

5.2.1. Understanding the phenotypic, differentiation, and metabolic profiles of unique radioresistant T cell subsets during recovery following TBI	142
5.2.2. Reducing the recovery of alloreactive donor T cells while enhancing the functional recovery of non-alloreactive donor T cells through metabolic regulation	143
5.2.3. NT-I7 integrates the requirement for thymic-dependent and -independent pathways, as well as metabolic demands for T cell growth and persistence, to induce rapid T cell recovery following radiation exposure.	145
References	148
Biography	163

List of Figures

Figure 1. T cell recovery kinetics in the peripheral blood is TBI dose-dependent.

Figure 2. Expression of luciferase in T-Luc mice is T cell-specific.

Figure 3. Establishing an in vivo imaging model to track T cell recovery.

Figure 4. Evaluating systemic T cell recovery through in vivo imaging.

Figure 5. TBI induced defects in total thymic output.

Figure 6. Preservation of T cell repertoire diversity following TBI.

Figure 7. Single-cell sequencing reveals distinct clusters unique to TBI groups.

Figure 8. TN & TM precede other subsets in pseudotime.

Figure 9. CD4 T cells upregulate lymphocyte proliferation and mitochondrial metabolic pathways during recovery after TBI.

Figure 10. T cells upregulate oxidative stress markers during recovery following irradiation.

Figure 11. Radioresistant T cell subsets demonstrate increased proliferation in response to in vitro stimulation.

Figure 12. Glut1 is required for donor T cells to induce acute GVHD.

Figure 13. Glut1 mediates the expansion of alloreactive donor T cells.

Figure 14. Glut1 modulates alloreactive T cell survival.

Figure 15. Transfer of donor T cells with Glut1 deletion inhibits GVHD development and spares GVL activity.

Figure 16. 2-DG treatment selectively suppresses alloreactive T cells.

Figure 17. 2-DG treatment ameliorates GVHD and leads to the functional recovery of donor T cells mediating GVL.

Figure 18. NT-I7 induces peripheral blood T cell recovery after total body irradiation.

Figure 19. NT-I7 induces peripheral blood T cell recovery in aged animals after total body irradiation.

Figure 20. NT-I7 induces changes in myeloid cell recovery after total body irradiation.

Figure 21. NT-I7 treatment induces systemic T cell recovery following TBI.

Figure 22. NT-I7 enhances T cell reconstitution through thymic-dependent and independent pathways.

Figure 23. NT-I7 alters the DN-to-DP transition as well as the relative abundance of SP4 and SP8 thymocytes during T cell development.

Figure 24. NT-I7 alters the frequency and number of stem and progenitor populations.

Figure 25. NT-I7 alters the differentiation potential of bone marrow cells after TBI.

Figure 26. NT-I7 treatment preserves T cell effector function and proliferation.

List of Abbreviations

TBI	Total body irradiation
NK	Natural killer
TCR	T cell receptor
Treg	Regulatory T cells
allo-HSCT	Allogeneic Hematopoietic Stem Cell Transplantation
GVL	Graft-Versus-Leukemia
MHC	Major Histocompatibility Complex
APCs	Antigen Presenting Cells
GVHD	Graft Versus Host Disease
OXPHOS	Oxidative Phosphorylation
FAO	Fatty Acid Oxidation
LAA	Leukemia-Associated Antigens
CMV	Cytomegalovirus
TN	Naïve T cells
TEM	Effector memory T cells
TEFF	Effector T cells
TCM	Central memory T cells
ROS	Reactive oxygen species

2-DG	2-Deoxyd-Glucose
LIP	Lymphopenia-Induced Proliferation
PI3K	Phosphatidylinositol 3-Kinase
MLR	Mixed Lymphocyte Reaction
Glut	Glucose transporter
PCA	Principle Components Analysis
UMAP	Uniform Manifold Approximation and Projection
GSEA	Gene Set Enrichment Analysis
ECAR	Extracellular Acidification Rate
OCR	Oxygen Consumption Rate
FACS	Fluorescence-Activated Cell Sorting
PBMCs	Peripheral Blood Mononuclear Cells
TCDBM	T cell-Depleted Bone Marrow
H&E	Hematoxylin-Eosin
CBC	Complete Blood Count
IR	Ionizing Radiation
GI tract	Gastrointestinal tract
BLI	Bioluminescent Imaging
BMT	Bone Marrow Transplant
HP	Highly Proliferative

mTORC1	Mammalian Target of Rapamycin Complex 1
Hsp90aa1	Heat Shock Protein 90 Alpha Family Class A Member 1
Prdx1	Peroxiredoxin 1
Txn1	Thioredoxin 1
CFSE	Carboxyfluorescein Succinimidyl Ester
HIF1 α	Hypoxia-Inducible Factor 1-Alpha
S6	Small Ribosomal Subunit 6
WT	Wild Type
IFN γ	Interferon Gamma
FDG	Fludeoxyglucose
TCR-tg	Transgenic T cell receptor
HSC	Hematopoietic Stem Cell
MPP	Multipotent Progenitor
HPC-1	Hematopoietic Progenitor 1
CFU-GM	Granulocyte-Macrophage Progenitors
BFU-E	Burst Forming Unit Erythroid
CFU-GEMM	Common Myeloid Progenitors
Gzmb	Granzyme B
TNF α	Tumour Necrosis Factor Alpha
JAK	Janus Kinase

STAT	Signal Transducer and Activator of Transcription
FcRN	Neonatal Fc Receptor
LMPP	Lymphoid-primed Multipotent Progenitors
CLP	Common Lymphoid Progenitor
GMP	Granulocyte-Monocyte Progenitors
MEP	Megakaryocyte-Erythroid Progenitors

Acknowledgements

I would like to acknowledge my mentors Dr. Nelson Chao and Dr. Benny Chen for their guidance over the years. I appreciate their patience, frequent discussions, and feedback. They have substantially contributed to my development as a scientist in terms of experimental design, data interpretation, scientific writing, and presentation skills. I am very grateful of my graduate student experience in the Nelson Chao lab. I am also thankful for my dissertation committee, professors Soman Abraham and Xiaofan Wang, for their valuable input and novel ideas to help improve my work. I would also like to thank Dr. Luigi Racioppi for exciting conversations of new scientific findings, as well as his intellectual feedback of my work. In addition, I am grateful to work with Dr. Yiqun Jiao, who has taught me various essential techniques during my training, providing valuable input and support for various projects. I am also thankful for the opportunity to work with scientists at NeoImmuneTech on the relevant projects as part of my dissertation. I would like to thank my parents, my partner Connor, friends, and my rabbit, Brad, for their continuous support throughout graduate school.

1. Introduction

1.1 T cell reconstitution following total body irradiation

Total body irradiation (TBI) is caused by exposure to ionizing radiation of the entire body, inducing various biological consequences. TBI leads to acute radiation injury that affects the gastrointestinal, cardiovascular, and central nervous system [1]. Bone marrow failure is another main source of radiation injury characterized by the destruction of the hematopoietic system, causing increased infection and hemorrhage. While both the innate and adaptive immune systems are affected, reconstitution of adaptive immune cells is a prolonged process that can take up to 2 years, a large window of increased susceptibility to opportunistic infections. In the current study, we focus on the T cell reconstitution process following TBI, which mediate protection against viral, fungal, and bacterial infections. By characterizing numerical, phenotypic, and functional aspects of T cell recovery, we hope to achieve a more comprehensive understanding of essential mechanisms during the reconstitution process that will provide novel insights for medical countermeasures.

1.1.1 Background of total body irradiation exposure

Ionizing radiation can be generated through high energy alpha and beta particles, as well as electromagnetic radiation such as gamma rays and x-rays, leading to both direct and indirect biological consequences especially in the context of TBI [2]. Environmental and occupational exposure due to radiation accidents, as well as nuclear terrorism events

are main routes of TBI exposure. TBI can also be utilized as an important treatment component of hematological and solid tumors. In the case of hematological malignancies, TBI is used as a conditioning regimen in preparation for bone marrow transplantation to create a niche for donor-derived bone marrow engraftment.

The biological effect of TBI is characterized by increased apoptosis triggered damage of DNA and other essential cellular components such as cellular membrane and signaling molecules [3]. Cells undergoing active mitosis, such as lymphocytes and cells in the gastrointestinal tract, are more prone to radiation-induced cell death. Consequently, survival rate drops significantly with increasing radiation dose. Therefore, it is essential to study the biological effects of TBI exposure to improve medical countermeasures and reduce the rate of morbidity and mortality.

1.1.2 TBI leads to profound T cell depletion and increased risk of infections

Innate immune cells, such as monocytes and natural killer (NK) cells, recover at a much faster rate compared to adaptive immune cells after TBI exposure. Among adaptive immune cells, T cell recovery is a particularly prolonged process. Non-human primate studies have shown that in contrast to B cells, which recover above baseline level 180 days following high dose TBI, T cell recovery only yielded approximately 60% of baseline level [4]. The delay in T cell recovery is partially due to de novo T cell

generation, which is a prolonged process that begins with the seeding of bone marrow-derived progenitor cells into the thymus, followed by sequential stages of thymocyte selection before mature T cells are exported to the periphery. The reduced capacity of T cells in terms of number and TCR diversity can lead to increased susceptibility to opportunistic infections and impaired ability to mount an effective response against tumor development.

1.1.3 The recovery of various T cell subsets post-TBI

T cell subsets demonstrate a spectrum of sensitivity to ionizing radiation. In general, regulatory T cells (Tregs), NKT cells, and memory T cells are more radioresistant [5]. While Tregs can alleviate inflammation-induced tissue damage and autoimmunity, they can also limit immune response against tumor development and infections during the lymphopenic window. Other T cells, such as effector memory T cells, are more resistant to radiation-induced apoptosis than their naïve and central memory counterparts, partially owing to differences in histone acetylation and Bcl-2 expression [6]. Additionally, CD8 T cells are more prone to radiation-induced cell death compared to CD4 T cells, which can alter the long-term CD4:CD8 ratio in circulation. Therefore, T cell recovery can remain incomplete and TBI-induced imbalance of T cell populations may persist for long periods after exposure.

1.1.4 Thymic-dependent and independent pathways of T cell recovery after TBI

T cell recovery following TBI is primarily mediated through thymic-dependent and independent mechanisms. De novo T cell production through the thymus is a lengthy process that involves the steady influx of stem and early T lineage progenitor cells in the thymus, followed by thymocyte education. Therefore, damage to the bone marrow and thymic niche can delay and potentially alter the T cell reconstitution. Furthermore, impaired thymocyte selection can result in limited TCR repertoire diversity and impaired capacity to respond to a wide variety of pathogen challenges. Hence, the thymic-dependent mechanism is critical for long-term T cell reconstitution by exporting T cells that recognize a diverse range of antigens. Previous studies demonstrated that the number of early T lineage progenitors and frequencies of double negative (DN) thymocytes are altered in mice when exposed to TBI at a range of 0.5 gray (Gy) to 4 Gy [7]. However, whether the effect on progenitor and thymocyte populations differ is unclear at higher dose, such as 5 Gy to 7 Gy. Aging can also play a role in de novo T cell generation by reducing the number of lymphoid progenitors [8], exacerbating T cell depletion in older individuals upon radiation exposure, which also induces premature senescence of HSCs. Therefore, therapeutic interventions in response to TBI should also be assessed in association with age.

Radiation exposure can also perturb T cell homeostasis in secondary lymphoid organs and peripheral tissues, disrupting T cell survival and homeostatic proliferation. However, peripheral expansion, a thymic-independent T cell generation mechanism, can lead to recovery of T cell numbers at a much faster pace than de novo T cell generation. This process is most notable in memory T cells, which recover much faster than naïve T cells after TBI. Memory T cells that recover early after TBI may be able to provide some degree of protection against opportunistic pathogens.

1.2 T cell reconstitution following bone marrow transplantation

In bone marrow transplantation, TBI is used as a conditioning regimen that depletes recipient cells, including alloreactive cells that mediate rejection of donor cells, to create a niche for the engrafted donor cells. The lymphopenic environment formed as a result of TBI is a source of morbidity and mortality due to increased risk of infection. While residual radioresistant recipient-derived memory T cells can offer some protection via recall response, engraftment of donor T cells can also mediate protection against opportunistic infections and prevent relapse of primary malignancies by mediating anti-tumor activity. However, donor T cells are a double-edged sword that also induce graft-versus-host-disease (GVHD), an inflammatory process mediated by alloreactive T cells that lead to the destruction of recipient tissues upon alloantigen recognition. Therefore,

it is critical to selectively eliminate alloreactive T cells and induce the recovery of non-alloreactive donor T cells to prevent GVHD and preserve anti-tumor activity.

1.2.1 Recovery of pathogenic versus beneficial donor T cells following bone marrow transplantation

Allogeneic hematopoietic stem cell transplantation (allo-HSCT) is a critical curative option for many types of hematologic malignancies [9; 10]. T cell recovery from the donor bone marrow cells is critical for reestablishing various hematopoietic lineages following lymphopenia caused by the high-dose conditioning regimen such as TBI [11]. However, T cell reconstitution from hematopoietic stem cells, which can take 12-24 months post-transplantation [12], is a prolonged process that renders patients susceptible to opportunistic infections. Specifically, this prolonged window of T cell depletion leads to increased susceptibility to fungal and viral infections, including aspergillus, candida, and cytomegalovirus, and Epstein-Barr virus [12]. While higher stem cell doses may enhance the rate of immune reconstitution [13], it is crucial to maximize the preservation of donor-derived memory T cells that recognize specific pathogens. Furthermore, it is also essential to consider the preservation of donor T cell-mediated protection known as graft-versus-leukemia (GVL) effect in order to prevent relapse of primary malignancies [14]. However, donor T cells that recognize recipient alloantigens can also contribute to GVHD, the primary cause of non-relapse mortality [15]. Nonspecific treatments such as T cell depletion therapies and broad immunosuppressants are linked to elevated rates of relapse and opportunistic infections

[16; 17; 18]. Novel approaches are therefore necessary for selectively targeting alloreactive donor T cells to preserve non-alloreactive T cells that mediate anti-tumor immunity.

1.2.2 Recovery of alloreactive donor T cells enables the development of GVHD

Acute GVHD is a primary complication in major histocompatibility complex (MHC)-mismatched bone marrow transplants that affect target organs such as skin, liver, and the gastrointestinal tract upon donor T cell recognition of alloantigens [15]. Aside from TCR engagement, additional signals are required to trigger donor T cell-mediated disease progression. The conditioning regimen, which includes radiation and chemotherapy, induces the release of proinflammatory cytokines that enhance the activation and recruitment of antigen presenting cells (APCs) [19]. Upon maturation, APCs can provide co-stimulation signals and induce activation of alloreactive T cells that migrate to secondary lymphoid organs. This process is further amplified, leading to enhanced recovery of alloreactive donor T cells during the expansion phase, followed by trafficking through the blood and lymph to reach the target organs, inducing tissue destruction [19]. Importantly, both CD4 and CD8 T cells can mediate tissue damage through cytotoxicity and release of proinflammatory cytokines. Therefore, it is important to assess the recovery of both T cell subsets in the current study.

1.2.3 Alloreactive donor T cell recovery and pathogenicity are associated with T cell metabolic reprogramming

The current understanding in T cell function is tightly linked to the metabolic state, prompting the use of metabolic modulation to dampen harmful inflammatory responses. Naïve, memory T cells and effector T cells adopt distinct metabolic profiles to support survival and functional requirements. In contrast to naïve and memory T cells, activated effector T cells become highly dependent on aerobic glycolysis to fulfill biosynthetic demands for cell growth and division [20; 21], cytokine production [22; 23], which promote pathogenic T cell responses in various inflammatory conditions [24; 25; 26; 27; 28]. Alloreactive donor T cells also undergo extensive metabolic reprogramming to become activated and induce GVHD upon alloantigen encounter. It is generally thought that glycolysis, which promotes T cell growth and clonal expansion, is employed in this process. However, conflicting data have been reported regarding the requirement of glycolysis versus other metabolic pathways to induce T cell-mediated GVHD [29]. Specifically, one group reported that alloreactive T cells activated in vivo are primarily dependent on OXPHOS and fatty acid oxidation (FAO) [30; 31]. In contrast, in vivo studies by Nguyen et al. showed that alloreactive T cells preferentially utilize glycolysis metabolite and gene expression analyses [29]. Due to the lack of treatments that selectively target the metabolism of alloreactive T cells, the role of glycolysis in T cell-mediated GVHD requires further characterization.

1.2.4 Recovery of non-alloreactive donor T cells promotes GVL and protects against opportunistic infections

While alloreactive donor T cells contribute to GVL effect through recognition of alloantigens expressed on recipient malignant cells, they are also the primary mediator of GVHD in allogeneic bone marrow transplantation. Previous studies demonstrated that donor non-alloreactive T cells can also facilitate GVL through recognition of leukemia-associated antigens (LAA) as well as protection against DNA viruses such as CMV, a significant source of morbidity and mortality [32]. In the clinical setting, it is advised that the infection history of the donor be taken into consideration to optimize the conditioning regimen prior to bone marrow transplantation, as functional donor memory T cells specific for CMV can protect against infections during the lymphopenic period [33]. In addition to reducing the risk of opportunistic infections, non-alloreactive T cells can prevent tumor development through recognition of different types of LAAs, including neoantigens in acute myeloid leukemia and self-antigens that are overexpressed on malignant cells [34; 35].

1.2.5 Anti-tumor capacity and memory T cell persistence are dependent on different metabolic pathways compared to activated alloreactive T cells

T cell metabolism is tightly linked to the differentiation status, and functions. More differentiated T cells, such as TEM and terminally differentiated effector cells (TEFF), are characterized by increased metabolic activity compared to TN and TCM [36]. Importantly, increasing differentiation status and higher metabolic activity are correlated to decreased anti-tumor capacity [36]. In particular, TEFF exhibit increased dependence on aerobic glycolysis for expansion and cytokine production [37], but suffer at the cost of reduced longevity in vivo, a critical component in sustaining anti-tumor response. Mechanistically, ROS generated through increased metabolic activity facilitates loss of quiescence and limits long-term self-renewal capacity [36; 38]. Furthermore, compared to activated alloreactive T cells, which are highly dependent on glycolysis, memory T cells with increased long-term persistence are characterized by mitochondrial fusion and enhanced fatty acid oxidation (FAO) [39]. In mouse models of melanoma, glycolysis inhibitors such as 2-DG has been linked to reduced T cell differentiation status and enhanced anti-tumor function [40]. Therefore, the metabolic distinction between anti-tumor T cells and alloreactive T cells can be exploited to selective suppress alloreactive T cells through metabolic manipulation.

1.3 IL-7 integrates T cell generation mechanisms and metabolic demands to support T cell recovery

IL-7, a γ_c cytokine, is an essential component in T cell development and mature T cell homeostasis. Indeed, mice harboring a mutation in IL-7Ra exhibit defective thymocyte development and undergo severely impaired lymphopenia induced proliferation (LIP) [41]. IL-7 also regulates metabolism in mature T cells. Specifically, IL-7 facilitates glucose uptake and glycolysis to support T cell survival and growth through Akt activation. As a critical factor that integrates T cell survival, homeostatic proliferation, and metabolic regulation, IL-7 is a promising candidate to restore T cell numbers and function.

1.3.1 IL-7 is critical for de novo T cell generation and homeostatic proliferation of mature T cells

IL-7 has unique roles at different stages of thymocyte development. At the T lineage progenitor stage, defective IL-7 signaling can lead to reduced early thymocyte progenitors (ETPs) [42]. IL-7 also serves as a growth factor for double negative (DN) thymocytes to support survival and proliferation of DN2 thymocytes. Moreover, IL-7 signaling is essential for the survival and transition of double positive (DP) thymocytes into mature CD8 T cells.

Beyond thymopoiesis, IL-7 also regulates the mature T cell pool in the periphery. LIP of naïve T cells, also known as homeostatic proliferation, is dependent on IL-7 and high affinity self-pMHC ligands. During T cell depletion, IL-7 concentration is increased, inducing LIP to fill the lymphopenic niche with proliferating naïve T cells that gradually acquire a “memory phenotype” without encountering the cognate antigen [43; 44]. At low concentrations, IL-7 promotes T cell survival by upregulating the expression of anti-apoptotic proteins such as Bcl-2 through STAT5 activation [45]. Besides IL-7, other γ_c cytokine cytokines such as IL-15, can also mediate homeostatic proliferation, even in the absence of lymphopenic conditions [45]. IL-15-mediated proliferation is much stronger than IL-7 and selectively drives CD8 TN proliferation over CD4 TN, favoring the generation of central memory T cells [46]. Memory T cells are generally dependent on a mixture of IL-7 and IL-15 for survival and homeostatic proliferation, although the specific requirements vary based on the memory T cell subset [45]. Specifically, antigen-specific memory CD8 T cells generated during acute infections are more dependent on IL-7 for survival compared to memory phenotype CD8 T cells, which are primarily depend on IL-15 for homeostatic proliferation. In contrast, both antigen-specific memory CD4 T cells and memory phenotype T cells are highly dependent on IL-7 for both survival and homeostatic proliferation.

1.3.2 IL-7 supports T cell persistence and growth through regulation of distinct metabolic processes via PI3K/Akt axis and STAT5 activation

In addition to regulating thymocyte development and homeostatic expansion, IL-7 also plays a role in the metabolic regulation of T cells. Previous studies revealed that IL-7 maintains glycolysis by controlling Glut1 and hexokinase 2 expression through PI3K/Akt activation, which is critical in regulating the metabolic state, cell growth and survival [47]. Specifically, T cells harboring a deletion in IL-7R, which is essential for activation of downstream pathways, showed significant reduction in glycolytic flux. Importantly, this phenotype was reversed through IL-7R^{flox} transgene expression in T cells on an IL-7R-deficient background, restoring glycolysis utilization and T cell survival. IL-7 is also essential for preventing T cell atrophy and promoting cell division in vivo in a glycolysis-dependent manner. In addition to regulating glycolytic metabolism, IL-7 also promotes CD8 memory cell longevity by regulating triglyceride synthesis and fatty acid oxidation through glycerol transport, which ensures metabolic fitness and supports accelerated recall response [48].

1.3.3 NT-I7, a long-acting recombinant human IL-7 that boosts T cell recovery in various disease states in clinical trials, potentially supports T cell recovery post-TBI

Total body irradiation (TBI) causes profound suppression of hematopoiesis and T cell depletion, increasing chances of infection. Currently, therapeutic options for improving

recovery of the T cell compartment following radiation exposure are not available. Exogenous administration of IL-7 has been shown to increase peripheral blood (PB) T cell levels in mice and humans [49; 50]. However, this effect can be offset by the short half-life (<10 hours) of IL-7 in circulation. NT-I7 (efineptakin alfa) is a long-acting homodimeric recombinant human IL-7 fused with a hybrid Fc fragment. The Fc region consists of heavy chain regions from both human IgD and IgG4 [51], which enhances the half-life in vivo through neonatal Fc receptor-mediated recycling [52]. Additionally, as increased molecular size correlates with less efficient system clearance through the kidneys, its large molecular size of 104-kDa relative to endogenous IL-7 (25-kDa) also contributes to enhanced persistence. Importantly, clinical trials have demonstrated that NT-I7 is not only well-tolerated with minimal adverse effects, but also persistently increases T cell counts at a dose-dependent manner [51]. Therefore, NT-I7 is a long-lasting form of IL-7 that can be further assessed for its ability to rescue compromised T cell immunity, including the window of TBI-induced lymphopenia.

1.4 Significance and study objective

1.4.1 Characterizing the phenotypic, differentiation, and metabolic profile of T cell recovery following total body irradiation

Although previous studies demonstrated variations in survival advantages within T cell populations, differences in proliferation kinetics and mechanisms have not been comprehensively examined [4; 6]. Moreover, T cell populations unique to TBI exposure

and their gene expression profile during active T cell recovery have not been extensively characterized. In the context of peripheral expansion, there are very few findings for the unique gene expression for T cells that undergo homeostatic proliferation. In one murine study, 9 candidate genes were assessed for their potential role in homeostatic proliferation through quantitative PCR. However, only one gene with no homologies in nonrodent species was found to be consistently increased in T cells that undergo homeostatic proliferation [53]. Moreover, the lack of comprehensive characterization of radioresistant T cell populations and their transcriptional landscape during the active recovery window following ionizing radiation prompts us to assess the unique gene signatures of radioresistant T cells and mechanisms involved in systemic T cell recovery. A more comprehensive approach is required to address the transcriptional signature of radioresistant T cells during recovery from TBI. In the current study, we investigated the phenotypic, metabolic, and functional aspects of T cell recovery after radiation exposure. In addition, we also characterized the role of thymic-dependent and peripheral expansion pathways following TBI to achieve a more comprehensive understanding of essential mechanisms during the reconstitution process. Implications from these findings will improve the identification and the optimal treatment window and therapeutic interventions.

1.4.2 Harnessing T cell metabolism to prevent the recovery of alloreactive donor T cells and promote the recovery of donor T cells against tumor development following bone marrow transplantation

In addition to radiation exposure as a result of nuclear accidents and terrorism events, TBI is also a core component of conditioning regimen in preparation for allogeneic bone marrow transplantations. In this setting, TBI-induced lymphopenia creates a niche for the engraftment of donor cells. Since donor cells include both alloreactive T cells and non-alloreactive T cells, donor T cell recovery can be a double-edged sword that mediates recipient tissue damage and prevents tumor relapse. Current transplant approaches to reduce GVHD include induction of immunosuppression, T cell depletion, and cyclophosphamide administration. However, the selectivity of these treatments is limited, leading to simultaneous suppression of T cells mediating protection against common viruses and bacterial infections, as well as tumor antigen-specific T cells. Selective depletion of alloreactive T cells ex vivo offers a different approach to preserve non-alloreactive donor T cells. The ex vivo depletion approach features a mixed lymphocyte reaction (MLR) of purified donor T cells and irradiated recipient antigen presenting cells or lymphocytes, followed by photodepletion or addition of antibodies that target activated T cells [32]. However, these treatments have shown limited depletion efficiency and off-target effects that also affect nonalloreactive T cells. We hypothesize that specific inhibition of alloreactive donor T cells through metabolic manipulation will enhance the preservation of T cells mediating GVL effects.

Despite the large body of studies, the role of glycolysis in the pathogenicity of alloreactive T cells and the sparing of GVL activity with glycolysis blockade remain poorly understood [29; 30; 31; 54; 55]. Previous studies indicated that alloreactive T cells activated *in vivo* are primarily dependent on OXPHOS and fatty acid oxidation (FAO) [30; 31]. In contrast, *in vivo* studies by Nguyen et al. showed that alloreactive T cells preferentially utilize glycolysis through metabolite and gene expression analyses (20). However, these studies could not exclude the dependence of antigen presenting cells (APCs) on glycolysis due to the systemic treatment with glycolysis inhibitors [29; 56; 57; 58]. Non-specific treatments using metabolic inhibitors can affect the function and survival of other cell types and cannot be assumed to accurately reflect the biology of alloreactive T cells. Other groups also demonstrated indirect connections between glycolysis and T cell-mediated GVHD [59; 60]. More importantly, whether glycolysis inhibition is capable of preserving anti-tumor effects of non-alloreactive T cells is unknown. It is imperative to evaluate GVL effects in preclinical studies to prevent tumor relapse prior to the introduction of glycolysis inhibitors to the clinical setting. A model limiting the utilization of glycolysis exclusively in T cells is necessary to address its role in T cell-driven GVHD and the preservation of GVL effects. Glucose uptake in T cells can be facilitated through glucose transporter (Glut) family members Gluts 1, 3, 6, and 8 [27]. Glut1, the primary glucose transporter in T cells, is upregulated as soon as 2 hours following activation [27]. Transgenic animals that constitutively express Glut1 are

susceptible to the development of systemic inflammatory diseases [61; 62]. Given the discordant findings [29; 30; 31; 54], we previously utilized animals harboring a T cell-specific genetic deletion for Glut1 (Glut1^{T-KO}) to address the role of glycolysis in GVHD [27]. However, whether the effect on disease progression is a strain-specific phenomenon, the mechanisms leading to the differences in GVHD development, and impacts on GVL effects were not examined. Donor T cells derived from these animals are functionally deficient for glycolysis, allowing for the examination of glycolysis in T cell-mediated GVHD. In the current study, we examined the molecular pathways by which glycolysis modified the pathogenic phenotype of alloreactive T cells through proliferative response and cell death mechanisms, demonstrating a key role for glycolysis without confounding factors from other glycolysis-dependent cell types [56; 57; 58]. We also evaluated for the first time the therapeutic potential and feasibility for the separation of GVL from GVHD through ex vivo glycolysis inhibition using the small molecule inhibitor, 2-Deoxyd- glucose (2-DG).

1.4.3 Enhancing T cell reconstitution using long-acting recombinant human IL-7, which integrates T cell generation mechanisms and metabolic demands during T cell recovery.

As a critical component during T cell development and maintenance, IL-7 facilitates de novo T cell generation and homeostatic expansion in the periphery. Clinical trials have demonstrated that IL-7 administration promotes peripheral T cell expansion, leading to enhanced TCR repertoire diversity [63]. These mechanisms contribute to enhancing

survival and proliferation in both naïve and memory T cells, which are directly linked to regulation of metabolic activity. Previous studies revealed that IL-7 supports T cell survival, growth, and cell division through glycolysis regulation [47]. Hence, IL-7 is a promising candidate that integrates multiple requirements for T cell recovery, including metabolic regulation and diverse T cell generation mechanisms. However, these IL-7-mediated T cell recovery mechanisms can be compromised by its short-half life in vivo. NT-I7, a long-acting recombinant human IL-7, consists of homodimeric IL-7 fused to human Fc fragments IgD and IgG4 [51]. Studies have shown that NT-I7 has a significantly extended half-life due to neonatal Fc receptor recycling mechanisms associated with the recombinant human Fc fragments fused to IL-7. Both mouse and human studies consistently show that NT-I7 administration consistently enhance T cell counts. We propose that NT-I7 can rescue systemic T cell recovery following TBI exposure in both lymphoid organs and peripheral blood, shortening the lymphopenic window. Moreover, we further propose that NT-I7-mediated T cell recovery is linked to both thymic-dependent and -independent pathways, as well as inducing changes at the HSC and progenitor stage, which may also lead to the reestablishment of other hematopoietic lineages. Due to the extended half-life of NT-I7, we hypothesize that the effect on T cells can be sustained even after the administration of NT-I7, leading to both numerical and functional T cell recovery.

2. Methods

2.1 T cell recovery following Total body irradiation

2.1.1 Mice

The B6.129-*Gt(ROSA)26Sor^{tm2(ACTB-Luc)Tyj}*/Nci strain (common strain name: ROSA26-pCAGGs-LSL-luciferase) on the C57BL/6 background was originated from the Jackson Laboratory and obtained via the NCI mouse repository. Live mice were obtained through in vitro fertilization at Duke University Medical Center. The B6.Cg-Tg(Cd4-cre)1Cwi/BfluJ (CD4Cre) strain, C57BL/6 strain, and B6(Cg)-Tyr^c-2J/J strain were purchased from Jackson laboratories (Bar Harbor, ME). T-Luc mice were generated by crossing the ROSA26-pCAGGs-LSL-luciferase strain to the CD4Cre strain to generate heterozygotes. Chimera mice were generated using white C57BL/6 recipients and T-Luc donors. Following 10.5 Gy TBI, white C57BL/6 recipients were transplanted with 1×10^6 whole bone marrow from T-Luc donors. Following reconstitution, BLI was performed to determine T cell reconstitution from donor cells. All mice were maintained in a specific pathogen-free facility at Duke University. All experimental procedures were approved by the Institutional Animal Care and Use Committee (IACUC) of Duke University Medical Center.

2.1.2 TBI model

Mice were given sublethal TBI doses at 0 Gy, 2 Gy, 5 Gy, and 7 Gy using a Mark I-68A ¹³⁷Cs irradiator (JL Shepherd and Associates, San Fernando, CA). For 7 Gy BMT

treatments, mice were given either T cell depleted (TCD) (1×10^7 /mouse) or lineage-negative bone marrow cells (0.5×10^6 /mouse) through tail vein.

2.1.3 Bioluminescent imaging

Mice were anesthetized using isoflurane, followed by D-Luciferin injection (30 mg/kg, PerkinElmer, CT) 10 minutes prior to imaging. Imaging was performed using a Xenogen IVIS 100 imaging system (Xenogen Corporation, Alameda, CA) for maximal signal intensity at 4-minute exposure time. Living Image 2.5 software (Caliper, Newton, MA) was used for imaging analyses.

2.1.4 TCR sequencing

Splenocyte cell pellets were isolated (1 million splenocytes per mouse), flash frozen in 10% DMSO, sent to Adaptive Biotechnologies for DNA extraction and sequencing. TCR β deep sequencing was performed via the ImmunoSEQ platform using a multiplex PCR amplification method that resolves CDR3 sequences in the TCR β region. Total productive rearrangements and Shannon entropy for each sample are provided in the supplementary section.

2.1.5 TCR repertoire analyses

The sequencing data were accessed from the ImmunoSEQ platform. Clonality, Shannon entropy, rearranged nucleotide and amino acid sequences, V resolved, D resolved, J resolved, productive frequencies of single clones were downloaded from the Adaptive server. Shannon entropy was computed for all clones found within each VJ combination.

2.1.6 Single-cell sequencing library preparation

Single cell expression libraries were prepared using the Chromium Single Cell Next GEM 3' v3.1 Gene Expression Assay (cat# 1000121, 10x Genomics, Pleasanton, CA, USA). Briefly, cell suspensions from FACS purified live CD45.1⁻CD45.2⁺CD3⁺CD4⁺CD8⁻ and CD45.1⁻CD45.2⁺CD3⁺CD4⁻CD8⁺ cells were mixed with reverse transcription reagents and loaded on the 10x Genomics Chromium Controller Single-Cell Instrument (10x Genomics, Pleasanton, CA, USA) along with gel beads and oil to generate single-cell gel bead in emulsions (GEMs). GEM-RT was performed in an Eppendorf Mastercycler Pro (cat#950030020, Eppendorf): 53 °C for 45 min, 85 °C for 5 min; held at 4 °C. After reverse transcription, GEMs were lysed and full-length cDNA was purified with DynaBeads MyOne Silane Beads (cat#37002D, Thermo Fisher Scientific). cDNA was amplified using the Eppendorf Mastercycler Pro (cat#950030020, Eppendorf): 98 °C for 3 min; cycled 11-13 × : 98 °C for 15 s, 67 °C for 20 s, and 72 °C for 1 min; 72 °C for 1 min; held at 4 °C. Amplified cDNA product was purified with the SPRIselect Reagent Kit (0.6 × SPRI)

(cat#B23318, Beckman Coulter). Standard NGS dual indexed libraries were constructed using the reagents in the Chromium Single-Cell 3' v3.1 Library Kit, following these steps: (1) fragmentation, end repair and A-tailing; (2) SPRIselect cleanup; (3) adapter ligation; (4) postligation cleanup with SPRIselect; (5) sample index PCR; (6) post index PCR cleanup. The barcoded sequencing libraries were quantified by quantitative PCR (cat#KK4824, KAPA Biosystems Library Quantification Kit for Illumina platforms). Sequencing libraries were transferred to the Duke University Center for Genomic and Computational Biology (GCB) and were loaded on a Nextseq 500 (Illumina, San Diego, CA, USA) for sequencing. Libraries were pooled to equimolar concentration to a total of 1.4pm and sequenced in single index mode (28x8x91) with a 5% PhiX spike-in.

2.1.7 Single-cell sequencing sequencing data processing and analyses

The raw reads were processed using the 10x Genomics Cell Ranger pipeline (v.3.0.2). The ``cellranger mkfastq`` command was used to demultiplex libraries to FASTQ format files. The ``cellranger count`` was used to identify cell barcodes and feature counts to the mouse transcriptomes (refdata-cellranger-mm10-3.0.0). Libraries were anchored and integrated using the top 2000 variable features per library calculated via the “vst” method in Seurat package (v 3.1.1). Default normalization and reduction on these 2000 features between the libraries was calculated, and the first 20 dimensions used as input for anchoring. Post anchoring, data were scaled by ``ScaleData`` function with default

setting, PCA was performed and the first 20 PC's were used for UMAP dimensionality reduction and subsequent clustering using resolution 0.5. Marker genes per cluster were calculated using Seurat's `FindAllMarkers` function and the "wilcox" test option and only return positive markers.

Datasets were further filtered based on cells of interest (CD4 & CD8) and clustering was performed again on the subsets of these cells using resolution 0.5. Combining multiple libraries using the integration strategy described in Stuart and Butler allowed for calculation of differential expression, not only between clusters, but within clusters across libraries using default parameters in Seurat [64]. This allowed calculation of differential expression within cell type between Control, Day 5 and Day 21. Differential expression of relevant cell marker genes was visualized on UMAP plot to reveal specific individual cell types. Additional downstream analyses included examining the cellular distribution of a priori genes of interest, closer examination of genes associated with cell clusters, and the refined clustering of cells in order to identify further resolution of cell types, in addition to comparing differences between experiments of different states.

2.1.8 Gene ontology enrichment analysis

Gene Set Enrichment Analysis (GSEA) was performed using Broad's GUI (Graphical User Interface) GSEA tool for Windows Operating System. Hallmark signature

database version 7.2 was used as gene set to find out differentially regulated pathways between Day21 and Control.

2.1.9 Trajectory analyses

The cell trajectory analysis was performed using R package Monocle2 that uses reversed graph embedding to describe multiple fate decisions in a fully unsupervised manner [65].

The dimensionality was reduced by performing a Principle Components Analysis (PCA) followed by t-SNE to project cells into two dimensions (Monocle2 Documentation).

Density peak clustering, based on each cell's local density (P) and the nearest distance (Δ) of a cell to another cell with higher distance, identifies cell clusters in 2-D t-SNE space [65].

The top significant genes across all clusters as input for the RGE algorithm were used to define progress through the trajectory (Monocle2 Documentation).

2.1.10 Metabolic assays

Extracellular acidification rate (ECAR) and oxygen consumption rate (OCR) assays were performed using the XF24 extracellular flux analyzer (Seahorse Bioscience) as previously described [66]. ECAR was measured at indicated time points following sequential compound injections (10 mM glucose, 1 μ M oligomycin, and 20 mM 2-DG). Basal OCR was measured prior to compound injection. Glucose uptake assays were described previously (Wieman et al., 2007). 2-Deoxy-d-[H^3] glucose (2 mCi/reaction) was added to

T cell cultures and quenched by 200 μ M phloretin (Calbiochem, San Diego, CA).

Radioactivity of solubilized cell pellets was measured using a scintillation counter.

2.1.11 Murine cell preparation and T cell stimulation

Lymphocytes were isolated from blood, spleens, bone marrow, and thymi. For blood collection, 50 μ l of peripheral blood, collected using EDTA-coated syringe, were stained with monoclonal antibodies for 15 minutes at room temperature. The stained samples were then processed using BD FACS Lysing Solution (BD Biosciences) to lyse red blood cells. Splenocytes were isolated, filtered through a 70 μ M cell strainer, and depleted of red blood cells with ACK lysis solution. Thymi were collected, filtered through a cell strainer. Lineage negative bone marrow was prepared using the Lineage Cell Depletion Kit (Miltenyi Biotec, Germany) for reconstitution of the 7 Gy BMT recipients via tail vein injection.

2.1.12 Flow cytometry

The following Abs were used to detect surface expression of corresponding proteins:

anti-CD4-APC-Cy7 (clone GK 1.5), anti-CD8-PE-Cy7 (clone 53-6.7), anti-CD44-PE-Cy5.5 (clone IM7), anti-CD25-APC (clone PC61), anti-CD3-PE (clone 145-2C11), anti-B220-PerCP-Cy5.5 (clone RA3-6B2), anti-CD49b-FITC (clone DX5). All antibodies were purchased from BD Pharmingen (San Diego, CA), BD Biosciences (Franklin Lakes, New

Jersey), Biolegend (San Diego, CA), and eBioscience (San Diego, CA). Fixable Viability Dye eFluor 780 (catalog 65-0865) was used to distinguish viable cells (eBioscience, San Diego, CA). Stained samples were analyzed using FACSCanto flow cytometer (BD Biosciences). Data were analyzed using FlowJo software (Tree Star, Ashland, OR).

2.1.13 Statistics

Data were analyzed using Prism Graphpad (Version 6, San Diego, CA). Error bars represent mean \pm SEM. Unpaired two-tailed student's t tests, one-way ANOVA with Tukey's multiple comparisons test, were utilized for group comparisons. Survival curve comparisons were performed using Log-Rank (Mantel-Cox) test. P-values < 0.05 were considered statistically significant. The differences of Shannon entropy were tested by two-way ANOVA followed by Tukey's honestly significant difference test.

2.2. T cell recovery in Bone marrow transplantation

2.2.1 Mice

C57BL/6 (H-2^b, CD45.2), C3H/HeJ (H-2^k, CD45.2), BALB/c (H-2^d, CD45.2), B6.SJL (H-2^b, CD45.1) mice were purchased from Jackson laboratories (Bar Harbor, ME). Glut1T-KO (Glut1^{fl/fl} x CD4Cre) mice, Glut1^{fl/fl} mice, and TCR-tg 4C mice are in the C57BL/6 background as described previously (15, 28–30). Wildtype (WT) animals include both C57BL/6 and littermate controls. All mice were maintained in a specific pathogen-free

facility at Duke University. All experimental procedures were approved by the Institutional Animal Care and Use Committee (IACUC) of the Duke University Medical Center.

2.2.2 Murine cell preparation and T cell stimulation

Splenocytes were isolated, filtered through a 70 μ M cell strainer, and depleted of red blood cells with ACK lysis solution. Thymi were collected, filtered through a cell strainer. Murine total, CD4+, or CD8+ T cells were isolated from splenocytes by negative selection using mouse Pan T Cell Isolation Kit II (Miltenyi, Germany). Dendritic cells (DCs) were isolated from splenocytes using CD11c Microbeads UltraPure (Miltenyi). Bone marrow cells were collected from femurs and tibia by flushing using a syringe and passing through a strainer. To prepare T cell depleted bone marrow (TCDBM), bone marrow cells were first incubated with anti-CD90.2 antibody (clone 30H12; BD Pharmingen, CA) on ice for 1 hour. Subsequently, cells were treated with Low Tox-M Rabbit Complement (Cedarlane, Burlington, Canada) for 1 hour at 37°C and washed twice for injection. For in vitro T cell stimulation, 7.5×10^5 T cells isolated from donor spleens were incubated in 12 wells, flat-bottomed plates with 1.5×10^5 BALB/c irradiated DCs (20 Gy) at 37°C in 5% CO₂ for 16 hours; irradiated BALB/c splenocytes (20 Gy) were used when indicated. T cells isolated from the recipient spleens were utilized for in vivo expansion analyses. For antibody stimulation in vitro, 12 wells, flat-bottomed plates

were coated with goat anti-hamster IgG antibody (Invitrogen) at 20ug/ml overnight, followed by wash with PBS prior to stimulation with anti-CD3 at 1ug/ml (BD Pharmingen, clone 145-2C11) and anti-CD28 at 0.3ug/ml (Invitrogen, clone 37.51) antibodies. For metabolic assays, T cells were co-cultured with BALB/c irradiated DCs or IL-7 (0.3 ng/ml) for 120 hours. For intracellular staining of TNF α , WT or Glut1T-KO T cells were stimulated with purified BALB/c DCs for 72 hours, with the addition of PMA (Sigma, 20ng/ml), ionomycin (Sigma, 1uM), and monensin (ThermoFisher) 4 hours prior to collection. For ex vivo inhibition assays, 1×10^6 T cells were first stimulated with irradiated BALB/c splenocytes (20 Gy) for 16 hours in complete RPMI with 10% fetal bovine serum. Following 16 hours, T cells were washed and stimulated with freshly isolated BALB/c splenocytes (irradiated) for an additional 24 hours, 48 hours, 72 hours, or 96 hours in the presence of media control or 2-DG at a final concentration of 8mM.

2.2.3 Human cell preparation and T cell stimulation

Human T cells were purified using RosetteSep human T cell enrichment cocktail (STEMCELL Technologies, Vancouver, Canada) from donor peripheral blood mononuclear cells (PBMCs). T cells (1.25×10^5 cells) were co-cultured with irradiated PBMCs (20 Gy) from unrelated donors (5×10^5 cells) for 16 hours, followed by 24-hour incubation with 2-DG, washed and incubated with PBMC stimulators or Dynabeads human T-Activator CD3/CD28 for 72 hours (Thermo Fisher, Waltham, MA). Human

samples from de-identified healthy donors were obtained from American Red Cross under an approved protocol.

2.2.4 GVHD model

Recipient mice were lethally irradiated at 9.5 Gy for C3H/HeJ, 8.5 Gy for BALB/c, or 10.5 Gy for C57BL/6 mice using a Mark I- 68A 137Cs irradiator (JL Shepherd and Associates, San Fernando, CA) and transplanted via tail vein injection within 4 hours following irradiation. Recipients were transplanted with 1×10^7 TCDBM cells/mouse from C57BL/6 donors with or without 1×10^6 T cells from WT or Glut1^{T-KO} mice. Survival, weight change, skin changes (hair loss and ruffling, erythema), hunching posture, diarrhea, and activity were monitored daily for clinical grading. Mice that met humane endpoints were sacrificed according to Duke University IACUC protocols.

2.2.5 GVL model

Recipient BALB/c mice were lethally irradiated at 8.5 Gy, followed by transplantation with 1×10^7 TCDBM cells/mouse from C57BL/6 donors with or without T cells from WT or Glut1T-KO mice, along with 5×10^5 Luc-EGFP BCL1 cells or 1×10^5 Luc-EGFP A20 cells. Survival and weight loss were recorded daily. Recipients were further monitored for tumor growth by bioluminescent imaging (BLI) and GVHD evidence by skin changes, activity, posture, and diarrhea. Biopsies were taken from spleen and liver for

evidence of tumor growth. Mortality due to GVHD or tumor was distinguished by BLI, necropsy, and histology. In the absence of tumor detection, the cause of death was ruled as GVHD.

2.2.6 Tumor cell lines

Luciferase (Luc)- and the enhanced green fluorescent protein (EGFP)-expressing (Luc-EGFP) BCL1 cells, a B-cell leukemia/ lymphoma cell line of BALB/c origin, were a generous gift from Dr. Defu Zeng (City of Hope, Duarte, CA). A20 cells, another Bcell leukemia/lymphoma cell line of BALB/c origin, were initially purchased from ATCC (Manassas, VA). A20 cells expressing the Luc-EGFP gene were made by lentivirus-mediated gene transduction. Briefly, 293T cells cultured in Dulbecco's Modified Eagle Medium (DMEM) media (Sigma-Aldrich, St. Louis, MO, USA) were co-transfected with pLEX (ThermoFisher)-EF1a-luciferase-EGFP together with the packaging plasmids, pMD2.G (a gift from Didier Trono (Addgene plasmid # 12259) and psPAX2 (A gift from Didier Trono (Addgene plasmid # 12260)), by calcium phosphate precipitation. After 24 hours, the DMEM media was replaced with fresh medium. At 48 hours after transfection, medium containing lentivirus was harvested and filtered through a 0.45 μ M syringe filter. Viral infection was carried out in a 12-well plate using 5×10^5 A20 cells with 0.5 ml of lentiviral medium containing 10 μ g/mL polybrene (Sigma-Aldrich, St. Louis, MO). At 24 hours after infection, cells were selected with 1 μ g/mL puromycin

for 7 days and clonal Luc-EGFP positive cells were then selected by FACS sorting. Periodically, cells were treated with puromycin to weed out cells which had silenced reporter gene expression.

2.2.7 Bioluminescent imaging

Mice were anesthetized using isoflurane, followed by D-Luciferin injection (30 mg/kg, PerkinElmer, CT) 10 minutes prior to imaging. Imaging was performed using a Xenogen IVIS 100 imaging system (Xenogen Corporation, Alameda, CA) for maximal signal intensity at 5-minute exposure time. Living Image 2.5 software (Caliper, Newton, MA) was used for imaging analyses.

2.2.8 Mixed lymphocyte reaction

Purified T cells (2.5×10^5 cells) were incubated in 96-wells, flatbottomed plates with 5×10^5 irradiated (20 Gy) BALB/c splenocytes for indicated periods at 37°C in 5% CO₂. Cells were pulsed with ³H-thymidine (1mCi [0.037MBq]/well) 16 hours before being counted by a MicroBeta Trilux liquid scintillation counter (EG&G Wallac, Turku, Finland).

2.2.9 Metabolic assays

ECAR and OCR assays were described in 2.1.10

2.2.10 Enzyme-linked immunosorbent assay

Supernatants from T cell cultures were collected and assessed by enzyme-linked immunosorbent assay (ELISA) using antibodies against interferon γ (IFN γ) and interleukin-2 (IL-2) (BD Pharmingen, San Jose, CA) as described previously.

2.2.11 Flow cytometry

The following antibodies were used to detect surface protein expression: anti-CD4-PE (clone H129.19), anti-CD4-APC (clone RM4-5), anti-CD8-PE-Cy7 (clone 53-6.7) were purchased from BD Pharmingen (San Diego, CA) and BD Biosciences (Franklin Lakes, New Jersey); anti-CD69-PerCP-Cy5.5 (clone H1.2F3) was purchased from Biolegend (San Diego, CA). Fixable Viability Dye eFluor 780 (catalog 65-0865) was used to distinguish viable cells (eBioscience, San Diego, CA). For intracellular staining, anti-pS6-PE (eBioscience, clone cupk43k) and anti-Bim-PE (CST, Danvers, MA, clone C34C5) were used; anti-Mcl-1 (clone Y37) and anti-Noxa (clone 114C307) primary antibodies were purchased from Abcam (Cambridge, UK). Secondary antibodies, anti-rabbit IgG Fab2-AF647 (catalog ab181347) and anti-mouse IgG Fab2-AF647 (catalog ab169358) were purchased from Abcam. For intracellular staining, cells were first stained with antibodies for surface proteins, fixed with 4% PFA, then permeabilized using 0.5% Tween 20 in PBS. For staining of TNF α , eBioscience Foxp3/Transcription Factor Staining Buffer Set was used (ThermoFisher). Cells were fixed and permeabilized at 4 degrees

Celsius for 30 minutes, followed by washing with 1x permeabilization buffer, intracellular staining for 20 minutes. Following staining, cells were washed twice before running. For secondary staining, secondary antibodies were added following addition of unconjugated primary antibodies. For isotype controls, Rabbit IgG XP (R)-PE (CST, catalog 5742S), mouse IgG1k-PE (BD Pharmingen, clone MOPC-21), Rabbit IgG (Abcam, ab37415), mouse IgG1k (Abcam, clone B11/6) were used. For apoptosis assay, the Apoptosis Detection Kit (BD Pharmingen), which includes Annexin V-PE and 7-Amino-Actinomycin D (7AAD), was used. Stained samples were analyzed using FACSCanto Flow Cytometer (BD Biosciences) and data were analyzed using FlowJo software (Tree Star, Ashland, OR).

2.2.12 Western blotting

Cells were lysed with Pierce™ IP Lysis Buffer (ThermoFischer), which contains 25mM Tris-HCl pH 7.4, 150 mM NaCl, 1% NP- 40, 1 mM EDTA, 5% glycerol, supplemented with protease inhibitor (Thermo Scientific) and phosphatase inhibitor (Thermo Scientific). Cell debris was then removed by spinning for 5 minutes at 4°C. Protein concentrations were determined using the Pierce BCA Protein Assay Kit (Thermo Scientific). Whole cell extracts (50mg of proteins) were fractionated by SDSPAGE and transferred to a nitro cellular membrane using a transfer apparatus according to manufacturer's instructions (Bio-Rad). Membranes were blocked with LICOR blocking

buffer, washed and incubated with primary antibodies (1:1000 in blocking buffer) at 4°C for 12 hours. After washing, membranes were incubated with a 1:10000 dilution (in blocking buffer) of fluorescent 700 or 800 anti-rabbit or anti-mouse antibodies for 1 hour at room temperature. Blots were washed with TBST five times and scanned using LICOR machine. Anti-Puma antibody (ab9643), anti-Noxa antibody (clone 114C307, ab13654), and anti- Mcl-1 antibody (clone Y37, ab32087) were purchased from Abcam. Anti-Mdm2 antibody (clone D-7, sc-13161) was purchased from Santa Cruz Biotechnology Inc. (Dallas. TX).

2.2.13 Histology

Biopsy samples were taken from skin, small and large intestines, liver, and spleen and were stored in neutral buffered formalin. Specimens were embedded in paraffin, cut into 5-mm sections, and stained with hematoxylin-eosin (H&E). Coded slides were assessed by D.C. single blinded to the GVHD status. Histological GVHD was graded using a semi-quantitative system based on histologic changes in the small intestine, colon, skin, and liver. Histological characteristics used for scoring included inflammatory infiltrates, apoptosis of keratinocytes, separation of dermal-epidermal junction, and formation of cleft, follicular dropout, and fibrosis in the skin; inflammation, apoptosis of bile duct epithelial cells, apoptosis of hepatocytes, cholestasis, fibrosis, and parenchyma in the

liver; and lamina propria inflammatory cell infiltrate, crypt regeneration, crypt epithelial cell apoptosis, crypt loss, mucosal ulceration, and fibrosis in the intestine.

2.2.14 Statistics

Data were analyzed using Prism Graphpad (Version 6, San Diego, CA). Error bars represent mean \pm SEM. Unpaired two-tailed student's t tests, one-way ANOVA with Tukey's multiple comparisons test, were utilized for group comparisons. Survival curve comparisons were performed using Log-Rank (Mantel-Cox) test. P-values < 0.05 were considered statistically significant.

2.3. Role of NT-17 in T cell recovery

2.3.1 Mice

Generation of T-Luc chimera mice was described as shown in 2.1.1. C57BL/6 mice were purchased from Jackson laboratories (Bar Harbor, ME). All mice were maintained in a specific pathogen-free facility at Duke University. All experimental procedures were approved by the Institutional Animal Care and Use Committee (IACUC) of Duke University Medical Center.

2.3.2 CBC

Peripheral blood was drawn via retro-orbital bleed. Blood was collected with K2EDTA (Beckton Dickinson) and analyzed using an automatic hematology analyzer (HEMAVET HV950FS; Drew Scientific).

2.3.3 Murine cell preparation and T cell stimulation

Isolation of bone marrow, spleen, blood, thymi, and lineage negative cells were as described in 2.2.11. T cell stimulation in vitro was described in 2.2.2.

2.3.4 Bioluminescent imaging

Bioluminescent imaging was performed as described in 2.1.3

2.3.5 Flow cytometry

Antibodies used for peripheral blood and thymocyte immunophenotyping were described in 2.1.12. The remaining antibodies used are as follows: anti-CD48-FITC (clone HM48-1), anti-CD150-APC (clone TC15-12F12.2), anti-Sca1-PE (clone D7), anti-c-Kit-PE-Cy7 (clone 2B8), anti-Lineage-PerCP-Cy5.5 antibodies (catalog 561317) BD. All antibodies were purchased from BD Pharmingen (San Diego, CA), BD Biosciences (Franklin Lakes, New Jersey), and Biolegend (San Diego, CA). Fixable Viability Dye eFluor 780 (catalog 65-0865) was used to distinguish viable cells (eBioscience, San Diego,

CA). Intracellular staining was performed as described in 2.2.11. Stained samples were analyzed using FACSCanto flow cytometer (BD Biosciences) and BD LSRII flow cytometer. Data were analyzed using FlowJo software (Tree Star, Ashland, OR).

2.3.6 Statistical analysis

Data were analyzed using Prism Graphpad (Version 6, San Diego, CA). Error bars represent mean \pm SEM. Unpaired two-tailed student's t tests, one-way ANOVA with Tukey's multiple comparisons test, were utilized for group comparisons. Survival curve comparisons were performed using Log-Rank (Mantel-Cox) test. P-values < 0.05 were considered statistically significant.

3. Results

3.1 Characterizing phenotypic, differentiation, and metabolic profile of T cell recovery following total body irradiation

Evaluation of recovery kinetics and gene expression profile of radioresistant T cell subsets, as well as mechanisms of T cell reconstitution is essential for determining the window susceptibility post-TBI, optimal window of treatment, and identifying therapeutic candidates that modulate mechanisms of T cell generation. Here, we assessed absolute T cell counts in various tissues along with immunophenotyping and single-cell sequencing to characterize the transcription and functional profile of radioresistant T cell populations, as well as the contribution of thymic-dependent and thymic-independent pathways to T cell reconstitution.

3.1.1. Investigating kinetics of T cell recovery in the peripheral blood (nadir, window of susceptibility, radiation dose-dependent)

Blood and lymphatic vasculature serves as highways connecting T cells to secondary lymphoid organs and peripheral tissues. Peripheral blood T cell are sensitive to IR and can be used as an indicator for tissue damage in response to radiation. To investigate the kinetics of peripheral blood T cell recovery, cell counts were assessed at baseline, day 3, then weekly over the course of 180 days. Additionally, to determine whether T cell reconstitution is radiation dose-dependent, peripheral blood T cell reconstitution dynamic was monitored following TBI at 2 Gy, 5 Gy, and 7 Gy. Untreated mice as well

as mice treated with 7 Gy TBI followed by bone marrow transplantation were included as unirradiated control and positive control for T cell reconstitution, respectively. T cell numbers decreased drastically on day 3 in a dose-dependent manner. Specifically, T cells in the 7 Gy-treated group were depleted more than 50- to 300-fold in CD4 and CD8 T cells, respectively ($19 \pm 14/\mu\text{L}$ blood, CD4 T cells, $p < 0.05$; $4 \pm 2/\mu\text{L}$ blood, CD8 T cells, $p < 0.05$) (Figure 1). TBI dose at 5 Gy yielded $32 \pm 14/\mu\text{L}$ blood in CD4 T cells ($p < 0.05$) and $10 \pm 8/\mu\text{L}$ blood in CD8 T cells ($p < 0.05$). In contrast, more T cells survived on day 3 at 2 Gy TBI, accounting for 10% of pretreatment cell numbers ($123 \pm 27/\mu\text{L}$ blood, CD4 T cells, $p < 0.05$; $93 \pm 36/\mu\text{L}$ blood, CD8 T cells, $p < 0.05$). T cell numbers continued to decline and reached the nadir on day 7 for all TBI groups. Following the continuous decline immediately after TBI, all groups underwent a steady rise in T cell numbers from day 14 to day 42 at a radiation dose-dependent manner. As expected, T cell numbers in the transplant group recovered more rapidly and exceeded 7 Gy TBI group on day 14. Although the dose-dependent difference remained apparent on day 14, this trend was gradually diminished as differences among T cell numbers began to diminish from day 21 to day 42, suggesting active endogenous T cell reconstitution of the peripheral blood. Interestingly, aside from the low dose group (2 Gy), TBI groups receiving higher doses at 5 Gy and 7 Gy also demonstrated T cell recovery comparable to unirradiated controls on day 21. From day 42 to day 180, T cell numbers recovered to levels similar to unirradiated and transplant controls. These results suggest that peripheral blood T cell

recovery is delayed with increasing doses of radiation exposure, indicating a window of susceptibility to opportunistic infections. At the sublethal doses examined in this study, both CD4 and CD8 T cells recovery back to baseline on day 180, suggesting a quantitative reconstitution of peripheral blood T cells.

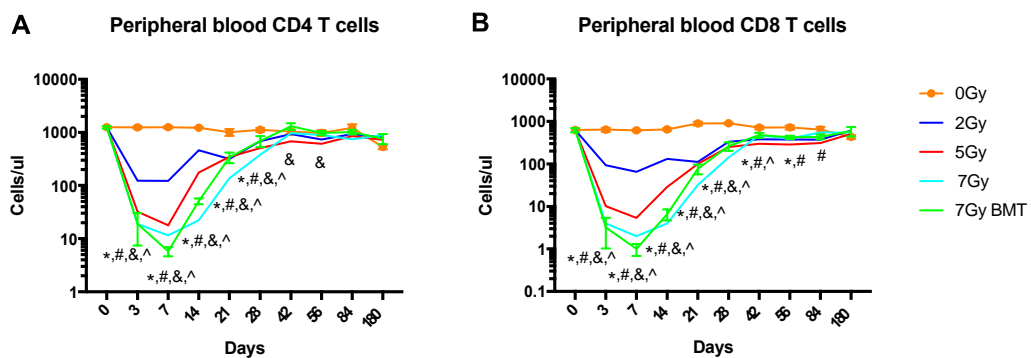


Figure 1. T cell recovery kinetics in the peripheral blood is TBI dose-dependent.

C57BL/6 mice were unirradiated (0 Gy), sublethally irradiated at 2 Gy, 5 Gy, 7 Gy, or irradiated at 7 Gy and transplanted with 1×10^7 /mouse TCDBM cells from C57BL/6 mice. Blood was collected at indicated time points. Numbers of CD4⁺ (A) and CD8⁺ (B) T cells were determined by flow cytometry. Data are means \pm SEM. * P < 0.05, 0 Gy vs. 2 Gy; # P < 0.05, 0 Gy vs. 5 Gy; & P < 0.05, 0 Gy vs. 7 Gy; ^ P < 0.05, 0 Gy vs. 7 Gy BMT; multiple unpaired t test. BMT, bone marrow transplant.

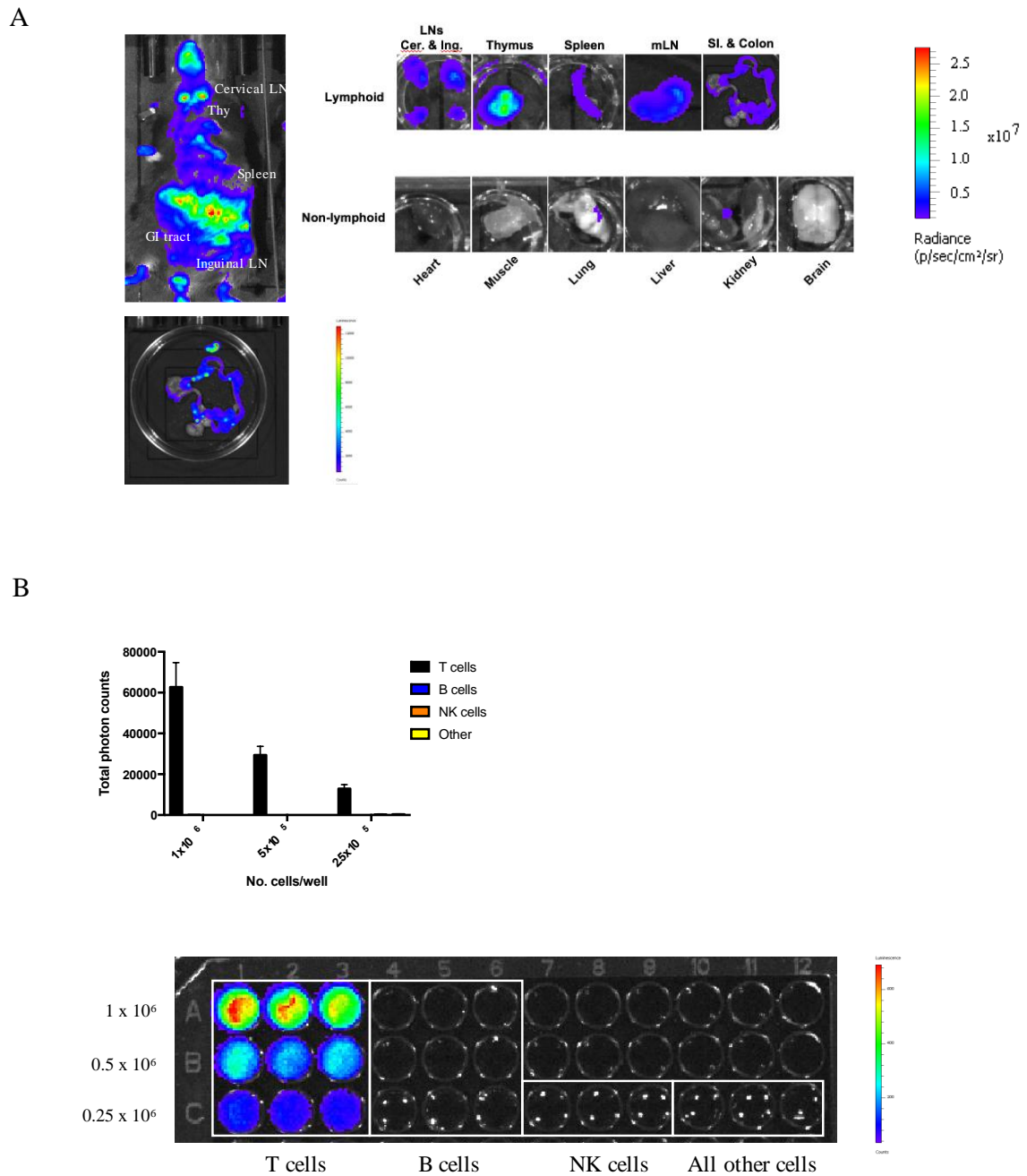
3.1.2. Establishing an imaging system to track T cell recovery in vivo

Previous studies have benefitted from the organ donor network, which provides access to a wide variety of tissues to examine T cell maintenance in addition to the peripheral blood [67; 68; 69]. Although peripheral blood cell counts are used as a

surrogate marker for tissue damage in radiation biodosimetry [70], investigating T cell recovery at the systemic level will provide a more comprehensive understanding of the process.

To visualize T cell recovery in vivo, we sought to generate a reporter strain that specifically expresses luciferase in both CD4 and CD8 T cells through CD4-driven Cre expression, which is active in late double negative and early double positive thymocytes [71]. To establish a T cell-specific luciferase reporter strain for bioluminescent imaging (BLI), Luc^{flox/flox} strain was crossed to CD4-Cre strain to generate CD4-Cre x Luc^{flox/flox} (T-Luc) animals. This allows for the constitutive expression of luciferase induced by CD4-Cre promoter during thymic development. To assess luciferase expression in vivo, whole body imaging was performed on T-Luc mouse given D-luciferin (Figure 2A, top left panel), allowing for the visualization of cervical lymph nodes, thymus, spleen, inguinal lymph nodes, as well as the gastrointestinal (GI) tract. Upon dissection of lymphoid organs and non-lymphoid organs, luciferase expression was primarily detected in lymphoid organs rather than non-lymphoid organs (Figure 2A, top right panel). Notably, imaging of T-Luc mice also allowed for the detection of Peyer's Patches (Figure 2A, middle panel). Next, to determine whether luciferase expression is restricted to T cells, we sorted splenic T cells (CD3⁺CD4⁺ and CD3⁺CD8⁺), B cells (B220⁺CD3⁻), NK cells (CD49b⁺CD3⁻B220⁻), and all other cell types (CD49b⁻CD3⁻B220⁻) by FACS. Sorted

cells were plated at various concentrations for imaging (Figure 2B). While luciferase activity was not detectable in non-T cell populations, luciferase activity in T cells was proportional to the number of cells in each well, further validating that luciferase expression in T-Luc mice is restricted to T cells.



To assess T cell reconstitution kinetics, T-Luc mice were subjected to 5 Gy TBI, followed by weekly BLI to visualize T cell locations following irradiation. Following TBI, T cells were visible in cervical lymph nodes, thymus, and GI tract (Figure 3A). However, pigmentation in the original C57BL/6 background limits the detection sensitivity when small numbers of T cells are present, particularly during early stages of recovery from radiation. Furthermore, the limited numbers of available T-Luc mice greatly reduce the number of biological replicates. Additionally, the shaving was performed weekly prior to imaging to improve detection of T cells. To address these issues, we sought to generate chimera mice using congenic white C57BL/6. Following 10.5 Gy TBI, white C57BL/6 recipients were transplanted with 1×10^6 whole bone marrow from T-Luc donors (Figure 3B). Following reconstitution, monthly BLI was performed to determine T cell reconstitution from donor cells. 3 months following transplantation, T-Luc-derived T cells populated both primary and secondary lymphoid organs (Figure 3C), indicating stabilized chimera generation that simulates the presence of T cells in the physiological condition without TBI. Therefore, the chimeras with stabilized T cell reconstitution can be used to subsequent evaluation of T cell recovery in TBI model.

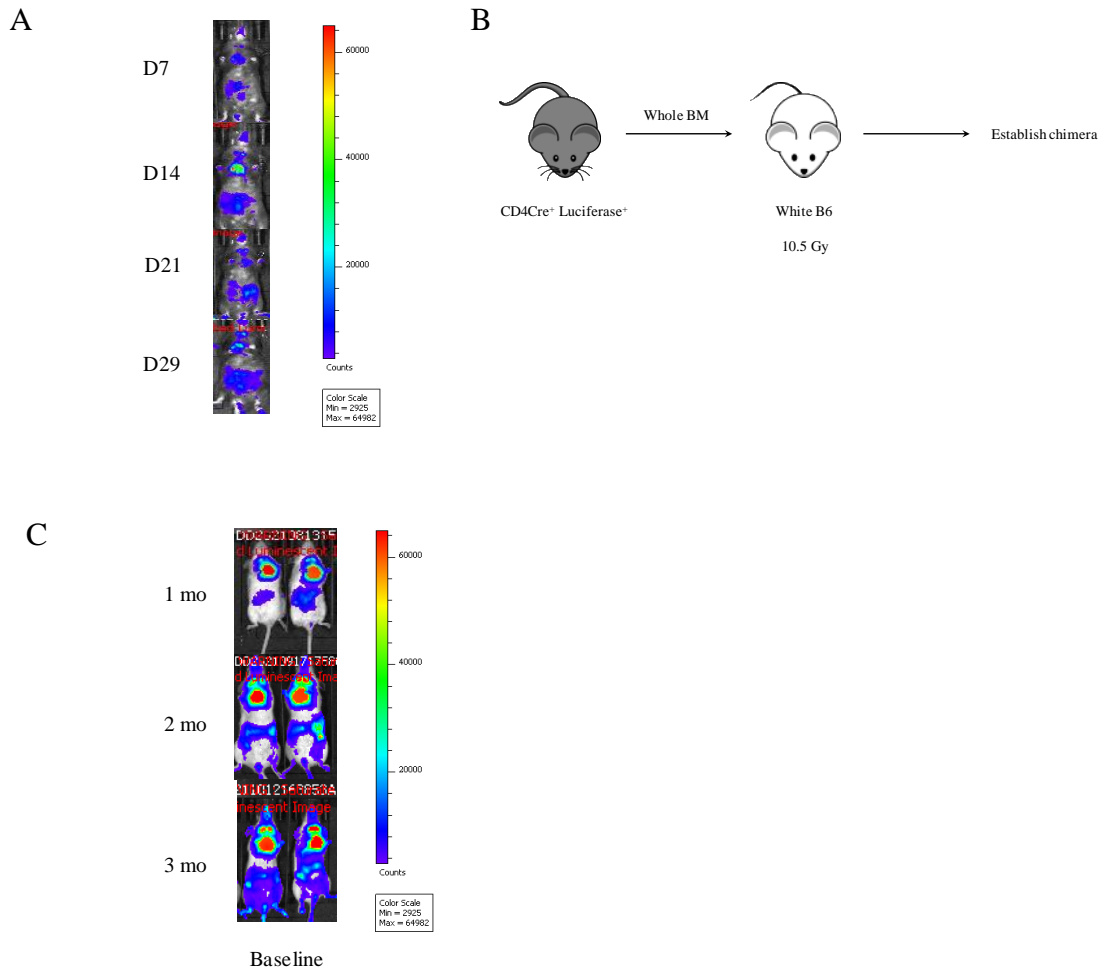


Figure 3. Establishing an in vivo imaging model to track T cell recovery.

(A) T cell recovery following 5 Gy TBI of T-Luc mice. Mice were shaved prior to imaging. BLI, bioluminescent imaging. **(B)** BLI of T-Luc mice treated with vehicle of NT-17 following 5 Gy TBI. **(C)** Generation of white C57BL/6 chimeras using donor bone marrow from T-Luc mice. 1×10^6 whole bone marrow was transferred per white C57BL/6 recipient following 10.5 Gy TBI. BM, bone marrow. **(D)** BLI of baseline chimera screening for T cell reconstitution at 1 month, 2 months, and 3 months after transplantation.

3.1.3. Investigating kinetics and mechanisms of systemic T cell recovery following TBI

We have shown that chimera recipients of T-Luc donors can be utilized to study T cell recovery after stable reconstitution by bone marrow cells (Figure 3). To evaluate kinetics of systemic T cell recovery, fully reconstituted chimeras (3 months after transplantation) were subjected to sublethal irradiation at 5 Gy. Location and magnitude of T cell recovery were monitored through in vivo imaging until day 98 (Figure 4A). Early following TBI (day 7, day 14, and day 28), BLI signal intensity was significantly reduced compared to baseline animals. (Figure 4A, top panel). Specifically, the lowest signal intensity was spotted on day 7, recapitulating kinetics observed in peripheral blood. Notably, both thymic activity and T cell presence in peripheral tissues were drastically decreased, followed by a slow and gradual recovery back to baseline levels (Figure 4A, bottom panel). Importantly, BLI imaging suggests that both thymic-dependent and thymic-independent pathways are involved during recovery from TBI, although further experiments are required to address the kinetics and relative contribution of each pathway.

A

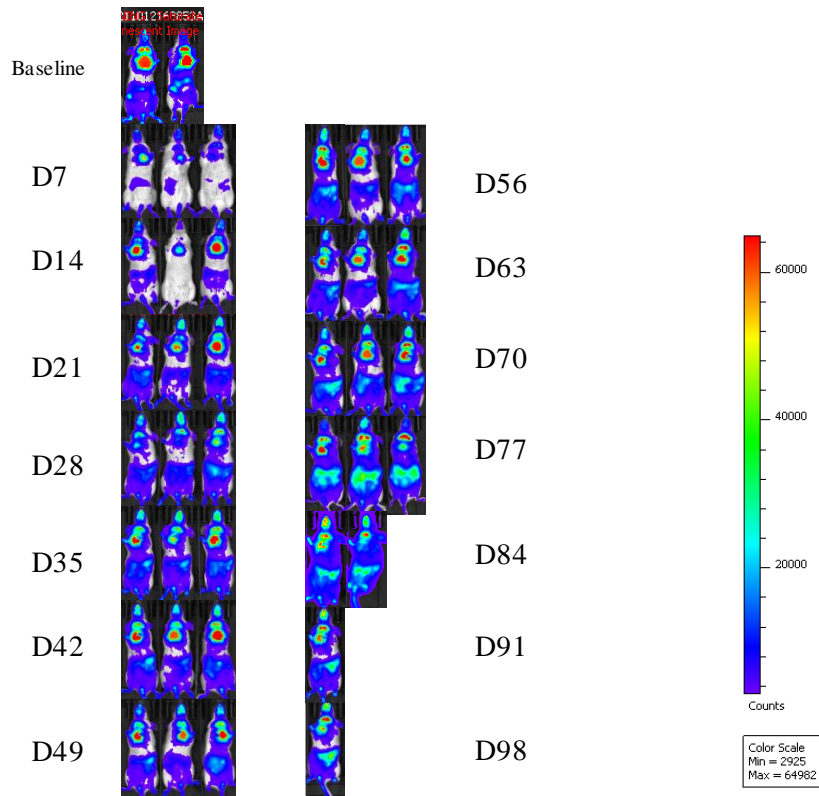


Figure 4. Evaluating systemic T cell recovery through in vivo imaging.

Chimera mice were generated by transferring 1×10^6 whole bone marrow per white C57BL/6 recipient following 10.5 Gy lethal irradiation. 3 months following transplantation, chimera mice were subjected to sublethal irradiation at 5 Gy

following stable reconstitution by donor bone marrow. Systemic T cell recovery was assessed through in vivo imaging until 98 days after radiation exposure (A). *P < 0.05 (day 14 vs. baseline; day 28 vs. baseline), **P < 0.01 (day 7 vs. baseline).

3.1.4. Role of TBI in thymic development during T cell recovery

Following development and maturation in the thymus, recent thymic emigrants migrate to various sites and contribute to the peripheral T cell pool (27-29). We hypothesize that increasing TBI doses induce waning thymic output, which may be mediated by a continuous decline in bone marrow-derived early thymic progenitors and radiation damage to the thymus.

Thymocytes were collected at 98 days after TBI treatments for total thymocyte numbers. Thymocyte numbers exhibited a trend for dose-dependent decline, with a significant defect at 7 Gy compared to unirradiated group (Figure 5A). For T cell development assessment, double-negative (DN) thymocyte frequencies were analyzed by CD44 and CD25 expression (Figure 5B). Overall, the above data revealed that TBI treatments caused a defect in total thymic output but did not affect T cell lineage commitment (DN2 to DN3) and β -selection (DN3 to DN4), as the frequencies for each DN stage were comparable across all groups (Figure 5C). There was an increase in the double-positive (DP) frequency at 2Gy, likely due to the corresponding drop in DN frequency (Figure 5D). However, it appears that positive selection was not impaired. Similarly, negative selection was unaffected as reflected by comparable SP populations.

Importantly, these data are in line with previous findings that thymic recovery is limited by the number of BM-derived settling progenitors (30-32), as the total DN frequency underwent a diminishing trend following increasing doses of TBI (Figure 5D).

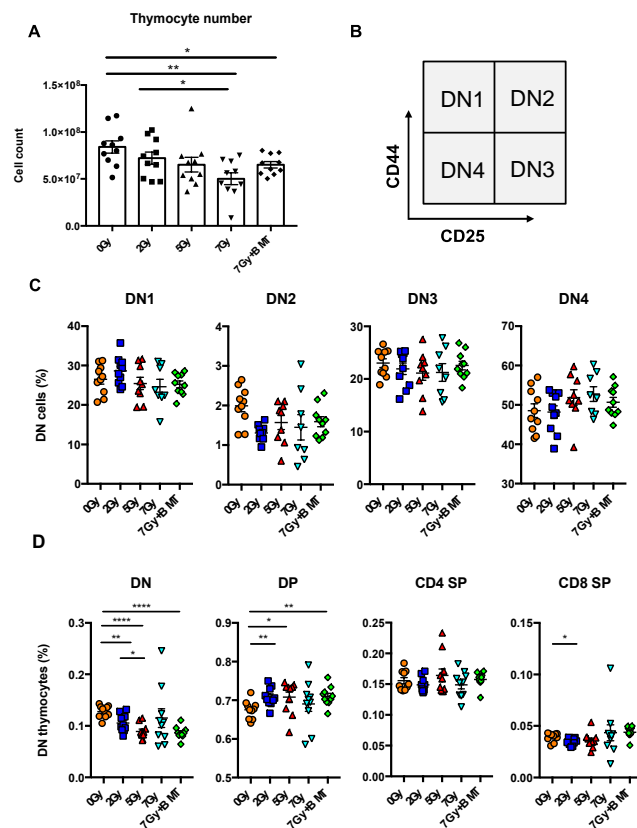


Figure 5. TBI induced defects in total thymic output.

At week 14, thymocytes were collected for total thymocyte numbers (A). DN thymocyte frequencies were analyzed by CD44 and CD25 expression (B) and shown in (C). CD4 SP, CD8 SP, and DP thymocyte frequencies separated by CD4 and CD8 expression were shown in (D).

3.1.5. TCR repertoire diversity is largely preserved following various doses of TBI exposure

De novo T cell generation through thymic development is the primary pathway to establish a T cell population bearing diverse TCRs that recognize a variety of antigens. We have shown that thymic activity is significantly reduced following TBI (Figure 5). It is essential to assess whether reduced thymic activity leads to reduced TCR repertoire diversity, an indicator of the capacity to respond to a diverse range of antigens. To determine whether various TBI doses lead to distinct repertoire diversity outcomes, we analyzed the clonal diversity of each group in splenic T cells using clonality as a measurement of the degree of dominance by expanded clones within the entire repertoire (Figure 6A). As expected, majority of the clones across all groups underwent minimal clonal expansion due to the lack of immunization with specific antigens. Furthermore, we observed an overall effective maintenance of repertoire diversity at low, intermediate, and high dose TBI, with a trend for decreased diversity for intermediate and high doses (higher clonality). We further assessed the Shannon entropy of observed clones assigned to each VJ recombination (Figure 6B), with the curve $\log_2 N$ representing the maximum diversity (highest possible entropy). The above data demonstrated that intermediate TBI dose significantly reduced the TCR diversity compared to unirradiated group. As expected, we observed a trend for decreased diversity across all TBI groups when compared to BMT group where thymic output was

increased by donor bone marrow progenitors. However, we did not detect a statistical difference between high dose TBI and unirradiated group, possibly due to limited sample size. To visualize the frequency distribution of individual clones, we analyzed the top 100 clones designated by distinct amino acid sequences of the CDR3 region (Figure 6C). Representing the relative frequencies of observed clones, the distributions of specific samples correspond to the degree of clonal expansion (samples 163 and 165 in intermediate dose TBI, sample 174 in high dose TBI). Overall, the TCR repertoire diversity across all TBI groups appeared to be effectively restored compared to unirradiated group, indicating no overt defect and possible underlying compensatory mechanisms to maintain diversity.

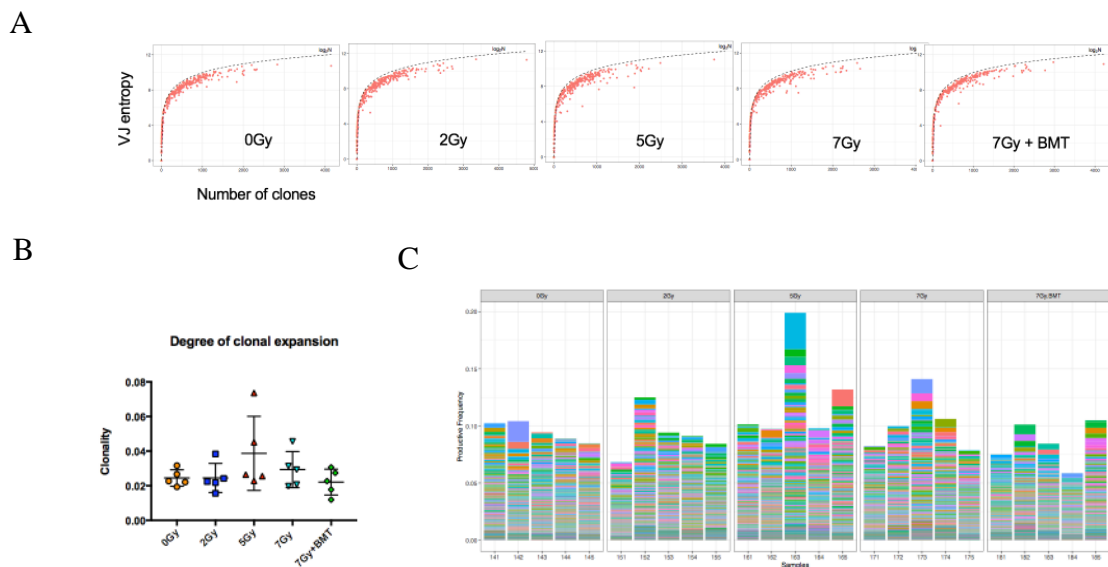


Figure 6. Preservation of T cell repertoire diversity following TBI.

C57BL/6 mice were sublethally irradiated at various doses. Splenocytes were isolated at week 14 and analyzed for clonality (A) and Shannon entropy for corresponding VJ

cassettes (B) using TCR β deep sequencing. Splenocytes were further analyzed for the frequency distribution of top 100 clones (C). $p < 0.05$, 0 Gy vs 5 Gy; 2 Gy, 5 Gy, 7 Gy vs. 7 Gy BMT.

3.1.6. Single-cell RNA-sequencing reveals distinct T cell populations unique to TBI treatment

We have demonstrated that both thymic-dependent and -independent pathways are actively involved during T cell recovery from TBI. Specifically, we showed that total thymocyte output is reduced in response to increasing TBI doses. However, the T cell subsets that actively undergo peripheral expansion is has not been comprehensively studied in the TBI setting. To address these questions, we utilized single-cell sequencing to characterize unique gene signatures of various radioresistant T cell subsets involved in peripheral expansion. Following exposure to lethal TBI (10.5 Gy) and bone marrow transplantation from CD45.1⁺ donors, we collected splenocytes from recipient-derived (CD45.2⁺) T cells of control (n = 3), 5 days (n = 6), and 21 days (n = 5) groups (Figure 7A). The distribution of various lymphocytes prior to purification is shown was assessed by flow cytometry (Figure7B). Early after TBI (day 5), T cell frequency was elevated compared to control group, along with an increase in NKT cell frequency. Later during recovery (day 21), total T cell frequency was reduced, likely contributed by increased proliferation of other cell types. In addition, although $\gamma\delta$ T cell frequency was elevated during recovery, $\alpha\beta$ T cells remained the predominate T cell population. To characterize

how distinct T cell populations respond and recover from TBI, splenic CD4 and CD8 T cells were purified by fluorescence-activated cell sorting (FACS) and pooled for library construction using the 10x Genomics Chromium platform, followed by sequencing using Illumina's NextSeq high output platform. Sequencing depth was approximately 50,000 reads per cell. Quality control was performed using Seurat to filter out doublets and lysed cells. Cells that passed quality control were kept for further analysis, including dimensionality reduction using Uniform Manifold Approximation and Projection (UMAP), differential gene expression analysis, and clustering. We first performed unsupervised clustering analysis, excluding NKT cells and regulatory T cells in attempt to further resolve the populations, yielding six distinct clusters (clusters 0, 1, 2, 3, 4, and 6) (Figure 7C). SingleR, an automatic annotation method was used to determine cell identities based on the reference cell types using the murine Immunological Genome Project (ImmGen) database. Clusters 0 and 1 strongly corresponded to CD4 and CD8 naïve T cells (TN), respectively (Figure 7D). Other top matches for cluster 1 includes CD8 effector and memory T cells (TEFF and TM), indicating heterogeneity within the cluster. By contrast, the identities of clusters 2, 3, 4, and 6 correlated primarily to TM or TEFF (Figure 7D). Notably, all four clusters matched strongly with thymocytes, indicating elevated proliferative capacity. To better identify each cluster, a second annotation method was applied using representative genes from known T cell subsets, including TN, TM, and TEFF (Figure 7E). In addition, genes

associated with cycling and proliferation were included for annotation. Overall, the phenotype of clusters 0 and 1 indicates the presence of predominately TN, along with some TM. In addition, the expression of cycling genes was considerably lower than the remaining clusters. Clusters 2, 3, 4, and 6 primarily exhibited the effector memory T cell (TEM) phenotype of both CD4 and CD8 T cell origins. The four clusters were further divided into 2 categories based on the relative expression of cycling genes: moderately (MP) and highly proliferative (HP) TEM1 and TEM2. The above annotation system of the unsupervised clustering analysis suggests that while naïve T cells were shared across control and TBI groups, four distinct proliferative TEM subsets were unique to irradiated animals. Furthermore, the emergence of proliferative TEM subsets indicates that T cells actively undergo homeostatic proliferation following radiation exposure.

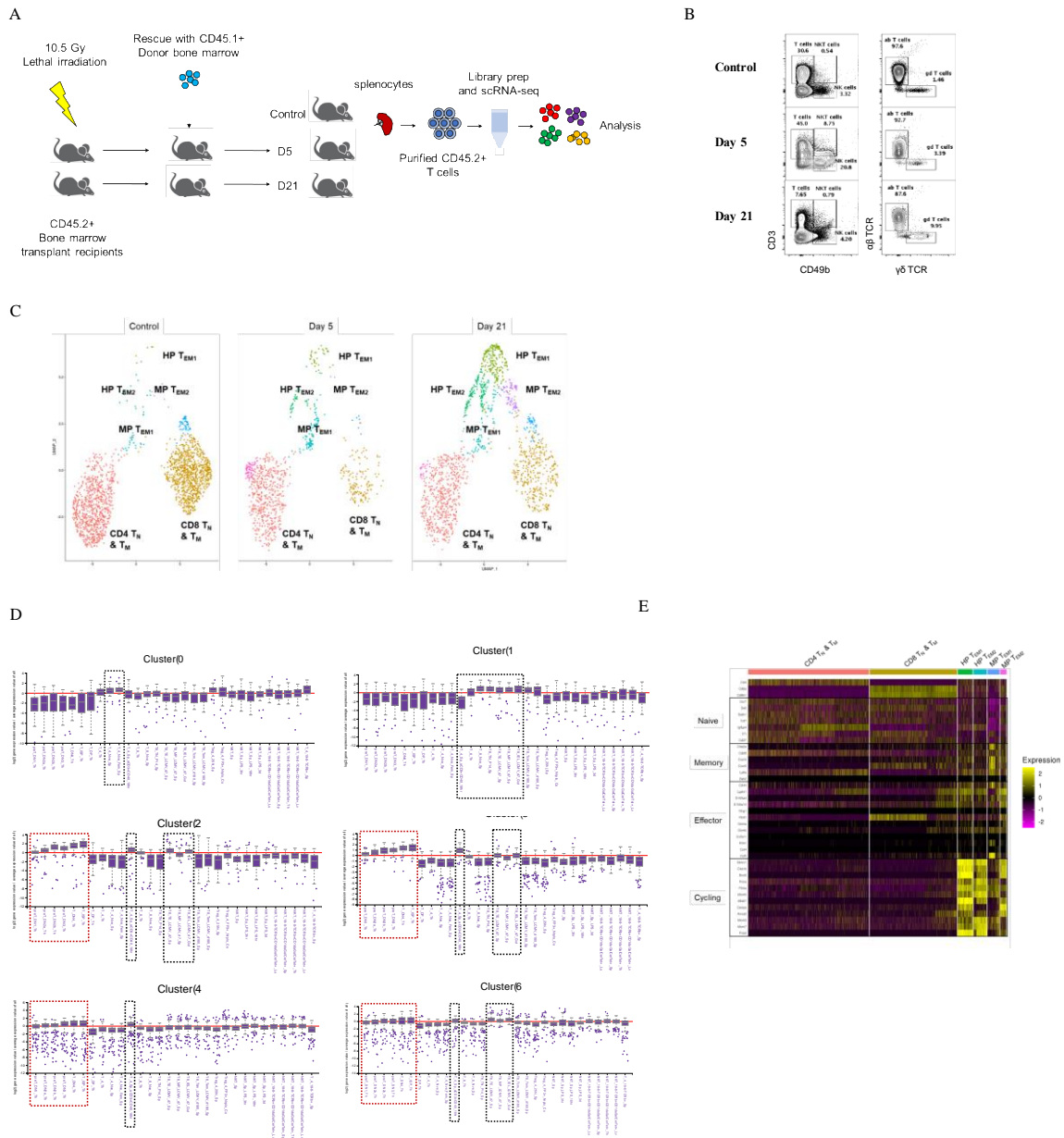


Figure 7. Single-cell sequencing reveals distinct clusters unique to TBI groups.

(A) Experimental design for scRNA-seq of splenic T cells from control and irradiated mice. Splenic T cells were pooled from each group (control, n = 3; day 5, n = 6; day 21, n = 5), isolated by FACS, subjected to library construction and RNA sequencing. scRNA-seq, single-cell RNA sequencing. (B) Distribution of distinct lymphocyte cell types prior to T cell purification analyzed by flow cytometry. (C) Clustering analysis reveals six main populations in control, day 5, and day 21 groups. NKT cells and

regulatory T cells were excluded from the analyses. Cells are represented by individual points, assigned to annotated cell types within each cluster. (D) Annotation of clusters 0 and 1 indicates the presence of primarily naïve T cells while Clusters 2, 3, 4, and 6 exhibit a distinct proliferative effector memory phenotype. Clusters were annotated by SingleR based on the ImmGen reference dataset of murine immune cells. Black boxes highlight matches T cell populations. Red boxes highlight similarity to proliferative thymocytes. (E) Annotation of various clusters using markers associated with known T cell subsets. Expression heatmap showing the relative expression of naïve, memory, effector, and cycling genes. The scale bar indicates expression level based on z-score distribution.

3.1.7. Trajectory analyses reveal thymic-independent generation of radioresistant T cells, which involves the acquisition of effector memory phenotype during recovery

To resolve the relationships of proliferative TEM populations and TN, unsupervised trajectory analysis for CD4 (Figure 8) and CD8 T cells (data not shown) was performed to determine the differentiation lineage, respectively. CD4 T cells were ordered along a pseudotime axis based on the progression of their transcription profile (Figure 8A). We also examined the placement of control, day 5, versus day 21 cells along the pseudotime trajectory (Figure 8B). Notably, while control and day 5 T cells are located toward the early and middle segments of the path, a great number of day 21 cells were ordered along the latter segments, indicating a progressive change in cellular phenotype over the course of recovery. To determine the identities of cells that are present within each segment, Seurat clusters were annotated along the trajectory (Figure 8C). While TN were primarily mapped along the root of the trajectory, followed by MP

TEM and HP TEM were located in the middle or at the end of the trajectory. Similar to analyses using CD4 T cells, the trajectory of CD8 T cells recapitulated the location of the above population along pseudotime. In addition, further analysis revealed that trajectory construction was based on the graded expression of proliferation markers. Collectively, these findings suggest the potential for radioresistant TN to serve as the primary source of recovery during homeostatic proliferation.

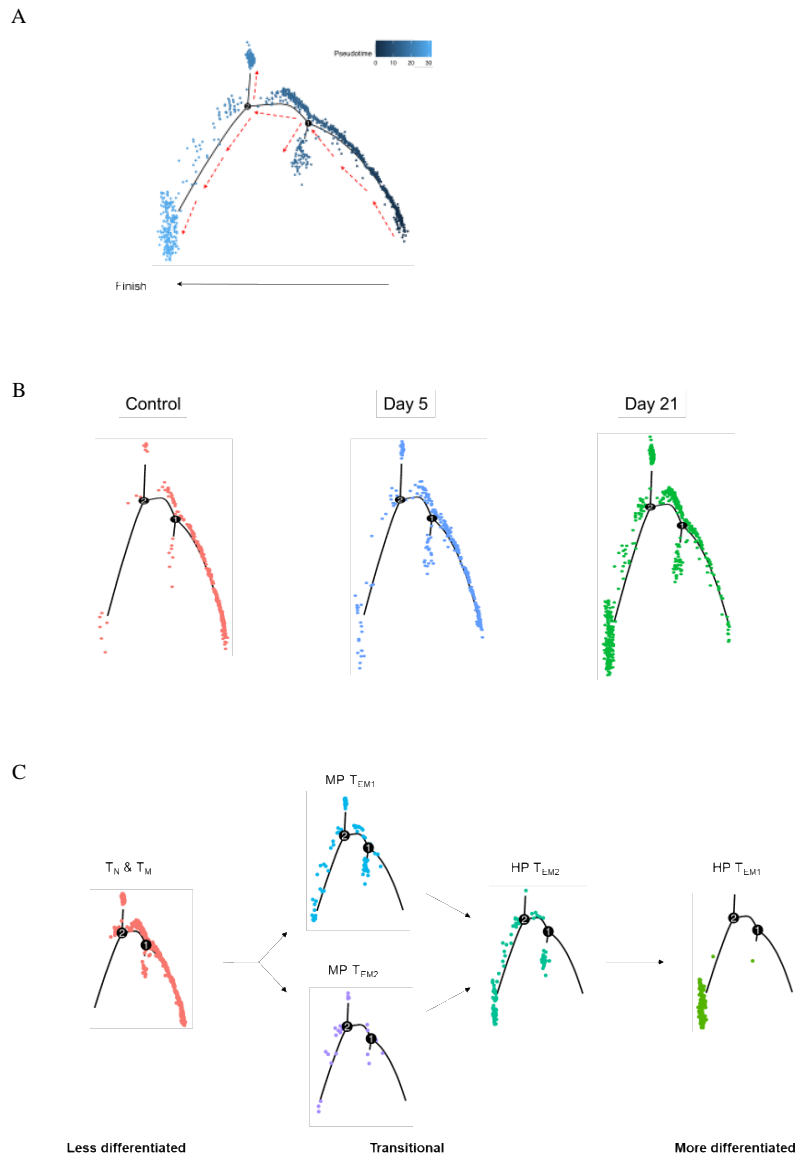


Figure 8. Figure 8. TN & TM precede other subsets in pseudotime.

Pseudotime analysis of CD4 T cells from control and day 5, day 21 irradiated groups. (A) Monocle pseudotime trajectory of T cells from all three groups. Cells are labelled along pseudotime progression. (B) Distribution of CD4 T cells from control, day 5 and day 21 after irradiation on the pseudotime trajectory. (C) Distribution of annotated T cell subsets were identified on the differentiation trajectory, ranging from less differentiated, transition, and more differentiated phenotypes.

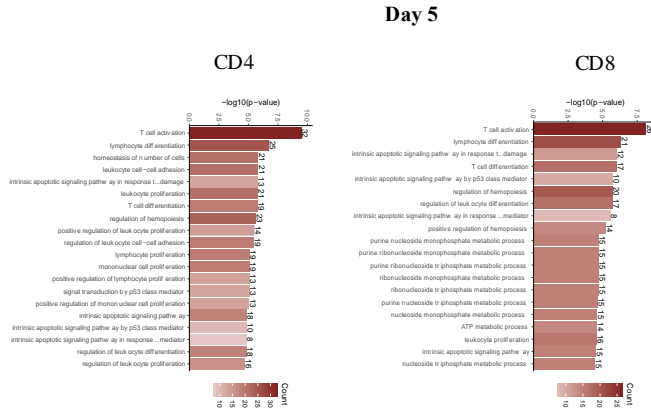
3.1.8. Radioresistant T cells demonstrate a preferential upregulation of mitochondrial activity and oxidative phosphorylation during the recovery process

To investigate T cell responses to irradiation after TBI, we utilized pathway enrichment analysis for biological processes and cellular components to determine pathways upregulated in irradiated T cells compared to control T cells. Analysis was performed for CD4 and CD8 T cells respectively to reveal the presence of shared pathways and potential differences during recovery. The kinetics of cellular responses can be visualized by comparing enriched pathways on day 5 and day 21 (Figures 9A and 9B). Early following TBI, CD4 T cells exhibited upregulation in lymphocyte proliferation and apoptotic pathways (Figure 9A, left panel). Later during recovery, cellular component analysis revealed upregulation of genes associated with mitochondrial activity (Figure 9B, left panel), indicating that mitochondrial metabolism may play a role in T cell persistence. Interestingly, CD8 T cells shared similar characteristics for increased mitochondrial activity (Figure 9A and 9B, right panels). However, upregulation of mitochondrial-associated pathways occurred on day 5 after irradiation, indicating that CD8 T cells may be more dependent on mitochondrial activity for persistence and recovery. These findings suggest that T cells rely on mitochondrial metabolism such as oxidative phosphorylation to promote survival and proliferation following TBI. GSEA analyses of day 21 T cells further showed that irradiated T cells upregulate mTORC1 signaling pathway (Figure 9C), which is linked to overall increase

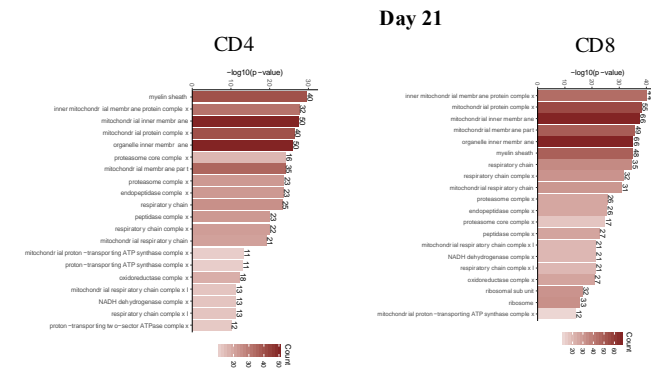
in metabolic activity. Moreover, both oxidative phosphorylation and glycolysis pathways were upregulated in day 21 T cells compared to control T cells. To confirm the metabolic state of day 21 T cells, freshly isolated day 21 or control T cells were subjected to Mito Stress Test to measure mitochondrial respiration (Figure 9D). Mito Stress Test, which examines mitochondrial function, revealed higher rate of oxygen consumption

rate (OCR) in radioresistant T cells. Further analysis showed that radioresistant T cells undergo enhanced basal respiration and maximal respiration.

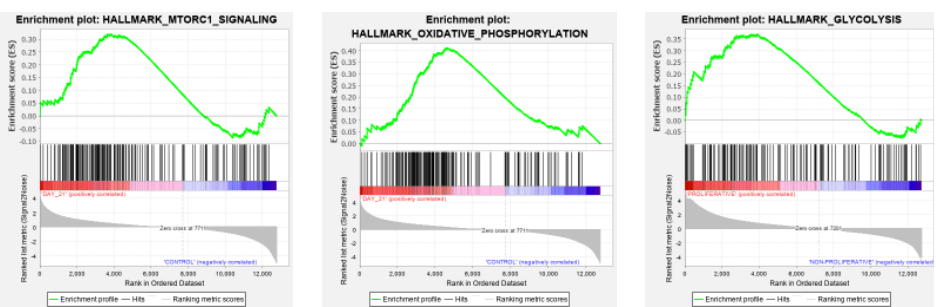
A



B



C



D

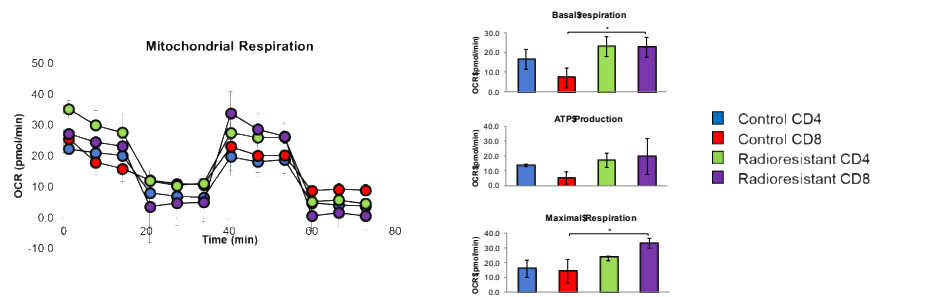


Figure 9. CD4 T cells upregulate lymphocyte proliferation and mitochondrial metabolic pathways during recovery after TBI.

(A) Naïve T cells (T_N) from 5 days after transplantation were analyzed for enriched pathways compared to control T cells. Pathways enriched in recipient-derived CD4 and CD8 T_N are displayed in the left and right panels, respectively. **(B)** Naïve T cells (T_N) from 21 days after transplantation were analyzed for enriched pathways compared to control T cells. Pathways enriched in recipient-derived CD4 and CD8 T_N are displayed in the left and right panels, respectively. **(C)** GSEA analysis of recipient-derived T cells shows upregulation of mTORC1 signaling pathway, oxidative phosphorylation, and glycolysis. **(D)** Control splenic T cells (CD45.2⁺) or recipient-derived irradiated T cells (CD45.1⁺) following transplantation were sorted by FACS, followed by Mito Stress Test to determine basal respiration, ATP production, and maximal respiration with an XF24 extracellular flux analyzer. Oxygen consumption (OCR) was measured following injection of oligomycin, FCCP, rotenone and anytimycin A.

The above findings indicate that radioresistant T cells increase the utilization of oxidative phosphorylation during the recovery phase. However, the metabolic alteration can also promote oxidative stress, potentially limiting the functional state and reconstitution dynamics. We next examined the expression of various oxidative stress markers, including Hsp90aa1, Prdx1, Prdx2, and Txn1 in control, day 5, and day 21 T cells (Figure 10A, left panel) and across previously annotated Seurat clusters (Figure 10A, right panel). As T cells gradually increases the utilization of mitochondrial respiration (Figure 9), the expression of oxidative stress markers steadily increases along pseudotime, which is further emphasized in Figure 10B, which shows the distribution of cells expressing low, intermediate, and high levels of stress markers across various groups. In day 5 and day 21 T cells, the majority of cells demonstrate higher level of

expression compared to control T cells. This was further recapitulated in the expression of different T cell populations (Figure 10A, right panel). As expected, later during the recovery process, clusters 2 through 6, which are annotated as memory T cells, showed greater oxidative stress compared to TN (clusters 0 and 1).

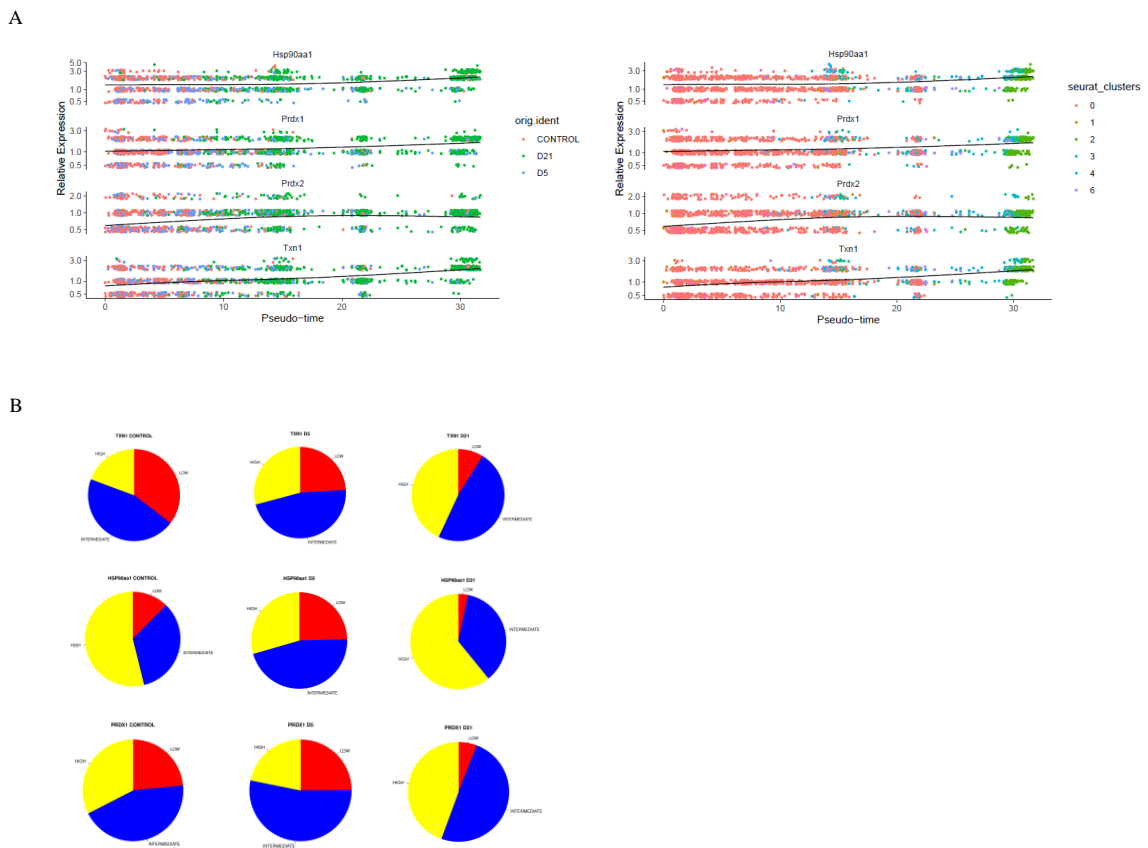


Figure 10. T cells upregulate oxidative stress markers during recovery following irradiation.

CD4 T cells from control, day 5, and day 21 were analyzed for the expression of oxidative stress markers. (A) Expression of Hsp90aa1, Prdx1, Prdx2, and Txn1 in control, day 5, and day 21 T cells (left panel), as well as among various seurat clusters annotated in Figure 1 (right panel) along pseudotime. (B) Pie chart representation of oxidative stress marker expression at low, intermediate, and high levels in control, day 5 and day 21 T cells.

3.1.9. During recovery, subsets of radioresistant T cells acquire increased proliferation capacity in response to different sources of stimuli in vitro

To characterize the phenotype and proliferative capacity of T cell subsets following irradiation, control or recipient-derived radioresistant T cells 21 days after transplantation were sorted based on TN (CD44⁺CD62L⁺), TCM (CD44⁺CD62L⁺), and TEM (CD44⁺CD62L⁻) phenotypes for subsequent assays. Each subset was then subjected to in vitro homeostatic stimulation in the presence of IL-7 and IL-15 to assess the proliferative capacity after labelling with carboxyfluorescein succinimidyl ester (CFSE). Five days following stimulation, both radioresistant CD4 and CD8 TN and TEM showed enhanced proliferation compared to control T cells. Radioresistant CD4 TCM showed moderately increased proliferation while CD8 TN showed decreased proliferation compared to control T cells (Figure 11A). In addition to homeostatic proliferation, surviving T cells can potentially mediate protection against opportunistic infections following radiation exposure. Therefore, it is critical to assess their capacity to respond to TCR stimulation. To evaluate the proliferative response of radioresistant T cells in the presence of TCR stimuli, sorted T cells were incubated with anti-CD3 and anti-CD28 antibodies. Although radioresistant memory T cells demonstrated comparable proliferation to control T cells, both CD4 and CD8 TN showed markedly increased ability to proliferate relative to control group (Figure 11B).

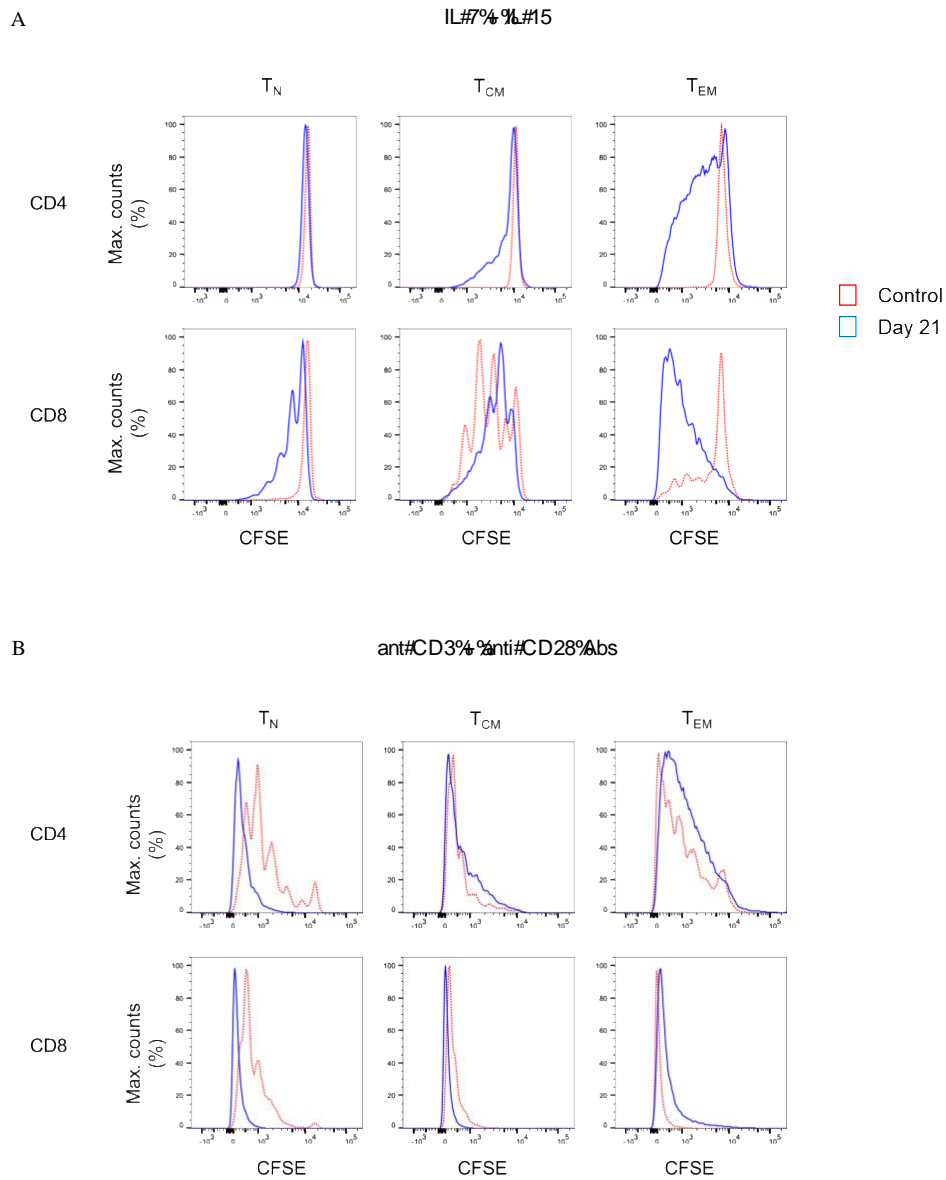


Figure 11. Radioresistant T cell subsets demonstrate increased proliferation in response to in vitro stimulation.

(A) Radioresistant naïve and effector memory T cells undergo enhanced homeostatic proliferation in vitro. Sorted T cells were labelled with CFSE and stimulated in vitro in the presence of IL-7 and IL-15 for 5 days. **(B)** Radioresistant naïve T cells demonstrate enhanced proliferation capacity in response to TCR stimulation. Sorted T cells were labelled with CFSE and stimulated in vitro in the presence of anti-CD3 and anti-CD28 antibodies for 5 days.

3.2. Manipulating donor T cell recovery following bone marrow transplantation

Compared to radioresistant T cell recovery after a single dose of TBI exposure, T cell recovery in the bone marrow transplant setting involves both donor and recipient T cells. Donor T cells consist of both alloreactive T cells, which mediate tissue damage upon recognition of recipient alloantigens, and non-alloreactive T cells. While recovery of alloreactive T cells mediate GVHD, an undesirable outcome, non-alloreactive T cells can prevent tumor development and provide protection against infections during the lymphopenic window. Therefore, it is critical to prevent the donor alloreactive T cell recovery while preserving non-alloreactive T cells. Studies have shown that donor T cell recovery following transplantation is primarily driven by activation and expansion in response to recipient alloantigens, a thymic-independent process associated with increased demand for aerobic glycolysis. In the current study, we propose to exploit the metabolic requirements to reduce alloreactive T cell recovery and preserve donor T cells with irrelevant specificities.

3.2.1. Donor T cell pathogenicity is fueled by glycolysis upon recognition of alloantigens, a thymic-independent process during donor T cell recovery

To manipulate the metabolic state of donor T cells, which are highly dependent on aerobic glycolysis, we utilized donor T cells derived from mice harboring Glut1 deletion, which diminishes glycolysis utilization by limiting glucose transportation into the cytosol. Previously, we demonstrated the role of Glut1 in T cell-mediated acute GVHD using the C57BL/6 → BALB/c major histocompatibility complex (MHC)-mismatched bone marrow transplant (BMT) model [27]. To confirm that the observation is not strain-specific, C3H/HeJ recipients were also utilized for the transfer of Glut1^{T-KO} or wild-type (WT) C57BL/6 T cells to induce acute GVHD. All WT recipients died from GVHD within 20 days while eight out of ten Glut1^{T-KO} T cell recipients survived long-term (Figure 12A). In addition, Glut1^{T-KO} T cell recipients showed comparable body weight and clinical scores with TCDBM recipients (Figures 12B-C). Therefore, consistent with the previous study, these findings further support a key role for Glut1 to promote donor cell pathogenicity.

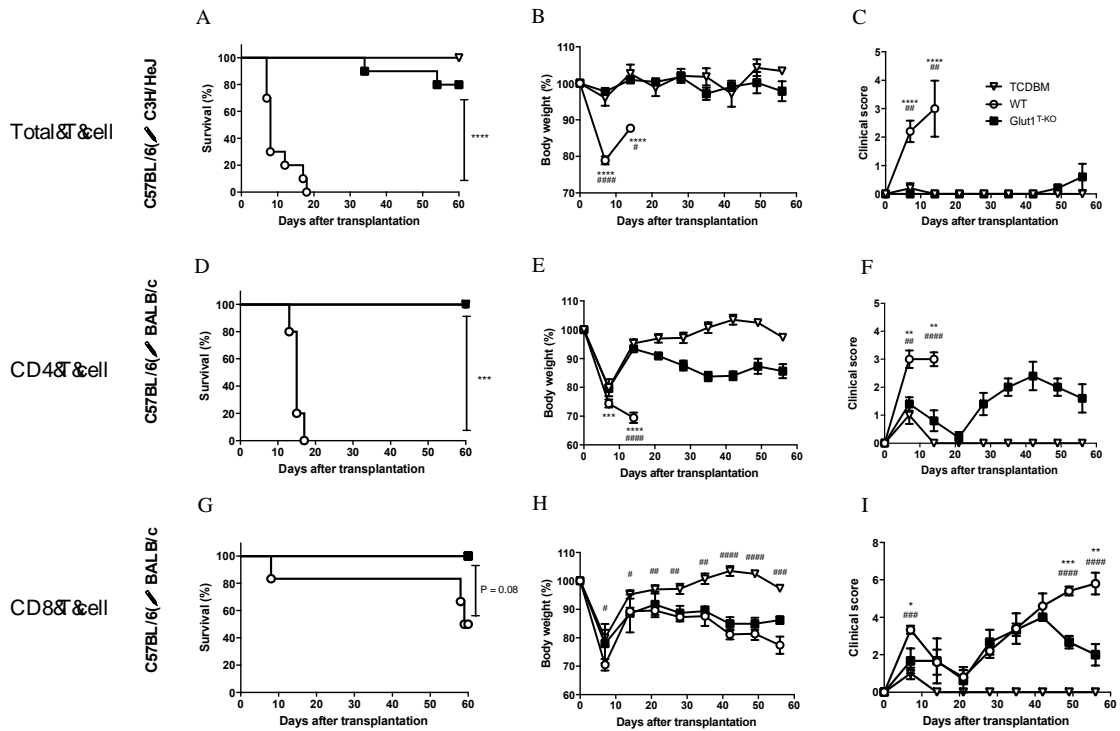


Figure 12. Glut1 is required for donor T cells to induce acute GVHD.

Acute GVHD was induced by transplantation of C57BL/6-derived 1×10^7 TCDBM or along with 1×10^6 WT or Glut1^{T-KO} total T cells into lethally irradiated (9.5 Gy) C3H/HeJ recipients (A-C). Lethally irradiated (8.5 Gy) BALB/c recipients were transplanted with 1×10^6 WT or Glut1^{T-KO} CD4⁺ (D-F) or CD8⁺ T cells (G-I), along with 1×10^7 TCDBM from C57BL/6 donors. Recipients were monitored for survival (A, D, and G), body weight (B, E, and H), clinical score (C, F, and I) up to 56 days after transplantation. Data were representative of three experiments. **** $P < 0.0001$, *** $P < 0.001$, log-rank test ($n = 10$ per group, A; $n = 5$ per group, D and G); data are shown as mean \pm SEM (B-C, E-F, H-I), * $P < 0.05$, ** $P < 0.01$, *** $P < 0.001$, **** $P < 0.0001$ (Glut1^{T-KO} vs. WT); # $P < 0.05$, ## $P < 0.01$, ### $P < 0.001$, #### $P < 0.0001$ (TCDBM vs. WT), 2-tailed Student t test.

We further examined whether Glut1 is required for CD4⁺ and CD8⁺ T cells to induce acute GVHD, respectively. In contrast to WT recipients, both CD4⁺ Glut1^{T-KO} and CD8⁺ Glut1^{T-KO} T cell recipients survived long-term (Figures 12D and 12G). However, the

kinetics of GVHD development and target organs affected differed. Both body weights and clinical scores in CD4⁺ Glut1^{T-KO} T cell recipients significantly improved early following BMT (Figures 12D-12F). In contrast, the kinetics of GVHD development in CD8⁺ T cell recipients is relatively delayed, leading to improvement in Glut1^{T-KO} T cell recipients later during disease progression compared to the control group (Figures 12G-12I). Target organ damage was also assessed by histology (data not shown). Both small intestine and colon exhibited reduced damage in CD4⁺ Glut1^{T-KO} compared to WT recipients. In contrast, skin damage was significantly reduced in CD8⁺ Glut1^{T-KO} recipients. Overall, transfer of either CD4⁺ or CD8⁺ Glut1^{T-KO} T cells significantly improved long-term survival and ameliorated acute GVHD.

3.2.2. Glut1 is required for the metabolic reprogramming and expansion of donor alloreactive T cells

T cells rapidly undergo metabolic reprogramming following activation, prioritizing glucose metabolism to promote growth and proliferation [72]. We first assessed whether alloreactive Glut1^{T-KO} T cells were able to initiate metabolic reprogramming. Glut1^{T-KO} T cells had significantly decreased glucose uptake following alloantigen stimulation (Figure 13A). Alloreactive Glut1^{T-KO} T cells were unable to utilize glycolysis, indicated by ECAR compared to WT T cells during glycolysis stress test (Figure 13B). Metabolic assays further confirmed deficient glycolysis, glycolytic capacity,

and glycolytic reserve of alloreactive $\text{Glut1}^{\text{T-KO}}$ T cells compared to control (data not shown). These results suggest that $\text{Glut1}^{\text{T-KO}}$ T cells display overall significant defects in glucose uptake and glycolytic metabolism upon alloantigen challenge.

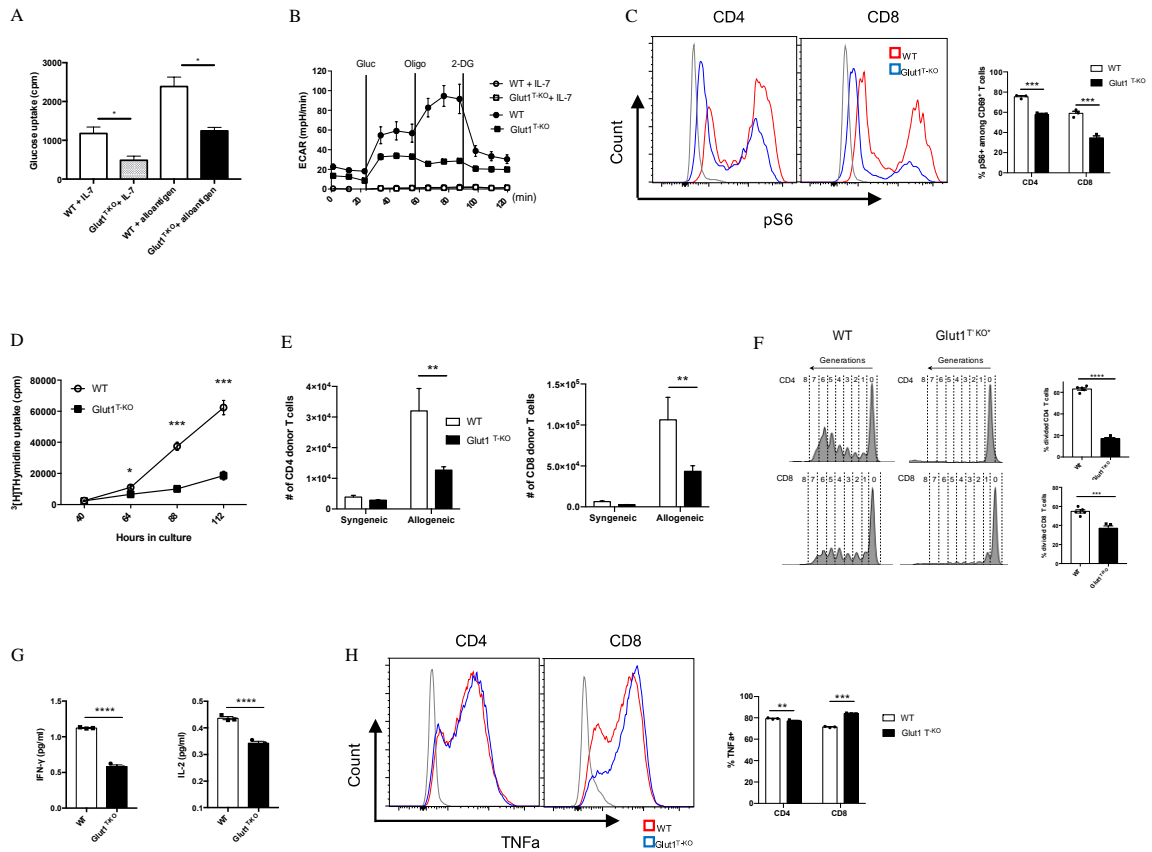


Figure 13. Glut1 mediates the expansion of alloreactive donor T cells.

WT or $\text{Glut1}^{\text{T-KO}}$ T cells were stimulated with BALB/c dendritic cells. After 5 days in culture, glucose uptake was measured (A). ECAR was assessed with the addition of glucose (gluc), oligomycin (oligo), and 2-DG (B). WT or $\text{Glut1}^{\text{T-KO}}$ T cells were stimulated for 16 hours using BALB/c DCs and analyzed by flow cytometry for phospho-S6 levels in CD69^+ T cells (C). Expansion in vitro was measured by ^3H -TdR incorporation assay at indicated time points after culture (D). Expansion in vivo was measured in T cells isolated from the spleen seven days after transplantation with 1×10^7 TCDBM from B6.SJL donors and 1×10^6 WT or $\text{Glut1}^{\text{T-KO}}$ T cells on the C57BL/6 background into BALB/c recipients (E). T cell proliferation following isolation from the spleen was analyzed (left panel) and measured by frequency (right panel) 58 hours following

transfer of CellTrace Violet (CTV)-labelled T cells along with B6.SJL TCDBM into BALB/c recipients (F). IFN γ and IL-2 production were assayed by ELISA using supernatants from T cell cultures (G). (H) WT or Glut1^{T-KO} T cells were stimulated with purified BALB/c DCs for 72 hours, with the addition of PMA (20ng/ml), ionomycin (1 μ M), and monensin 4 hours prior to intracellular staining for TNF α . Data are representative of two (F, n = 3) or three experiments (n = 3, A-D, and G; n = 5, E and F) and are shown as mean \pm SEM (B-F). *P < 0.05, **P < 0.01, ***P < 0.001, ****P < 0.0001 (Glut1^{T-KO} vs. WT), 2-tailed Student t test.

Mammalian target of rapamycin complex 1 (mTORC1) regulates glucose metabolism through HIF1 α and c-Myc to support biosynthesis and proliferation [72; 73]. Although rapamycin has been shown to dampen GVHD by inhibiting glycolysis [29], it is unclear whether glucose availability modulates mTORC1 activity to regulate alloreactive T cell response. We hypothesize that mTORC1, a nutrient sensor [73], responds to glucose availability to modulate donor cell pathogenicity. Alloreactive T cells positive for CD69 expression were assessed for the phosphorylation status of the small ribosomal subunit S6 (pS6), a downstream target for mTORC1 signaling. Phosphorylation of S6 (Ser235/236) in resting Glut1^{T-KO} T cells was significantly lower than WT T cells (Figure 13C). Following stimulation, Glut1^{T-KO} T cells demonstrated profoundly decreased phospho-S6 levels (Figure 13C). Glucose availability therefore leads to sustained mTORC1 activation in alloreactive T cells.

To determine the requirement for T cell expansion, tritium thymidine uptake was assessed in MLR. Glut1^{T-KO} T cells displayed drastically impaired thymidine uptake as

early as 64 hours following stimulation (Figure 13D). To test whether glycolysis is required for in vivo expansion upon alloantigen encounter, T cells were transferred into irradiated allogeneic or syngeneic recipients. While expansion in syngeneic recipients did not differ, Glut1^{T-KO} T cells exhibited significantly impaired capacity to undergo expansion compared to WT T cells in allogeneic recipients (Figure 13E). Furthermore, Glut1^{T-KO} T cells failed to undergo robust proliferation, indicated by the lack of subsequent generations following divisions (Figure 13F). Similar defects were observed in CD69⁺ alloreactive Glut1^{T-KO} T cells (data not shown). Glycolysis has also been linked to cytokine production through the sequestration of cytokine transcripts [22]. Expression of inflammatory cytokines IFN γ and IL-2 was measured in alloreactive T cells. Glut1^{T-KO} T cells displayed significantly reduced capacity to produce both cytokines compared to WT T cells (Figure 13G). TNF α expression was also assessed in WT and Glut1^{T-KO} T cells following 72 hours of stimulation with purified BALB/c DCs. While Glut1^{T-KO} CD4 T cells exhibited slightly reduced expression compared to WT group, Glut1^{T-KO} CD8 T cells demonstrated increased TNF α expression relative to WT T cells (Figure 13H). In summary, we demonstrated that glycolysis is indispensable for alloreactive T cell expansion and effector cytokine production.

3.2.3. Glut1 is required for the survival of alloreactive donor T cells

In addition to proliferation, alteration of survival signals is a potential modulator of pathogenicity. Glut1 expression has been shown to support resting T cell survival through the stabilization of pro-survival factors [74]. To determine whether the apoptotic pathway is involved in regulating viability in response to glucose metabolism, we assessed the expression of various candidate proteins 16 hours following activation by anti-CD3 and anti-CD28 antibodies. Proteins linked to the apoptotic pathway, including Mdm2, Puma, and Noxa, were drastically increased in activated Glut1^{T-KO} T cells relative to WT control (Figure 14A). By contrast, the anti-apoptotic protein Mcl-1 was significantly upregulated compared to WT T cells (Figure 14A).

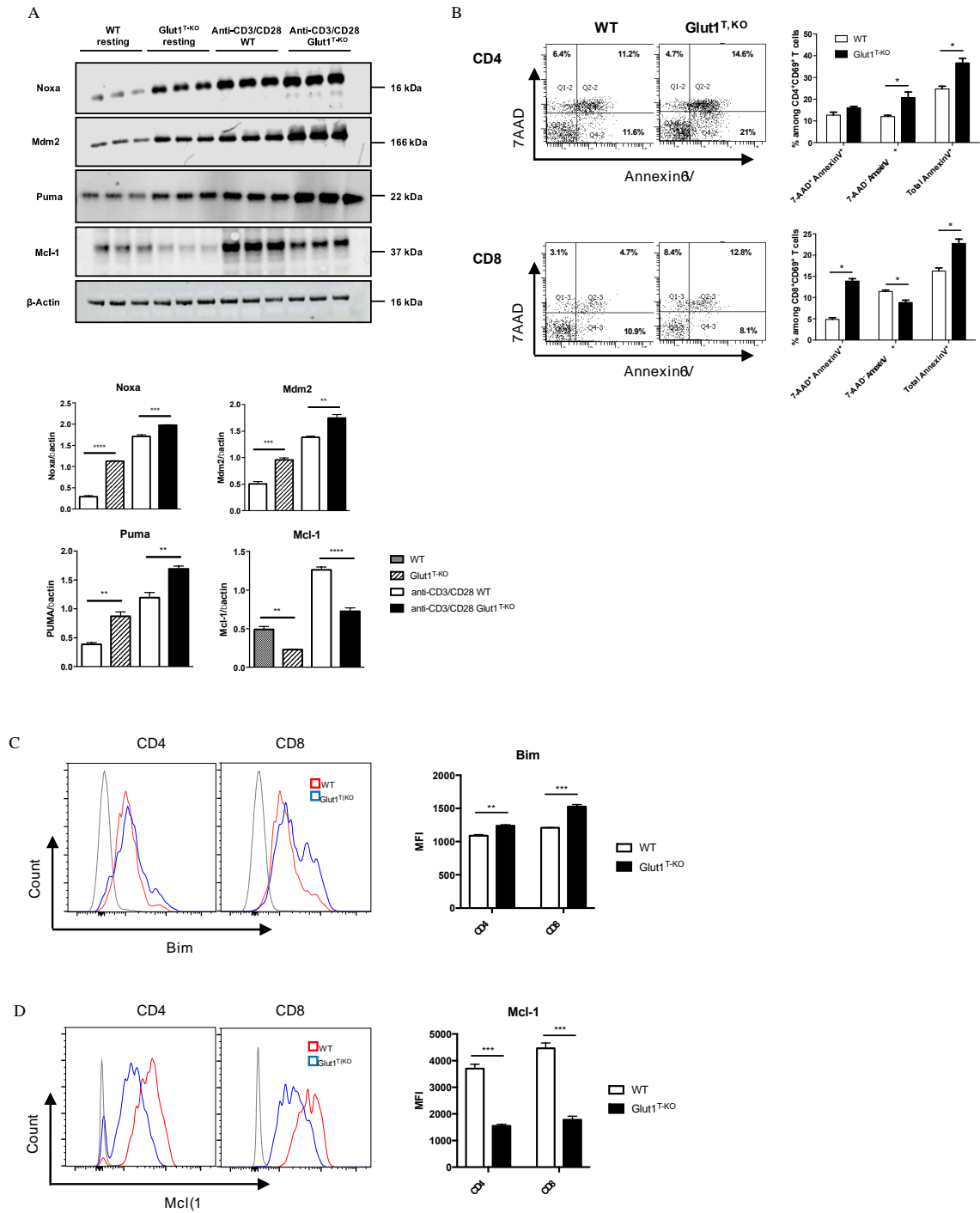


Figure 14. *Glut1* modulates alloreactive T cell survival.

(A) Freshly isolated WT or Glut1^{T-KO} T cells or those stimulated with anti-CD3 (1ug/ml) and anti-CD28 (0.3ug/ml) antibodies for 16 hours were assessed for the expression of Mdm2, Puma, Noxa, and Mcl-1 using Western blotting (upper panel). Results were quantified for fresh T cells and antibody-stimulated T cells (lower panel) (n = 3, one-way ANOVA with a Tukey's multiple comparisons test). (B) WT or Glut1^{T-KO} T cells were stimulated for 16 hours by irradiated (20 Gy) BALB/c DCs and analyzed by flow cytometry for Annexin V and 7AAD. T cells were gated on CD69⁺ CD4⁺ or CD8⁺ T cells. Bim (C) and Mcl-1 (D) expression were evaluated. Data are representative of three experiments (n = 3) and are shown as mean ± SEM. *P < 0.05, **P < 0.01, *P < 0.001, 2-tailed Student t test.**

We further assessed whether glycolysis is also involved in regulating cell survival in alloreactive T cells. Viability analysis demonstrated significantly less live Glut1^{T-KO} T cells compared to WT T cells following alloantigen stimulation in vitro (data not shown). Apoptosis was subsequently assessed using Annexin V and 7AAD staining. While both CD4⁺ and CD8⁺ alloreactive Glut1^{T-KO} T cells underwent increased apoptosis compared to WT T cells, the apoptosis kinetics differed. CD8⁺ CD69⁺ Glut1^{T-KO} T cells appeared to undergo apoptosis earlier than CD4⁺ CD69⁺ T cells inferred from percentages of Annexin V⁺ cells (Figure 14B).

Regulation of pro-apoptotic and anti-apoptotic protein expression can alter the survival outcome in response to cellular stress. Impaired glucose metabolism can lead to apoptosis in response to endoplasmic reticulum (ER) stress mediated by Bim, a pro-apoptotic Bcl-2-family protein [75]. Bim expression is higher in Glut1^{T-KO} T cells compared to WT T cells in both freshly isolated state (data not shown) and activated

state (Figure 14C). Though the demand for glycolysis is lower in resting T cells compared to activated T cells, a minimal rate of glycolysis is still required to meet basal energy demands [26], potentially contributing to the difference in baseline Bim expression. Regulation of anti-apoptotic Bcl-2 proteins such as Mcl-1 can also regulate survival [74; 76] Alloantigen-stimulated $\text{Glut1}^{\text{T-KO}}$ T cells failed to provide adequate survival signal through Mcl-1 compared to WT T cells (Figure 14D). Differences in Mcl-1 expression were readily detected in both anti-CD3 and anti-CD28 antibody activated T cells and alloreactive T cells (Figures 14A and 14D). Baseline differences in Mcl-1 expression between WT and $\text{Glut1}^{\text{T-KO}}$ T cells were detectable using Western blots (Figure 14A) but not flow cytometry (data not shown), which can be attributed to variation in detection sensitivity between methods of detection. In addition, the balance of Mcl-1 and Noxa, a BH3-only pro-apoptotic factor and a binding partner for Mcl-1, can be regulated by glucose availability [77]. Since Noxa expression was reduced in the presence of both anti-CD3 + anti-CD28 antibodies as well as alloantigens (Figures 14A), the skewed Noxa/Mcl-1 ratio may render $\text{Glut1}^{\text{T-KO}}$ T cells more prone to apoptosis.

3.2.4. Glut1 deficiency in donor T cells ameliorates GVHD while preserving GVL effects

It is crucial for GVHD treatments to selectively inhibit alloreactive T cells without compromising the GVL effect. To test the effect of glycolysis inhibition on GVL

preservation, lethally irradiated BALB/c recipients were engrafted with WT or Glut1^{T-KO} T cells, TCDBM, accompanied by challenge with BCL1 cells, a BALB/c-derived leukemia/lymphoma cell line.

TCDBM + BCL1 group succumbed to tumor challenge within 31 days following transplantation (Figures 15A and 15B), indicated by BLI (Figure 15C). Histology analysis further confirmed metastatic invasion of the liver parenchyma, indicated by enlarged and hyperchromatic nuclei of neoplastic cells (Figure 15D). While Glut1 deficiency did not completely protect recipients from GVHD as evidenced by gradual weight loss (Figure 15B), analyses of target organ histology indicated lower pathological scores in the skin and large intestine (data not shown). Furthermore, transfer of 1×10^6 Glut1^{T-KO} T cells significantly improved long term survival in majority of recipients compared to both TCDBM + BCL1 and WT T cell recipients, which all died from tumor or GVHD (Figures 15A to 15E). BLI analysis and necropsy revealed that Glut1^{T-KO} recipients remained tumor-free, demonstrating the preservation of GVL effects (Figure 15C-15E). In contrast, all WT T cell recipients succumbed to GVHD within 100 days (Figure 15E). To confirm that the GVL effect of Glut1^{T-KO} T cells is not restricted to a specific tumor model, a second lymphoma cell line of BALB/c origin (A20) was used to evaluate protection against tumor development. Transfer of Glut1^{T-KO} T cells significantly improved survival compared to TCDBM + A20 and WT recipients (Figure 15F). While body weights of Glut1^{T-KO} recipients were lower than that of TCDBM control groups due

to GVHD, they were significantly higher than WT recipients, demonstrating ameliorated GVHD development (Figure 15G). BLI analyses and necropsy showed that tumor growth was absent in all Glut1^{T-KO} recipients (Figure 15H and 15I), recapitulating protection against tumor using a different tumor model. A low dose of Glut1^{T-KO} T cells was also tested using the BCL1 tumor model and provided limited protection against tumor development (data not shown), suggesting a role for glycolysis in GVL. However, this limitation can be overcome by increased dose of Glut1^{T-KO} T cells, indicating that glycolysis is not absolutely necessary for donor T cells to exert anti-tumor effects. Collectively, these data indicate that transfer of Glut1^{T-KO} T cells at sufficient concentrations is capable of preventing tumor growth and mortalities caused by GVHD, supporting the hypothesis that glycolysis targeting selectively inhibits alloreactive T cells.

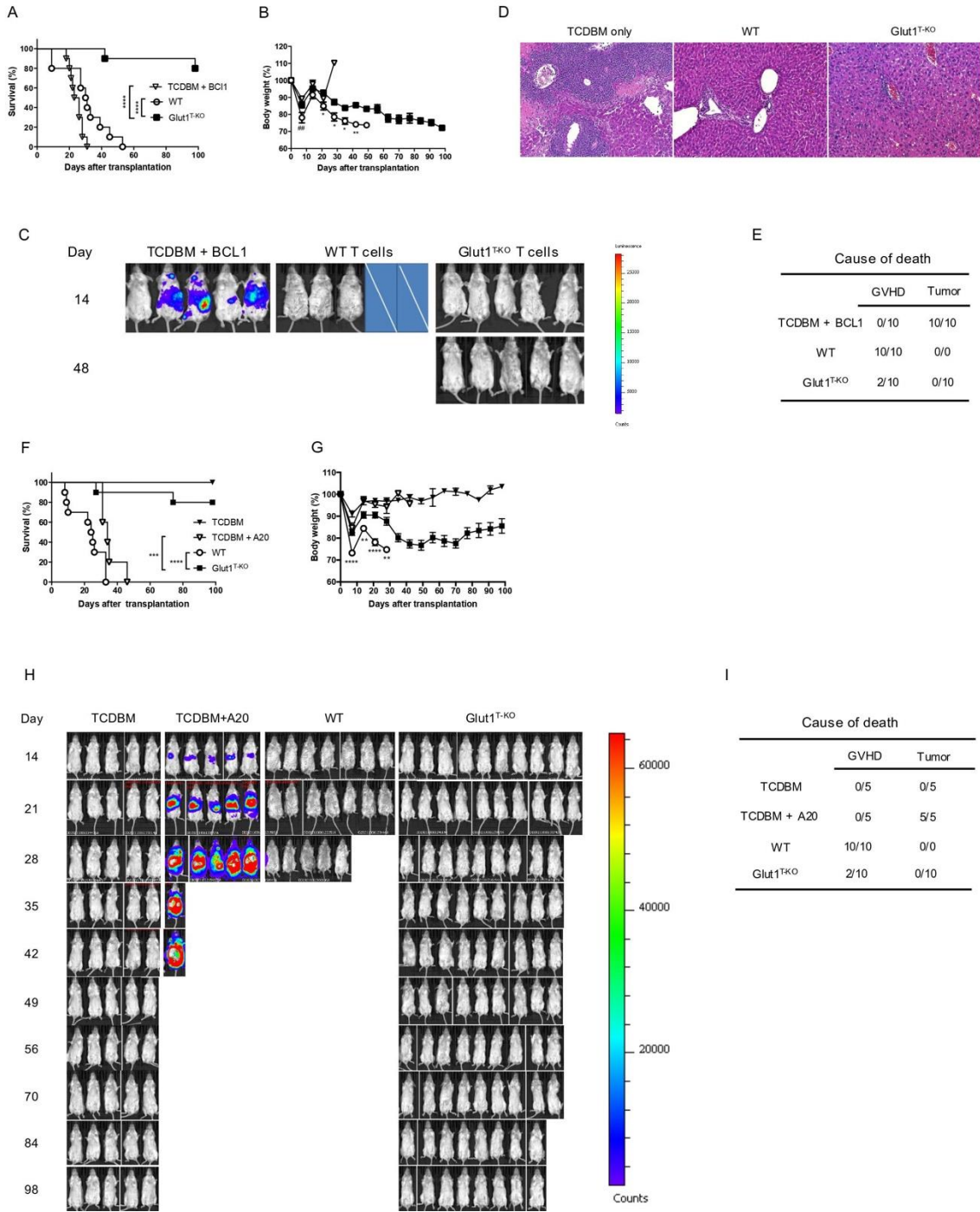


Figure 15. Transfer of donor T cells with Glut1 deletion inhibits GVHD development and spares GVL activity.

Lethally irradiated (8.5 Gy) BALB/c recipients were transplanted with 1×10^6 WT or Glut1^{T-KO} T cells, along with 1×10^7 TCDBM and 5×10^5 BCL1 cells. Recipients were monitored for survival (A) and body weight (B) up to 100 days after transplantation. Development of leukemia/lymphoma (C) was monitored by BLI. Cross symbols indicate death prior to BLI. H&E histology (10x & 40x) of liver (D) from recipients was assessed (time at sample collection: TCDBM + BCL1, day 21; WT, day 27; Glut1^{T-KO}, day 105). Cause of death due to GVHD or tumor development was summarized (E). (F) Lethally irradiated (8.5 Gy) BALB/c recipients were transplanted with 1×10^6 WT or Glut1^{T-KO} T cells, along with 1×10^7 TCDBM and 1×10^5 A20 cells. Recipients were monitored for survival (F) and body weight (G) up to 100 days after transplantation. Development of leukemia/lymphoma (H) was monitored by BLI. Cause of death due to GVHD or tumor development was summarized (I). **P < 0.01, **P < 0.001, log-rank test (A); *P < 0.05, **P < 0.01 (Glut1^{T-KO} vs. WT); #P < 0.01 (TCDBM vs. WT), 2-tailed Student t test (B). Data are representative of three experiments (n = 10 per group, 1×10^6 T cell recipients).

3.2.5. Inhibition of glycolysis by 2-DG selectively targets murine and human alloreactive T cells in vitro and preserves T cells with irrelevant specificities

A clinically-relevant approach for glycolysis inhibition to ameliorate GVHD has been previously explored, though systemic treatments [29] can induce toxicity in the brain and skeletal muscles [78; 79; 80]. To improve treatment specificity, donor T cells can be treated ex vivo in the presence of recipient alloantigens. A panel of small molecule inhibitors were evaluated for inhibition of alloreactive T cell proliferation. Both glucose analogs, fludeoxyglucose (FDG) and 2-DG, remarkably suppressed donor T cell response following stimulation (Figure 5A). 2-DG also showed potent inhibitory effect

on 4C CD4⁺ T cells bearing transgenic T cell receptors (TCR-tg) specific for BALB/c alloantigens (data not shown). The Glut1 inhibitor, WZB117, also inhibited alloresponse (Figure 16A). As 2-DG has been shown to dampen inflammatory T cell response and given its wide accessibility in clinical trials, 2-DG was selected for subsequent assays [81; 82; 83; 84].

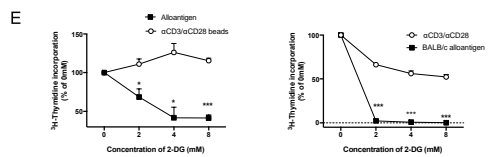
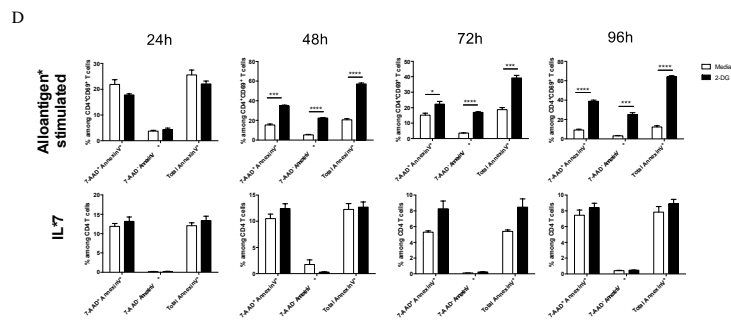
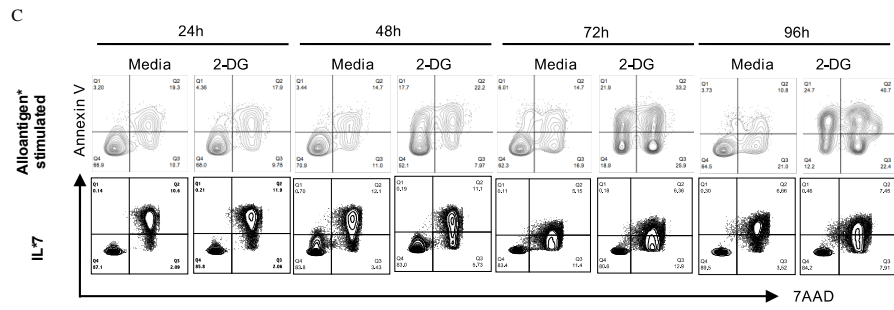
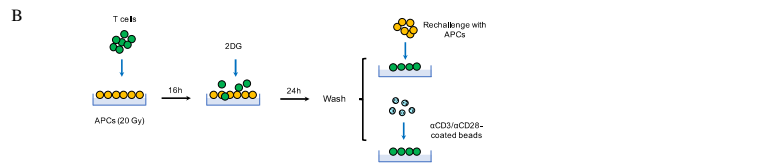
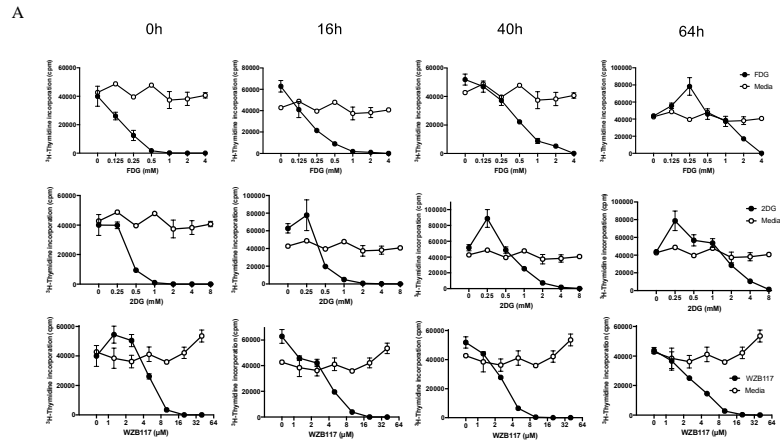


Figure 16. 2-DG treatment selectively suppresses alloreactive T cells.

WT or $\text{Glut1}^{\text{T-KO}}$ T cells were stimulated for 0 hour, 16 hours, 40 hours, or 64 hours using irradiated (20 Gy) BALB/c splenocytes, followed by the addition of various concentrations of small molecule inhibitors and cultured for a total of 112 hours for the assessment of thymidine incorporation. T cell response was determined following the addition of FDG or media only (H_2O), 2-DG or media only (H_2O), WZB117 or media only (EtOH) (A). Schematic diagram of T cells stimulated with irradiated MHC-mismatched APCs for 16 hours, followed by the addition of various concentrations of 2-DG, washed, then rechallenged with alloantigens or anti-CD3 and anti-CD28 antibodies (B). WT T cells were first stimulated with irradiated (20 Gy) BALB/c DCs for 16 hours, followed by incubation with freshly isolated irradiated DCs in the presence of media control or 8mM 2-DG for 24-96 hours; WT T cells were cultured in IL-7 (10ng/ml) for 16 hours plus 24-96 hours, and analyzed for Annexin V and 7AAD (C) and (D). T cells were gated on $\text{CD4}^+ \text{CD69}^+$ for alloantigen-stimulated samples and CD4^+ for IL-7-treated samples. (E) The proliferative response of mouse (left panel) and human T cells (right panel) cultured according to (B) was measured by $^3\text{H-TdR}$ incorporation assay. * $P < 0.05$, 2-tailed Student t test. ** $P < 0.01$, *** $P < 0.001$; data are representative of two experiments (n = 3 per group).

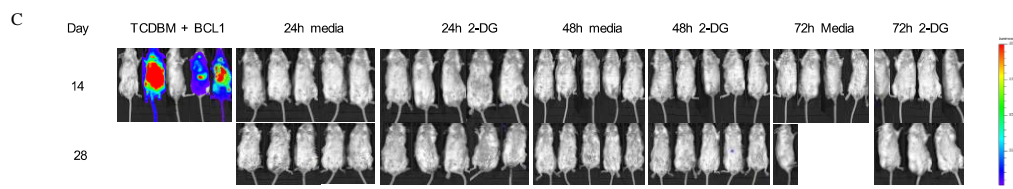
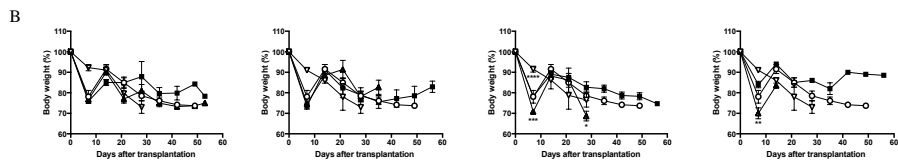
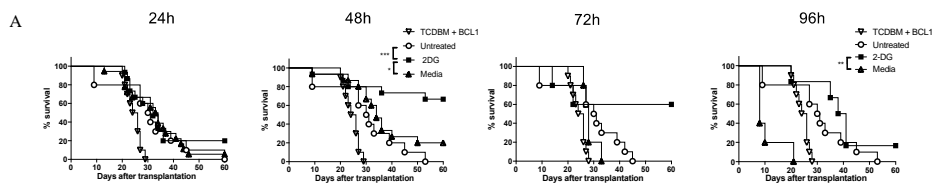
Incubation of recipient antigen-stimulated donor T cells with glycolysis inhibitors prior to BMT can spare non-alloreactive T cells, reducing toxicity to graft recipients and selectively suppressing alloresponse (Figure 16B). Incubation with 2-DG selectively triggered apoptosis in activated alloreactive T cells, indicated by a profound and consistent increase in AnnexinV⁺ populations and a corresponding decrease in the absolute number of alloreactive CD4 T cells (Figures 16C and 16D, upper panels). In contrast, 2-DG did not impact cell death outcomes in non-activated T cells treated with IL-7 (Figures 16C and 16D, lower panels). Similar findings were observed in alloantigen-stimulated versus IL-7-treated CD8 T cells. Following 2-DG incubation, secondary challenge with either alloantigens or anti-CD3- and anti-CD28-coated beads

demonstrated that only alloresponse was significantly inhibited (Figure 16E). Importantly, as inhibition occurs exclusively during the ex vivo stimulation process, suppression of alloresponse by 2-DG prevents toxicity due to non-specific systemic treatments. Similarly, to test the efficacy in human T cells, purified donor T cells were first primed with irradiated PBMCs from irrelevant allogeneic donors, incubated with 2-DG, and followed by PBMC rechallenge or anti-CD3 and anti-CD28 antibody stimulation. Alloreactive responses underwent a dose-dependent reduction compared to non-specific stimulation, indicating that the proliferative capacity of alloreactive T cells is highly dependent on the ability of T cells to perform glycolysis (Figure 16E). Therefore, the optimal concentration of 2-DG at 8mM was utilized for subsequent in vivo assays.

3.2.6. 2-DG-mediated inhibition of glycolysis ex vivo significantly reduces donor T cell-mediated GVHD while sparing T cells mediating GVL, demonstrating functional recovery of donor anti-tumor T cells

Given that Glut1^{T-KO} T cells preserved GVL effect and the promising in vitro data, we next tested the therapeutic potential of T cell-specific glycolysis inhibition using a clinically relevant model. Alloantigen-activated T cells were treated with 2-DG as shown in Figure 5B for 24-96 hours, followed by transfer into recipients along with TCDBM and BCL1 cells. Ex vivo inhibition for 24 hours demonstrated limited potency in GVHD

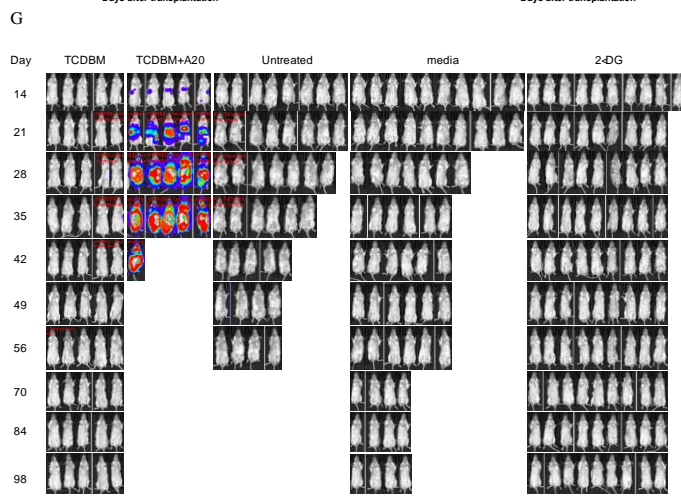
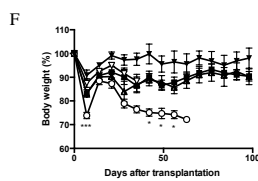
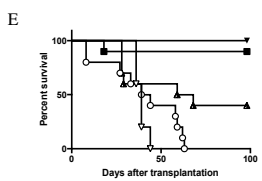
prevention, while longer incubation periods (48-96 hours) with 2-DG significantly limited GVHD development without impairing GVL activity as demonstrated by survival, body weight, BLI tumor screening, and clinical scores (Figures 17A-17D). Body weights of 72-hour-treated T cell recipients were significantly higher than those receiving media control T cells later following transplantation (Figure 6B). Interestingly, recipients for donor T cells treated with 2-DG for 48 hours gained an optimal survival advantage compared to those receiving uncultured and untreated T cells and those incubated with media control, resulting in the least amount of deaths by proportions caused by GVHD (Figure 17A and 17D). Protection against both GVHD and tumor development conferred by 48-hour-treated T cells was further assessed in a second tumor model using the A20 cell line. Ex vivo 2-DG treatment significantly improved survival compared to TCDBM + A20, WT T cell, and media control recipients (Figure 17E). Furthermore, transfer of 2-DG-treated T cells improved body weight compared to WT T cell recipients, as well as exhibiting reduced GVHD severity relative to both WT and media control recipients (Figures 17F). Together with BLI analyses and necropsy results (Figures 6G and 6H), we demonstrated that GVHD and tumor development can be attenuated using ex vivo 2-DG treatment. The results from these experiments provide further evidence that targeting glycolysis in alloantigen-specific T cells ex vivo preserves T cell response against irrelevant antigens, potentially providing protection against malignancies and opportunistic pathogens.



D

Cause of death

	24h		48h		72h		96h		Untreated	
	GVHD	Tumor	GVHD	Tumor	GVHD	Tumor	GVHD	Tumor	GVHD	Tumor
TCDBM	0/10	10/10	0/10	10/10	0/10	10/10	0/10	10/10		
Untreated									10/10	0/10
Media	14/15	0/15	12/15	0/15	5/5	0/5	5/5	0/5		
2-DG	12/15	0/15	5/15	0/15	2/5	0/5	4/5	0/5		



H

Cause of death

Treatment	Cause of death	
	GVHD	Tumor
TCDBM	0/5	0/5
TCDBM + A20	0/5	5/5
Untreated	10/10	0/10
Media	6/10	0/10
2-DG	1/10	0/10

Figure 17. 2-DG treatment ameliorates GVHD and leads to the functional recovery of donor T cells mediating GVL.

1 x 10⁶ T cells from C57BL/6 donor spleens were first stimulated for 16 hours with irradiated BALB/c splenocytes, followed by addition of 8mM 2-DG or media control for indicated periods. T cells treated ex vivo or untreated control T cells at the same dose were transplanted into BALB/c recipients, along with 1 x 10⁷ TCDBM from C57BL/6 donors and 5 x 10⁵ BCL1 cells. Recipients were monitored for survival (A), body weight (B), and tumor growth in TCDBM and TCDBM + BCL1, 24-hour, 48-hour and 72-hour media control or 2-DG-treated groups. Tumor development was detected using BLI imaging on day 14 and day 28 following transplantation (C). Cause of death due to GVHD or tumor development was summarized for different groups (D). 1 x 10⁶ T cells treated as shown in (A) for 48 hours or untreated control T cells at the same dose were transplanted into BALB/c recipients, along with 1 x 10⁷ TCDBM from C57BL/6 donors and 1 x 10⁵ A20 cells. Recipients were monitored for survival (E), body weight (F), and tumor growth (G). Cause of death was summarized for various groups (H). *P < 0.05, **P < 0.01, ***P < 0.001, log-rank test; data are representative of two experiments (n = 15 per group, recipients for 24-hour and 48-hour ex vivo cultured T cells; n = 5, recipients for 72-hour and 96-hour ex vivo cultured T cells).

3.3. NT-17 is a promising therapeutic agent that integrates requirements for various T cell recovery pathways

Radiation exposure leads to profound immune suppression, including delayed systemic T cell recovery. Currently, there is no FDA-approved reagent that specifically promotes the reconstitution of T cells, which is critical in facilitating cell-mediated and humoral immunity. Prolonged T cell recovery following radiation can contribute to increased susceptibility to opportunistic infections and tumor relapse.

IL-7, a cytokine that integrates the requirement for thymic-dependent and -independent pathways, as well as metabolic demands for T cell growth and persistence,

is a promising therapeutic candidate to induce rapid T cell recovery following radiation exposure. NT-I7 is a long-acting human recombinant IL-7 that is well-tolerated in clinical trials [51]. Therefore, we sought to investigate whether NT-I7 accelerates the T cell reconstitution process following radiation exposure.

3.3.1. NT-I7 promotes peripheral blood T cell reconstitution following TBI

To assess the effect of NT-I7 on peripheral blood T cell recovery following radiation, C57BL/6 mice underwent sublethal irradiation at 5 Gy, followed by vehicle or NT-I7 treatments via subcutaneous injections. Two NT-I7 treatment regimens were performed weekly following TBI, starting at 24 hr or day 7 after radiation. CBC and flow analyses revealed that total white blood cell, lymphocyte, and CD3 T cell counts dropped 20- to 30-fold compared to baseline, reaching the nadir on day 7 (Figures 18A to 18C). Vehicle group underwent prolonged reconstitution of all cell types, taking at least 56 days to recover back to baseline. In contrast, NT-I7 induced rapid increase in all cell types examined. Specifically, accelerated recovery was observed in total CD3 cells, CD4, and CD8 T cells in NT-I7 groups (Figures 18C to 18K). Notably, NT-I7 treatment starting at 24 hr and day 7 (at the nadir) achieved similar T cell reconstitution kinetics. Further analysis revealed that NT-I7 improved recovery of various T cell subsets, including TN, TCM, and TEM (Figures 18E to 18G; 18I to 18K), rather than skewing towards a specific

subset of T cells. Interestingly, CD8 T cells appeared to be more sensitive to NT-I7-induced recovery compared to CD4 T cells, which can be contributed to changes in lineage commitment during thymic development or differential responsiveness to NT-I7 during homeostatic proliferation of mature T cells.

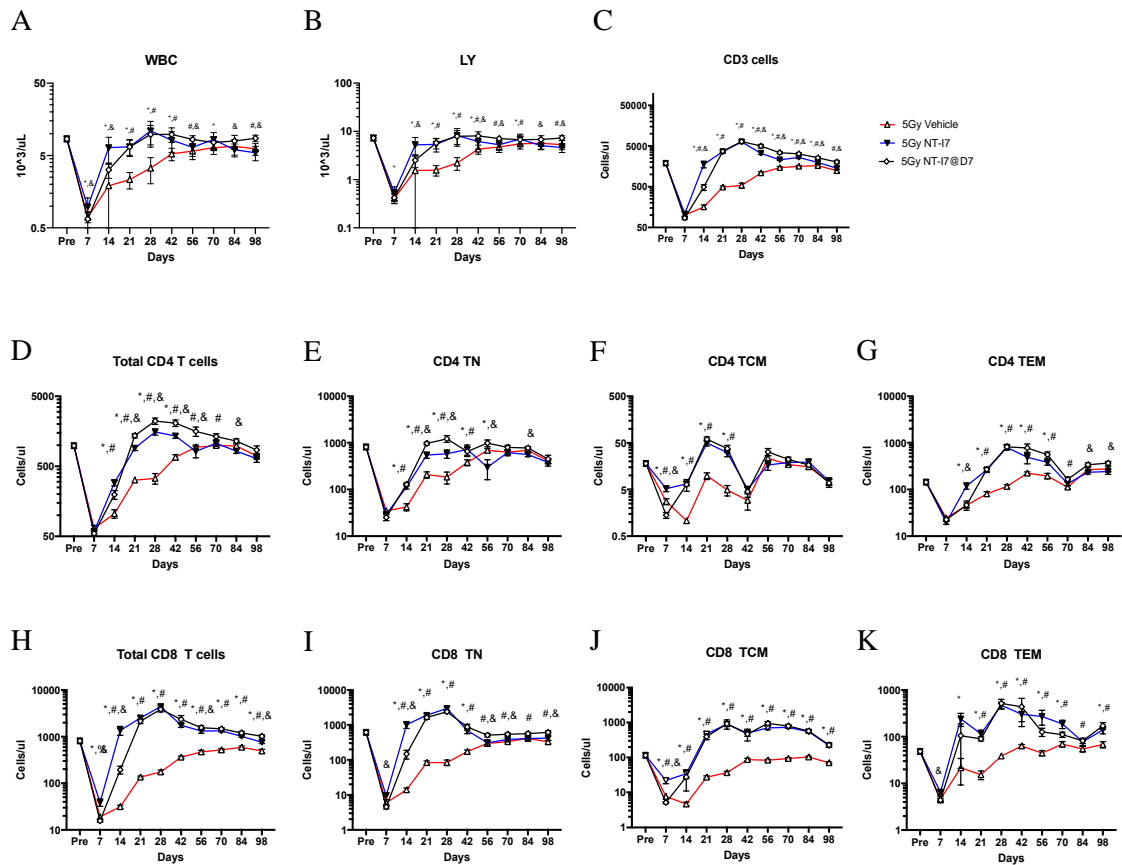


Figure 18. NT-I7 induces peripheral blood T cell recovery after total body irradiation.

C57BL/6 mice underwent 5 Gy TBI, followed by vehicle, NT-I7 injection at 10mg/kg at day 7, day 14, and day 21 or NT-I7 injection at 24 hr, day 7, day 14, and day 21. Complete blood count of WBC (A) and LY (B) were determined prior to irradiation (Pre) and until day 98 following TBI. Cell counts of total CD3 cells (C), CD4 T cells (D), CD4 TN (E), CD4 TCM (F), and CD4 TEM (G) were determined prior to irradiation and until day 98 following TBI. Cell counts of total CD8 T cells (H), CD8

TN (I), CD8 TCM (J), and CD8 TEM (K) were determined prior to irradiation and until day 98 following TBI. Data are means \pm SD. * $P < 0.05$, vehicle vs. NT-I7; # $P < 0.05$, vehicle vs NT-I7@D7; & $P < 0.05$, NT-I7 vs. NT-I7@D7; multiple t test. WBC, white blood cell; LY, lymphocytes; TN, naïve T cell, TCM, central memory T cell, TEM, effector memory T cell.

To determine whether NT-I7 also plays a role in T cell recovery in aged animals, we further assessed total CD3, CD4, and CD8 T cell counts in animals at 38-41 weeks and 62 weeks of age following TBI exposure. Similar T cell recovery trends were observed in NT-I7-treated mice, with a greater magnitude of CD8 reconstitution compare to CD4 T cells following the nadir (Figure 19). In addition to investigating the effect on T cells, we also examined whether NT-I7 altered the recovery of myeloid populations. Interestingly, NT-I7 also led to rapid recovery of neutrophils and monocytes compared to vehicle-treated mice (Figures 20A and 20B). However, the recovery of red blood cells and platelets was delayed with NT-I7 treatment (Figures 20C and 20D). These data indicate that NT-I7 induces accelerated T cell and specific myeloid subset recovery in the peripheral blood.

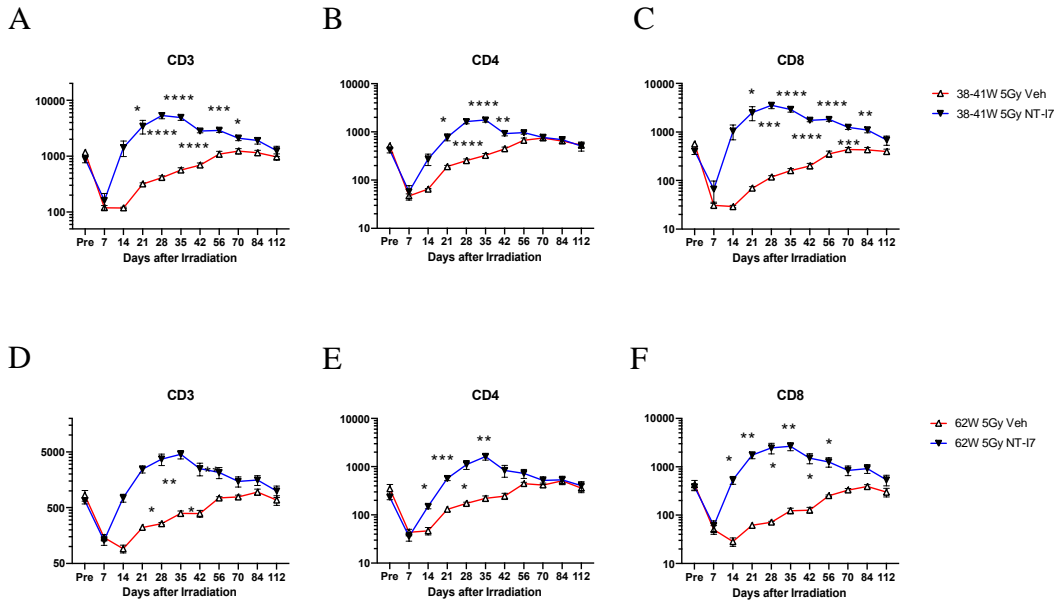


Figure 19. NT-I7 induces peripheral blood T cell recovery in aged animals after total body irradiation.

C57BL/6 mice underwent 5 Gy TBI, followed by vehicle or NT-I7 injection at 10mg/kg at 24 hr, day 7, day 14, and day 21. Cell counts of total CD3 cells (A), CD4 T cells (B), CD8 (C) in mice aged 38-41 weeks, and total CD3 cells (D), CD4 T cells (E), CD8 (F) in mice aged 62 weeks were determined prior to irradiation and until day 98 following TBI. Data are means \pm SEM. * $P < 0.05$, ** $P < 0.01$, *** $P < 0.001$, **** $P < 0.0001$ vehicle vs. NT-I7; multiple t test.

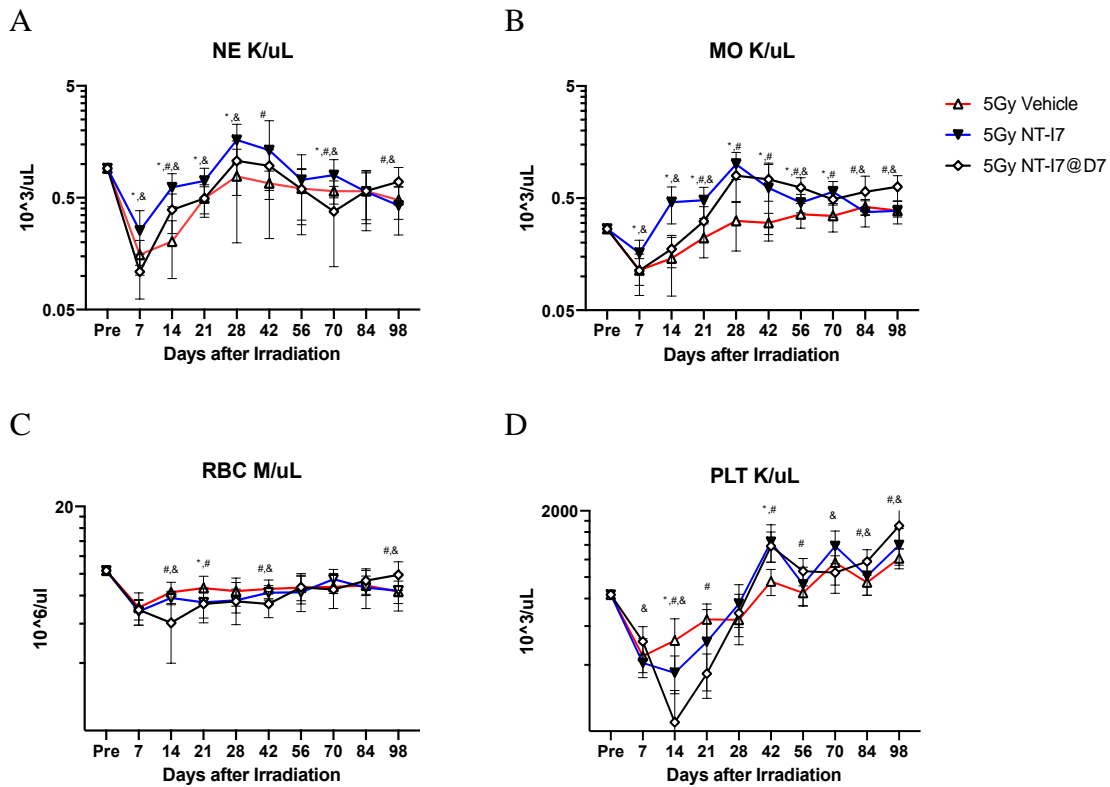


Figure 20. NT-I7 induces changes in myeloid cell recovery after total body irradiation.

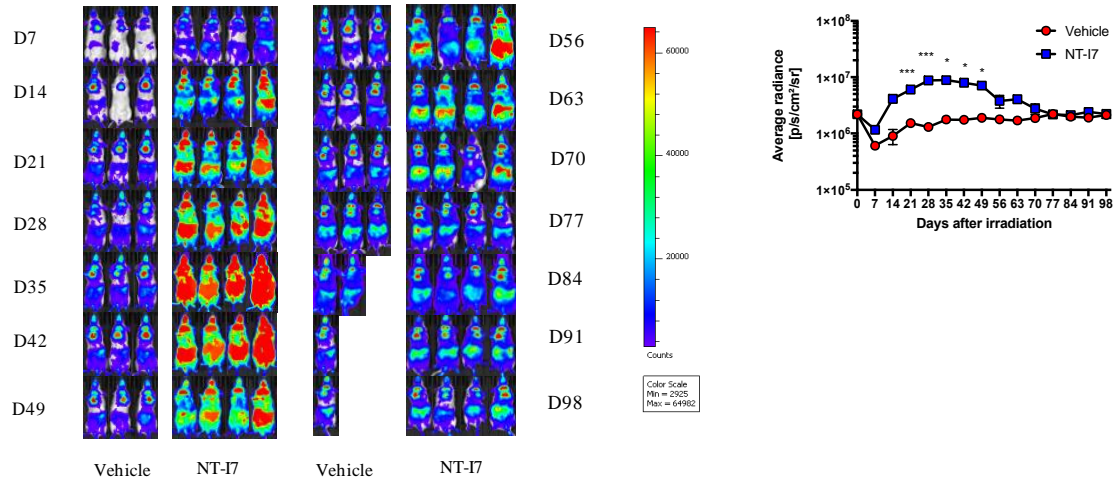
C57BL/6 mice underwent 5 Gy TBI, followed by vehicle, NT-I7 injection at 10mg/kg at day 7, day 14, and day 21 or NT-I7 injection at 24 hr, day 7, day 14, and day 21. Complete blood count of neutrophils (A), monocytes (B), red blood cells (C), and platelets (D) were determined prior to irradiation (Pre) and until day 98 following TBI. Data are means \pm SD. * $P < 0.05$, vehicle vs. NT-I7; # $P < 0.05$, vehicle vs NT-I7@D7; & $P < 0.05$, NT-I7 vs. NT-I7@D7; multiple t test. NE, neutrophil; MO, monocyte; RBC, red blood cells; PLT, platelets.

3.3.2. NT-I7 promotes systemic T cell recovery

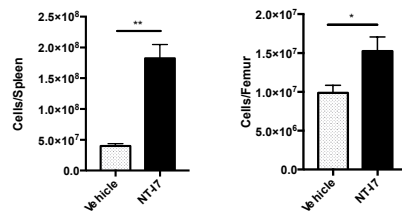
NT-I7 treatment induced rapid T cell recovery in the peripheral blood. However, mechanisms of T cell generation across various primary and secondary lymphoid organs vary, hence it is unclear whether similar reconstitution kinetics is recapitulated

systemically. To investigate whether the effect of NT-I7 is recapitulated in systemic T cell recovery, BLI imaging of chimera mice generated from T-Luc bone marrow donor cells (Figure 3) was utilized to determine recovery kinetics across different tissues. Weekly NT-I7 or vehicle injections were administered to chimeras starting at 24 hr and continued up to day 21 following 5 Gy TBI. Similar to preliminary findings using T-Luc mice, robust T cell recovery was observed in NT-I7 treated animals within the first few weeks following TBI (Figure 21A). Notably, the effect on T cell recovery persisted even after the last injection was administered. T cells were readily detected in the thymus, lymph nodes, spleen, and the GI tract in both groups. However, T cell signals were remarkably more saturated in NT-I7 treated mice since day 7 through day 63. From day 70, the signal intensity became more comparable between the two groups, indicating that the effect of NT-I7 is more robust early after TBI.

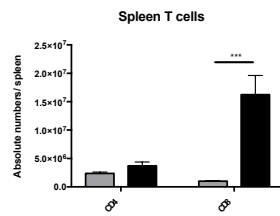
A



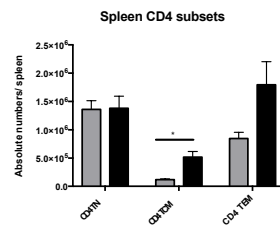
B



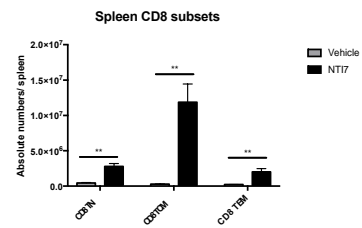
C



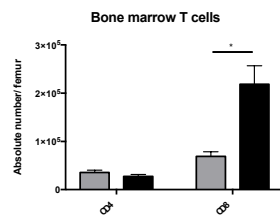
D



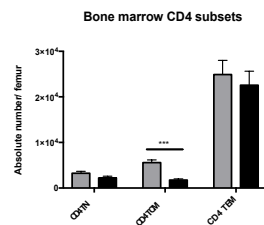
E



F



G



H

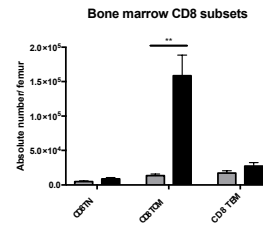


Figure 21. NT-I7 treatment induces systemic T cell recovery following TBI.

(A) Following chimera generation with T-Luc BM, NT-I7 or vehicle was given to chimeras following 5 Gy TBI, BLI was performed weekly to determine the kinetics of T cell recovery. C57BL/6 mice underwent sublethal irradiation at 5 Gy, followed by vehicle or NT-17 (10mg/kg) injections at 24h and day 7. Spleens and femur-derived bone marrow were collected 14 days after TBI. (B) Left; Cellularity of total splenocytes. Right: cellularity of total bone marrow cells per femur. Absolute cell counts of total T cells (C), CD4 T cell subsets (D), and CD8 T cell subsets (E) in the spleen. Absolute cell counts of total T cells (F), CD4 T cell subsets (G), and CD8 T cell subsets (H) in the bone marrow per femur. Data are means \pm SEM. *P < 0.05, **P < 0.01, and *P < 0.001; two-tailed unpaired t test. Data are representative of 5 biological replicates.**

Although imaging studies using chimera mice demonstrated that NT-I7 induces rapid T cell recovery at various peripheral sites following sublethal irradiation. However, it is unclear whether enhanced BLI signals correspond to cellularity changes in primary and secondary lymphoid organs. To determine whether T cell recovery through imaging is validated through corresponding changes in absolute cell counts, we collected spleens and bone marrow from C57BL/6 mice treated with vehicle or NT-I7 14 days following sublethal irradiation at 5 Gy. Absolute cell counts were significantly increased in NT-I7-treated mice relative to vehicle group in both the spleen and bone marrow (Figure 21B). In the spleen, total CD4 T cells counts were comparable between vehicle and NT-I7 groups (Figure 21C). However, CD4 central memory T cells (TCM) were increased compared to vehicle group (Figure 21D). Strikingly, total CD8 T cell numbers were significantly increased in NT-I7-treated mice (Figure 21C). T cell subset analyses further revealed that the increase in CD8 T cells is primarily contributed by

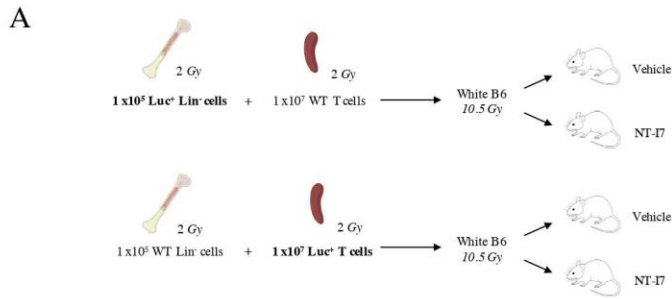
expansion of central memory T cells (TCM) in NT-I7 mice (Figure 21E). In addition, both CD8 naïve (TN) and effector memory (TEM) T cells were elevated in NT-I7 group, which is potentially beneficial for mounting both primary and secondary T cell responses against pathogen challenge. Interestingly, NT-I7-treated mice also exhibited significantly higher total CD8 T cells in the bone marrow (Figure 21F). In contrast, total CD4 T cells were comparable between vehicle and NT-I7 mice while CD4 TCM were reduced in the latter group (Figure 21G). Notably, CD8 TCM, which account for the majority of total CD8 T cells, were highly increased in the bone marrow of NT-I7 mice (Figure 21H). Bone marrow is known to provide a niche for antigen-specific memory T cells, which migrate from the peripheral following resolution of acute infection. Previous studies revealed that bone marrow memory CD8 T cells preferentially undergo proliferation in response to IL-7 and IL-15. It is possible that NT-I7, a long-acting IL-7, can induce rapid homeostatic expansion, supporting both the in vivo imaging results and the increase in absolute CD8 T cell counts. Additionally, CD8 memory T cells persisting in the bone marrow have been shown to mount effective secondary response against viral infections upon adoptive transfer [85]. It is possible that NT-I7 treatment further offers protection against secondary viral challenge to improve survival and antigen-specific CD8 memory T cells response. Additionally, further in vivo studies should be conducted to verify that rapid CD8 T cell recovery induced by NT-I7 is not accompanied by an inflammatory response in the absence of pathogen challenge or immunization. Taken together, these

findings demonstrate the clinical implication that NT-I7 treatment following radiation exposure induces rapid T cell recovery, which is critical for mediating protection against opportunistic pathogens when T cells are scarce.

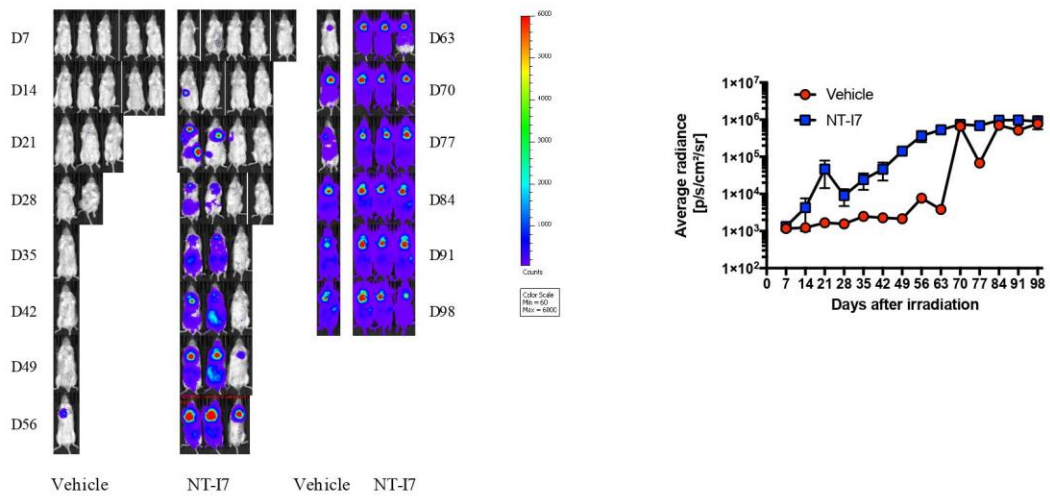
3.3.3. NT-I7 enhances T cell reconstitution through both thymic-dependent and independent mechanisms

Chimeras generated using T-Luc bone marrow demonstrated rapid induction of T cell reconstitution following TBI (Figure 4). However, it is unclear whether this process is primarily mediated through de novo generation of T cells through radioresistant hematopoietic stem cells during thymic development or through thymus-independent mechanisms such as peripheral expansion of radioresistant mature T cells. To this end, we utilized lethally irradiated white C57BL/6 mice transplanted with either T-Luc-derived lineage negative (Lin^-) cells from the bone marrow or mature T cells (Figure 22A), along with either Lin^- cells or T cells from wild type C57BL/6 donors. To simulate the effect of TBI on hematopoietic stem cells and mature T cells, both Lin^- cells and T cells were irradiated prior to transplantation so that the contribution of radioresistant Lin^- cells and T cells can be detected through imaging. Following transplantation, recipients were treated with either NT-I7 or vehicle as shown in Figure 22A. Imaging was performed weekly to visualize the T cell recovery in various locations. NT-I7-treated mice began to show T cell signal on day 14 and 21 after transplantation, primarily in the thymus, indicating that radioresistant Lin^- -derived cells began to

contribute to T cell development in the thymus (Figure 22B). Over the subsequent weeks, increased signal from the thymus was detected from day 28 through day 56. Moreover, increased T cell signal was detected in the cervical lymph nodes, spleen, and GI tract, suggesting that radioresistant Lin⁻ cells can contribute to the mature T cell pool in the periphery with NT-I7 treatment as soon as 21 days after transplantation.



B NT-17 enhances T cell reconstitution through thymic-dependent mechanisms



C NT-17 enhances T cell reconstitution through thymic-independent mechanisms

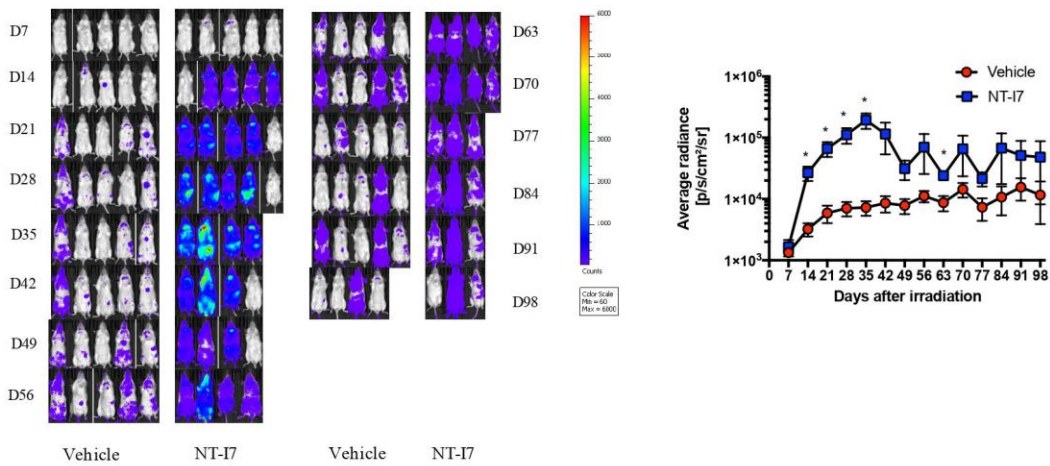


Figure 22. NT-I7 enhances T cell reconstitution through thymic-dependent and independent pathways.

(A) Schematic of experimental design to determine the mechanisms of NT-I7 during T cell recovery. lethally irradiated white C56BL/7 mice transplanted with either T-Luc-derived lineage negative (Lin⁻) cells from the bone marrow or mature T cells, along with either Lin⁻ cells or T cells from wild type C56BL/7 donors. Both Lin⁻ cells and T cells were irradiated at 2 Gy prior to transplantation. Recipients were subsequently treated with vehicle or NT-I7 as shown in Fig 7A. (B) BLI of recipients treated with vehicle or NT-I7 following transplantation with T-Luc-derived Lin⁻ cells and wild type C56BL/7 T cells. (C) BLI of recipients treated with vehicle or NT-I7 following transplantation with T-Luc-derived T cells and wild type C56BL/7-derived Lin⁻ cells. Data are means \pm SEM. *P < 0.05; two-tailed Welch's t test.

In contrast, thymopoiesis from T-Luc-derived Lin⁻ cells was not detected until day 56 in the vehicle group. These results indicate that in the absence of NT-I7 to boost T cell recovery, radioresistant Lin⁻ cells contribute to thymopoiesis albeit in a markedly delayed manner. In contrast, NT-I7 treatment considerably accelerates the repopulation of progenitor cells to induce thymopoiesis. These findings also suggest that intervention with NT-I7 following radiation exposure may be able to shorten the window of susceptibility to opportunistic infections. In the peripheral expansion model, T cell signals in the vehicle group were detected albeit at low intensity 21 days after transplantation (Figure 22C). The presence of T cells increased slightly over the course of 98 days. In contrast, T cells can be readily visualized in various secondary lymphoid organs and the GI tract in NT-I7-treated group as soon as 14 days after transplantation, at a remarkably higher intensity compared to vehicle-treated group, reaching peak intensity on day 35. The results suggest that NT-I7 enhances the peripheral expansion of

radioresistant T cells. These observations also recapitulated the findings in Figure 21 that the effect of NT-I7 persisted even after the end of treatment. Interestingly, NT-I7-mediated T cell reconstitution through thymic-dependent mechanisms underwent a continual and steady increase compared to vehicle group. In contrast, thymic-independent T cell recovery through NT-I7 is characterized by a large spike as soon as 14 days after TBI, plateauing at around 49 days. These observations indicate that rapid expansion of mature radioresistant T cells is the dominant mode of NT-I7-mediated T cell recovery early after radiation. De novo T cell generation in response to NT-I7 appears to be the predominant source of T cell recovery following the extensive peripheral expansion process. Altogether, results from the two distinct transplantation experiments support the role of NT-I7 in rapidly enhancing T cell reconstitution after radiation exposure through both thymus-dependent and peripheral expansion mechanisms.

3.3.4. NT-I7 alters DN-to-DP transition and enforces commitment to cytotoxic-lineage T cells

We observed that NT-I7-mediated thymic-dependent T cell recovery is characterized by a gradual increase approximately 21 days after radiation (Figure 23B), a relatively slow process compared to peripheral expansion of mature T cells. These observations were recapitulated in an endogenous T cell recovery model, where WT

mice were irradiated at 5 Gy, followed by vehicle or NT-I7 injections at 24 hr and day 7. As expected, thymocyte numbers are comparable 14 days after TBI in vehicle- and NT-I7-treated mice (Figure 23A). However, it is unclear whether thymic development and lineage commitment are altered by NT-I7 treatment.

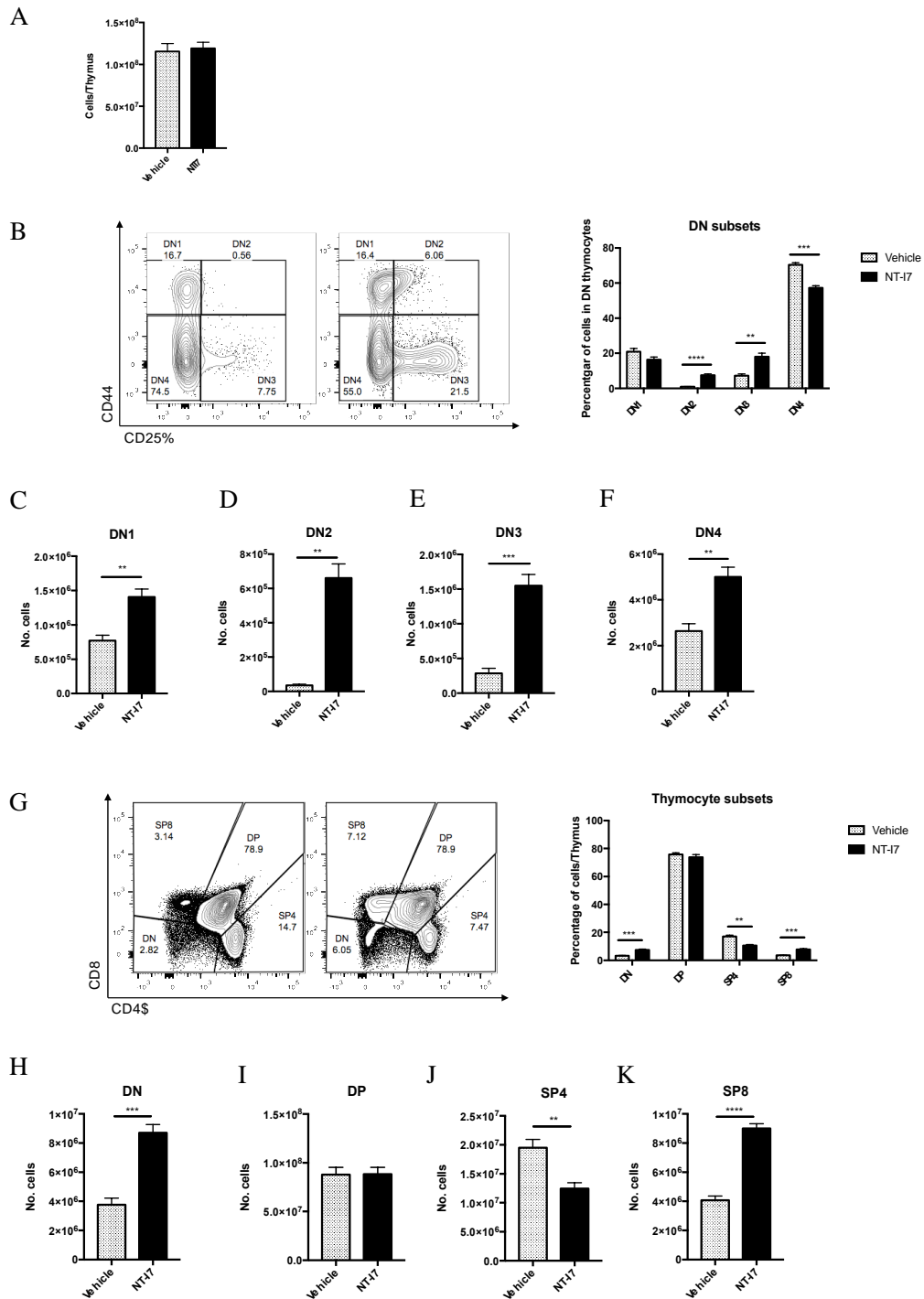


Figure 23. NT-17 alters the DN-to-DP transition as well as the relative abundance of SP4 and SP8 thymocytes during T cell development.

C57BL/6 mice underwent sublethal irradiation at 5 Gy, followed by vehicle or NT-17 (10mg/kg) injections at 24h and day 7. Thymi were collected for analysis. (A) Cellularity of thymocytes in vehicle- and NT-I7-treated animals. (B) Left: Representative gating strategy for DN1-to-DN4 transition. Right: Percentages of DN1, DN2, DN3, and DN4 thymocytes in vehicle- and NT-I7-treated animals. (C)-(F) Cellularity of DN1, DN2, DN3, and DN4 thymocytes in vehicle- and NT-I7-treated animals. (G) Left: Representative gating strategy for DN-to-DP transition. Right: Percentages of DN, DP, SP4, and SP8 thymocytes in vehicle- and NT-I7-treated animals. (H)-(K) Cellularity of DN, DP, SP4, and SP8 thymocytes in vehicle- and NT-I7-treated animals. Data are means \pm SEM. *P < 0.05, **P < 0.01, ***P < 0.001, and ****P < 0.0001; two-tailed Welch's t test. Data are representative of 5 biological replicates. Numbers indicate percentage of cells in gates.

Further analyses demonstrated that the composition of various thymocyte subsets is drastically altered in NT-I7 group, potentially leading to differences in CD4 vs. CD8 T cell numbers following export to the periphery. During thymocyte development, IL-7Ra expression is first detected at the DN2 stage [86]. IL-7 signaling is critical during β -selection at the DN3 stage to support survival and proliferation. FACS analyses indicate a significant increase in the frequencies of DN2 and DN3 thymocytes among all DN populations following NT-I7 treatment (Figure 23B). Furthermore, the absolute cell counts of all DN subsets are significantly increased compared to vehicle group (Figure 23C-23F), suggesting an increase in the total input of thymus-seeding cells such as common lymphoid progenitors or early thymic progenitors. Interestingly, IL-7Ra expression is downregulated beginning at the DN4 stage and cessation of IL-7 signaling facilitates positive selection in DP thymocytes. Following positive selection, IL-7Ra expression is re-induced in thymocytes for survival. The relative frequencies of DN, DP,

CD4⁺CD8⁻ (SP4), and CD4⁺CD8⁺ (SP8) thymocytes were further assessed to determine the effect of NT-I7 at distinct transition stages (Figure 23G). The results indicate that NT-I7 treatment selectively increases the frequency and absolute number of SP8 thymocytes, likely at the expense of SP4 thymocytes (Figures 23-23K). These findings are in line with previous reports regarding the role of intrathymic IL-7 in CD4 vs CD8 lineage commitment as IL-7 signaling enforces CD8 T cell fate. Therefore, NT-I7 enhances CD8 cytolytic lineage commitment relative to vehicle group. Following emigration to the periphery, increased CD8 total cell count in the spleen and bone marrow (Figure 21), which supports CD8 fate commitment during thymic development, may be critical for mounting effective cytotoxic response against pathogen challenges in NT-I7 mice.

3.3.5. NT-I7 alters the frequency and number of HSC and progenitors after TBI

Our peripheral blood data suggest that while T cells, neutrophils, and monocytes are increased, there was a delay in platelet and red blood cell recovery with NT-I7 treatment (Figure 20). It is possible that NT-I7 affects lymphoid and myeloid lineage commitment. We also showed that NT-I7 led to a significant increase in the bulk DN thymocyte population, including DN1 thymocytes which contains bone marrow-derived early thymocyte progenitors. These findings prompted us to investigate whether NT-I7 affects lineage commitment at the HSC and progenitor stage. We first examined the

composition of Lin⁻Sca1⁺cKit⁺ (LSK) cells, which consist of HSC, multipotent progenitors (MPP), hematopoietic progenitor 1 (HPC-1), and HPC-2 cells in the bone marrow. We showed that NT-I7 selectively increased the frequency and absolute numbers of HPC-1, a mixture of lymphoid- and myeloid-restricted progenitors that have lost the potential to differentiate into erythrocytes and megakaryocytes [87] (Figure 24). These data are consistent with increased T cells, neutrophils, monocytes in contrast to reduced platelet and red blood cell recovery in NT-I7-treated mice. Furthermore, the frequency and absolute number of MPP underwent a drastic increase in the presence of NT-I7. In contrast, the absolute number of HSCs was significantly reduced with NT-I7 treatment. Together with increased recovery of various white blood cell subsets, it is possible that NT-I7 treatment promotes the differentiation of HSCs into restricted progenitors. We further assessed the differentiation potential of bone marrow cells isolated from unirradiated control, vehicle, and NT-I7 mice. While TBI drastically reduced the total number of colonies in both vehicle and NT-I7 bone marrow, granulocyte-macrophage progenitors (CFU-GM) colonies are increased with NT-I7 treatment compared to vehicle (Figure 25). By contrast, Bone marrow from NT-I7 group generated significantly reduced burst forming unit erythroid (BFU-E) colonies, which give rise to red blood cells. However, the number of total colonies and common myeloid progenitors (CFU-GEMM) are reduced in NT-I7-treated group. Overall, we found that data from CFU assays are consistent with changes in corresponding populations in the peripheral blood.

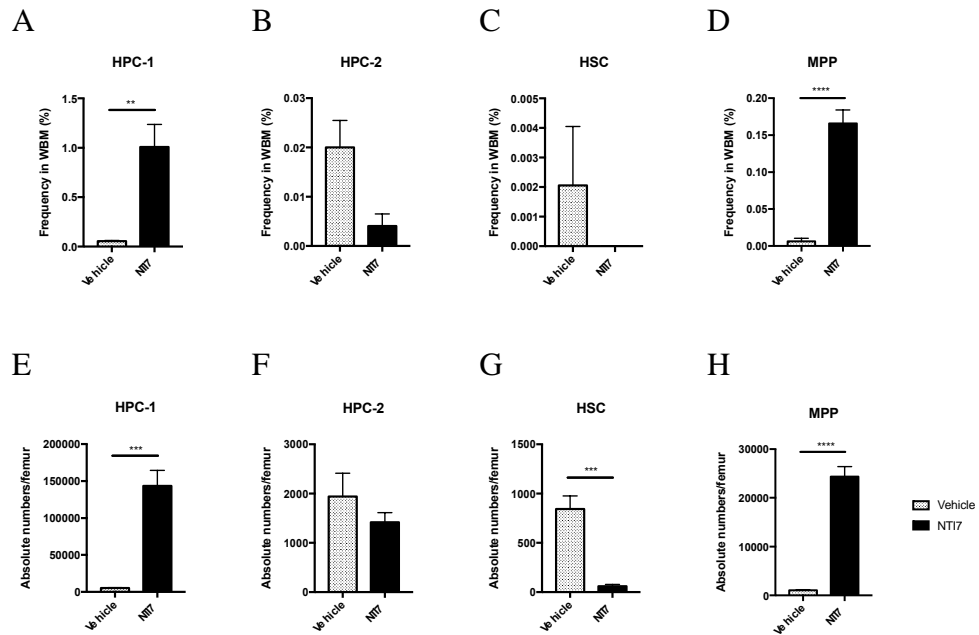


Figure 24. NT-I7 alters the frequency and number of stem and progenitor populations.

C57BL/6 mice underwent sublethal irradiation at 5 Gy, followed by vehicle or NT-17 (10mg/kg) injections at 24h and day 7. Femurs were collected for analyses. HPC-1, HPC-2, HSC, MPP are gated on live Lin⁻Sca1⁺cKit⁺ (LSK) bone marrow cells. Frequencies of HPC-1 (A), HPC-2 (B), HSC (C), and MPP (D) in whole bone marrow cells. Absolute numbers of HPC-1 (E), HPC-2 (F), HSC (G), and MPP (H) per femur. Data are representative of 5 biological replicates. Data are means \pm SEM. **P < 0.01, ***P < 0.001, and ****P < 0.0001; two-tailed unpaired t test. WBM, whole bone marrow cells.

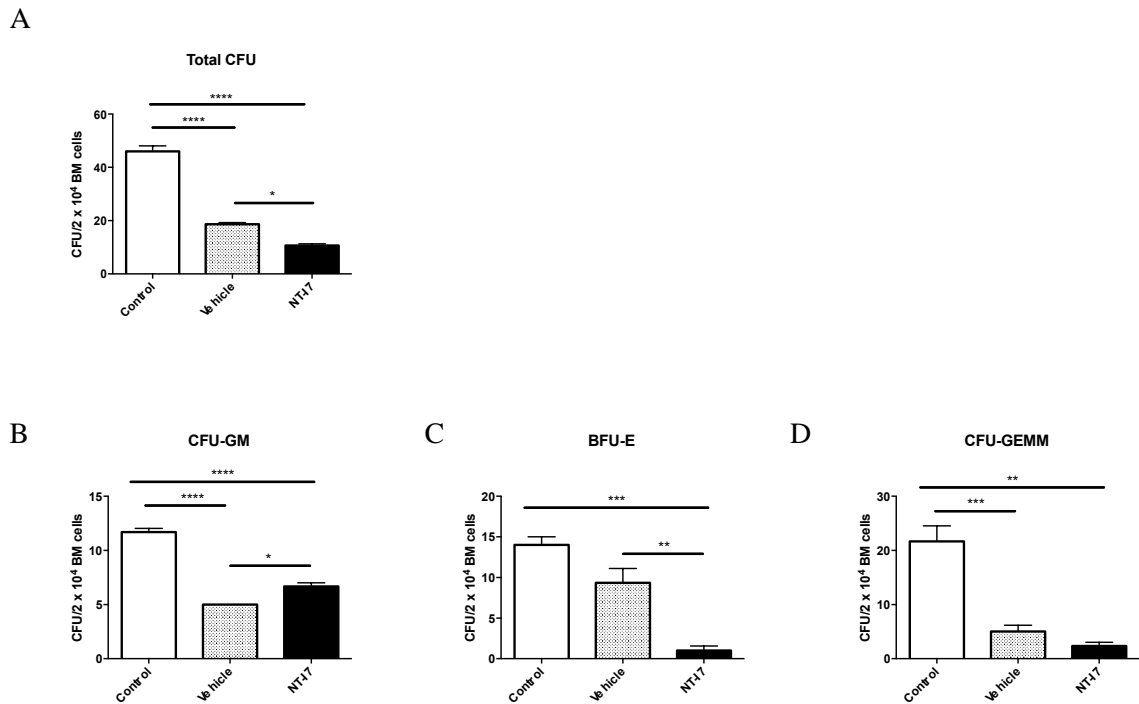


Figure 25. NT-I7 alters the differentiation potential of bone marrow cells after TBI.

C57BL/6 mice underwent sublethal irradiation at 5 Gy, followed by vehicle or NT-17 (10mg/kg) injections at 24h and day 7. Total bone marrow cells were plated for CFU assays at a concentration of 2×10^4 cells per 35mm dish. Total colonies (A), granulocyte-macrophage progenitor colonies (B), burst forming unit erythroid colonies (C), and common myeloid progenitor colonies (D) for counted. Data are means \pm SEM. * $P < 0.05$, ** $P < 0.01$, *** $P < 0.001$, and **** $P < 0.0001$; two-tailed unpaired t test. Data are representative of 5 biological replicates. Colony forming unit-granulocyte-macrophage progenitor, CFU-GM; burst forming unit erythroid, BFU-E; common myeloid progenitor, GEMM.

3.3.6. NT-I7 treatment preserves T cell effector function and proliferation in response to TCR stimulation

We demonstrated the contribution of NT-I7 to both thymic-dependent and -independent mechanisms, as well as the effect at the stem cell and progenitor stage.

Imaging analyses and lymphoid organ cellularity further revealed that NT-I7 promotes T cell recovery. However, it is unclear whether effector T cell function is retained following TBI exposure with NT-I7 treatment. To address these questions, we sought to measure the expression of the cytotoxic mediator granzyme B (Gzmb) as well as proinflammatory cytokines. Following stimulation with anti-CD3 and anti-CD28 antibodies, spleen-derived T cells were assessed for the frequency of Gzmb⁺ producers. While both groups demonstrated elevated Gzmb⁺ T cell frequencies compared to resting T cells (Figure 26A, left panel), T cells from NT-I7-treated mice exhibited significantly increased proportions of cytotoxic T cells compared to vehicle group (Figure 26A, right panel). We further measured pro-inflammatory cytokine expression. In both CD4 and CD8 T cells subsets, IFN- γ ⁺ producer frequencies were elevated (Figure 26B). However, the expression of TNF- α was comparable between NT-I7 and vehicle T cells (Figure 26C). In addition to effector functions, the effect of NT-I7 on T cell proliferation capacity was also assessed. Following in vitro stimulation, majority of T cells from both vehicle and NT-I7 groups underwent proliferation evidenced by the frequency of Ki67⁺ cells (Figure 26E), suggesting that both groups responded equally well to TCR stimulation. In summary, we show that T cell effector function is retained or enhanced following NT-I7 treatment after radiation exposure. We further show that proliferation capacity in response to TCR stimuli is preserved in vitro. Further studies will elucidate whether in vivo T cell response is altered through NT-I7 treatment.

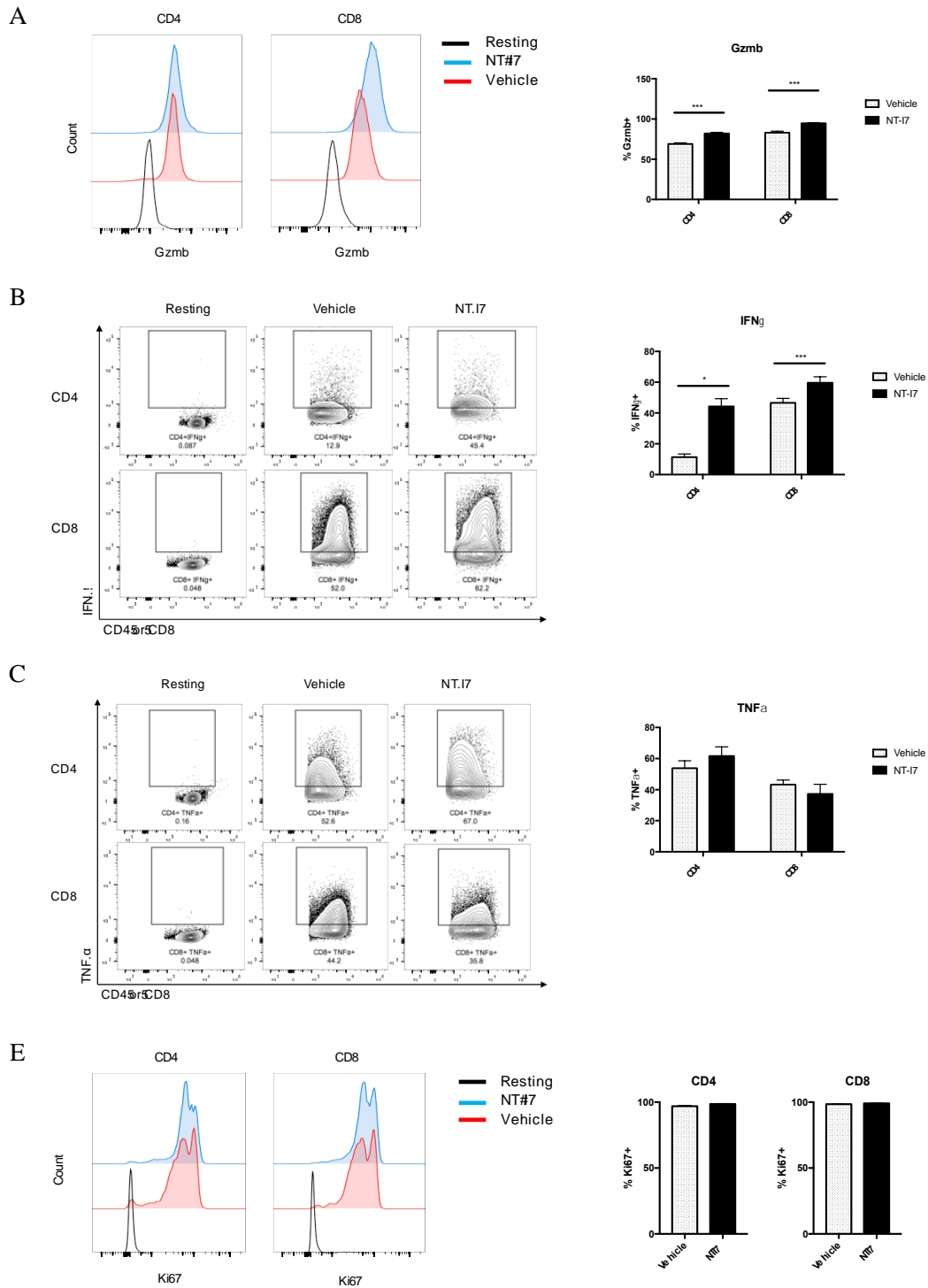


Figure 26. NT-I7 treatment preserves T cell effector function and proliferation.

C57BL/6 mice underwent sublethal irradiation at 5 Gy, followed by vehicle or NT-17 (10mg/kg) injections at 24h and day 7. Splenocytes were stimulated with anti-CD3 (1ug/ml) and anti-CD28 (0.3ug/ml) antibodies for 72h and analyzed for flow cytometry analysis. Splenocytes were incubated with PMA (20ng/ml) and ionomycin (1uM) 4 hours prior to collection for cytokine analysis. (A) Granzyme B expression in CD4 and CD8 T cells following stimulation. (B) IFN- γ expression in CD4 and CD8 T cells following stimulation. (C) TNF- α expression in CD4 and CD8 T cells following stimulation. (D) Frequencies of Ki67+ CD4 and CD8 T cells. Data are means \pm SEM. *P < 0.05 and ***P < 0.001; two-tailed unpaired t test. Data are representative of 5 biological replicates. Numbers indicate percentage of cells in gates. Numbers indicate percentage of cells in gates.

4. Discussion

In this study, we sought to investigate the T cell recovery process in response to ionizing irradiation in different settings, including TBI alone and TBI as a conditioning regimen for bone marrow transplantation. We further examined the role of NT-I7, a long-acting homodimeric recombinant human IL-7, in mediating T cell recovery after TBI.

4.1 Characterizing T cell constitution following TBI

Bone marrow failure and severe lymphopenia are major causes of morbidity and mortality associated with TBI exposure. Delayed immune reconstitution over the course of several months to years leads to compromised immunity against infections. In contrast to innate immune cells such as NK cells and monocytes that undergo accelerated recovery early, T cell recovery is a significantly prolonged process [88]. Studies have shown that even a single exposure to low dose (0.5 Gy) TBI can lead to long-term changes in the T cell pool [7]. However, few studies assessed the effect of higher dose TBI (> 5 Gy) on the reconstitution process through diverse T cell generation mechanisms. Moreover, there is a general lack of understanding in the mechanisms utilized by radioresistant T cells during homeostatic proliferation, which can have positive implications on the therapeutic approaches to enhance T cell recovery after TBI. In the current study, we characterized the dynamics and mechanisms of T cell

reconstitution to help predict T cell response to radiation, which can provide novel perspectives for optimizing the treatment options in the clinical setting.

We first characterized peripheral blood kinetics in response to various TBI doses. Peripheral blood T cells are severely depleted with the first week after TBI, reaching the nadir on approximately day 7. Both CD4 and CD8 T cells recovery back to baseline at around 42 days after exposure, including high dose TBI at 7 Gy (Figure 1), indicating a window of susceptibility for medical treatments to enhance T cell recovery.

Furthermore, we demonstrated that peripheral blood T cells undergo recovery in a TBI dose-dependent manner. It is unclear whether the kinetics observed in the peripheral blood is recapitulated systemically, including lymphoid organs and peripheral tissues where differences in homeostatic cues exist in the microenvironment. Specifically, during transit in the blood, naive T cells undergo minimal exposure to IL-7, a critical component regulating T cell survival and homeostasis. In contrast, secondary lymphoid organs are the primary site of IL-7 production [45]. However, there is no tool available to track the kinetics and magnitude of T cell expansion in various lymphoid organs and other peripheral tissues in vivo, which can provide a more comprehensive understanding on systemic T cell recovery. Using chimera mice reconstituted with donor cells that selectively express the luciferase reporter in T cells, we ventured to characterize how T cells respond to TBI from a systemic perspective. Visualization of T

cells in vivo offers a glimpse of T cell recovery mechanisms. The data indicate that both thymus and lymph nodes are actively involved during recovery. Interestingly, the GI tract is also a major site undergoing active T cell reconstitution. It is possible that homeostatic cytokines produced by intestinal epithelial cells [89], such as IL-7, contributes to mucosal T cell homeostasis in response to TBI. Overall, quantification of total signal intensity suggests that the nadir and the time it takes to recover back to baseline are similar to trends observed in the peripheral blood, highlighting the window of severe T cell depletion and optimal window of medical intervention.

Although in vivo imaging studies indicate an active role for thymic-dependent T cell recovery following TBI, whether thymocyte development is altered by radiation is unclear. To address this question, we analyzed thymocyte populations at various developmental stages. We demonstrated that reduction in total thymocyte numbers is radiation dose-dependent (Figure 5). Although, developmental checkpoints within DN1-DN4 were not significantly affected, TBI exposure reduced total DN thymocytes, suggesting that there may be a corresponding defect in number of early thymic progenitors seeding the thymus. The reduction in thymic cellularity may lead to a drop in TCR repertoire diversity, which can cause defective immune response against a diverse range of pathogens, as well as lack of response to immunizations. To determine whether TBI at various doses leads to reduced TCR diversity and expansion of selective

clones, we analyzed VJ entropy and the degree of clonal expansion. The data suggest that TCR repertoire diversity is relatively well-preserved even at high dose TBI in the current mouse model (Figure 6). However, it is worth noting that there is an intrinsic difference between mouse and human T cell maintenance. Peripheral T cell maintenance is less dependent on thymopoiesis in human than mice [90]. Specifically, maintenance of TN is highly dependent on thymopoiesis in mice throughout their entire lifespan. In contrast, TN in adult humans are maintained almost exclusively through homeostatic expansion. To further address the biological differences, future studies should also be conducted using non-human primate models. Additional factors that influence T cell recovery in response to TBI includes aging, which can lead to reduced stem cell and lymphoid progenitor output, as well as thymic involution, a direct contributing factor to a decline in de novo T cell generation. Specifically, TBI-induced thymopoiesis suppression can significantly exacerbate thymic involution in older individuals [7]. Gender can also affect the T cell recovery kinetics through the thymic-dependent pathway upon radiation exposure. Previous studies suggest that thymocytes undergo a rapid decline early following TBI in males [7]. By contrast, females exhibited a gradual trend in thymocyte reduction, which may be attributed to different rates of thymic involution depending on the gender.

In addition to assessing the effect of radiation on thymic-dependent T cell generation, we also investigated involvement of radioresistant T cells, which can undergo expansion in lymphopenic conditions to contribute to peripheral T cell recovery. Previous immunophenotyping and in vitro studies in mice and non-human primates showed that survival of radioresistant T cells is associated with the naïve versus memory status [4; 6]. In terms of the expansion process in lymphopenic conditions, one murine study assessed the gene signatures associated with homeostatic proliferation of normal T cells. However, there was only a small pool of candidate genes, which did not demonstrate consistent correlation with the homeostatic proliferating phenotype [53]. These early findings suggest a lack of unique transcription profile associated with T cell expansion in the lymphopenic environment. However, the pool of genes screened in earlier studies was limited by the number of gene sequences available in the microarray. Overall, very little is known about T cell populations that are actively involved during the expansion process in response to radiation. In the current study, we utilized single cell sequencing to characterize the subpopulations of radioresistant T cells, the unique gene expression profiles, and relevant pathways upregulated during T cell recovery. Unsupervised clustering analysis revealed 6 main clusters of radioresistant T cells, which were further annotated using the ImmGen database. We showed that while non-cycling naïve T cells and a small subset of memory T cells are shared between control and irradiated samples, there were four unique clusters of moderately and

highly proliferative memory T cell clusters (Figure 7C). To resolve the relationship among the radioresistant T cell populations, we utilized trajectory analyses to determine the differentiation paths. The data suggest that both naïve and memory T cells are actively involved during recovery following TBI (Figure 8), with naïve T cells gradually acquiring a “memory phenotype” in the absence of immunization or pathogen challenge. Furthermore, we assessed pathways that are upregulated at different time points during recovery to determine which mechanisms are utilized by proliferating radioresistant T cells. Pathway enrichment analysis revealed that various mitochondrial components involved in oxidative phosphorylation (OXPHOS) are highly upregulated on both day 5 and day 21 following TBI, indicating increased dependence on OXPHOS, in contrast to predominately relying on glycolysis in conventionally activated T cells. These findings were further validated by measuring oxygen consumption rate in freshly isolated radioresistant T cells, which exhibited enhanced basal and maximal respiration compared to control T cells (Figure 9D). Future experiments should investigate whether OXPHOS is specifically required for the recovery of radioresistant T cells through manipulation of genes critical for regulating mitochondrial OXPHOS, including the deletion of Drp1 and Opa1, which can lead to increased and decreased OXPHOS through regulation of mitochondrial fission and fusion, respectively. We also screened for the expression of oxidative stress markers, including Hsp90aa1, Prdx1, Prdx2, and Txn1 are upregulated in radioresistant T cells compared to unirradiated control T cells,

which can indicate increased level of reactive oxygen species (ROS) that can be associated with increased metabolism (Figure 10). A potential source of elevated oxidative stress is due to residual ROS as a result of TBI exposure on irradiated cells or ROS that are passed on to bystander cells [91]. However, the expression of stress-related genes is further increased later during expansion. The distribution of annotated Seurat clusters along pseudotime (Figure 10A, right panel) suggests that T cells undergo more oxidative stress as they acquire the memory phenotype following expansion. It is possible that active metabolic processes during proliferation can contribute to oxidative stress. However, they can also indicate reduced metabolic fitness, which is major limiting factor for T cell longevity [36]. Together, these results improved the current understanding of both the do novo T cell generation pathway and the homeostatic proliferation process in response to TBI.

Besides assessing the numerical recovery and the gene expression profile of T cells after TBI treatment, we further investigated whether TBI plays a role in altering the proliferative capacity of T cells. Interestingly, radioresistant naïve and effector memory T cells demonstrated markedly increased proliferation capacity compared to control T cells in response to homeostatic proliferation cues in vitro (Figure 11A). Radioresistant naïve T cells also showed increased enhanced proliferation in response to TCR stimulation (Figure 11B). The robust proliferation response in both the homeostatic

proliferation setting and conventional activation setting suggest that radioresistant T cells may be able to mediate protection against infections during the lymphopenic window, which requires future studies in vivo.

4.2. Manipulating T cell reconstitution following bone marrow transplantation

We characterized endogenous T cell recovery following TBI exposure. In the bone marrow transplant setting, TBI is incorporated as part of the conditioning regimen to make space for donor cell engraftment, a curative therapy for hematologic malignancies. In this setting, recovery of both donor and recipient T cells can contribute to protection against infections during the lymphopenia period. However, donor T cells can also lead to detrimental outcomes by mediating GVHD upon alloantigen recognition. In contrast, non-alloreactive donor T cells are critical for mediating anti-tumor immunity to prevent tumor relapse in addition to reducing risks of infections. Therefore, it is imperative to selectively prevent the recovery of alloreactive donor T cells and preserve the function of non-alloreactive T cells.

We exploit the metabolic preferences associated with activated alloreactive donor T cells in attempt to achieve optimal separation of GVL from GVHD. Activated T cells

are dependent on aerobic glycolysis to support growth, division, and effector functions [21; 55; 92]. Previous studies revealed conflicting results regarding the role of glycolysis in the pathogenesis of T cell-mediated GVHD [27; 29; 30; 31; 54]. In the current study, we utilized T cells genetically deficient for Glut1 to directly demonstrate the requirement for glycolysis in donor T cell-mediated acute GVHD without affecting glycolysis in antigen presenting cells. We established that glycolysis modulates the magnitude of T cell response through proliferation and survival. We further demonstrated ex vivo glycolysis inhibition that specifically targets alloreactive T cells to prevent acute GVHD while sparing GVL effect as a preventive approach.

Several studies reported that elevated glucose metabolism is strongly associated with donor T cell-mediated GVHD [93; 94]. Positron emission tomography studies revealed that glucose analog uptake is correlated with donor cell infiltration and GVHD symptoms [94]. A retrospective single-cell RNA sequencing study identified upregulated genes encoding glycolytic enzymes in GVHD patients [93]. Despite the phenotypic analyses and the existing paradigm for the dependence of activated T cells on glycolysis, other groups reported that alloreactive T cells in vivo are less glycolytic and are primarily dependent on oxidative metabolism, namely FAO [30; 31; 54]. However, the absence of conditioning-associated tissue damage in these models contributes to limited release of inflammatory cytokines during the priming phase of T

cells, subsequently altering the regulation of metabolic reprogramming and inflammatory response. Moreover, the evaluation of key glycolysis parameters and contribution of homeostatic expansion were not addressed. Contrary to this report, Nguyen et al. used a comprehensive metabolite analysis to demonstrate that alloreactive T cells derived from an irradiated model highly upregulate glycolysis compared to syngeneic recipients. The administration of glycolysis inhibitors in recipients alleviated disease progression. However, the systemic treatment led to off-target effects that compromised efficacy that could be attributed to organ toxicity [29]. Functional studies that specifically target glycolysis in T cells are therefore necessary to address the role of glycolysis in GVHD pathogenesis. To this end, we utilized donor T cells genetically deficient for Glut1, a major glucose transporter in activated T cells. We showed that in contrast to WT T cells, Glut1^{T-KO} alloreactive T cells showed significantly impaired capacity to adopt aerobic glycolysis (Figures 13A and 13B). Transplant experiments using Glut1^{T-KO} T cells remarkably prevented acute GVHD-associated clinical traits and improved survival (Figure 12). Glycolysis is required for both CD4⁺ and CD8⁺ T cell-mediated pathogenesis as transfer of Glut1^{T-KO} CD4⁺ or CD8⁺ T cells showed significant increase in body weight, reduced clinical score and target organ damage compared to controls (Figure 12). However, disease kinetics and target organ damage differed due to difference in natural disease progression associated with the transfer of CD4⁺ versus CD8⁺ T cells, with rapid improvement of disease progression and alleviated

gastrointestinal tract damage in CD4⁺ T cell recipients compared to delayed disease resolution and reduced skin damage in CD8⁺ T cell recipients. Glut1^{T-KO} T cell recipients in the C57BL/6 → BALB/c setting had not completely recovered their body weights when they were sacrificed after day +100. Even though we did not observe obvious signs of chronic GVHD at necropsy and histological analysis (data not shown), these observations do raise a question whether this strategy has any impact on chronic GVHD. More comprehensive analyses using chronic GVHD models will be needed to answer this question. Taken together, the above experiments demonstrated dramatically improved long-term survival compared to recipients of donor cells with intact glycolysis, providing solid evidence that glycolysis is selectively required for acute GVHD development.

mTORC1 activation has been shown to support cell growth, proliferation, and T_{eff} functions by promoting translation and anabolic metabolism [55; 95; 96; 97]. Nguyen et al. showed that mTORC1-deficient T cells have reduced ability to induce GVHD, accompanied by a less glycolytic phenotype [29]. However, it remains unclear whether the utilization of glycolysis directly promotes mTORC1 signaling in alloreactive T cells. As a sensor for metabolic cues, mTORC1 activity can be modulated by glucose availability [20]. Consistently, the current study (Figure 13C) demonstrated impaired mTORC1 activation as a direct consequence of impaired glycolysis. Additionally,

mTORC1 activity is negatively regulated by AMPK, an energy stress sensor that promotes catabolic pathways including FAO and OXPHOS [98].

Glycolysis has been implicated to support survival as well as antigen-specific expansion [27]. We first assessed the impact on T cell expansion. In vitro experiments indicated a profound defect in clonal expansion of alloreactive T cells upon antigen stimulation (Figure 13D). This observation was recapitulated in vivo by the numbers of donor T cells recovered (Figure 13E) and percentages of divided donor cells using proliferation dye (Figure 13F). The difference in response was exclusively seen in allogeneic recipients but not syngeneic controls (Figure 13E), indicating that alloreactive T cells are dependent on glycolysis for proliferation. Modulation of inflammatory cytokine secretion is also a critical determinant of T cell pathogenicity. Previous studies demonstrated a role for glycolytic enzymes in the translational regulation of inflammatory cytokines by engaging/disengaging glycolysis upon TCR crosslinking [22; 23]. Glycolysis inhibition has also been linked to diminished cytokine production in previous studies, where 2-DG was systemically delivered to BMT recipients [29]. However, glycolysis is also required for DC maturation and migration [56; 57; 58]. Proliferative T cell response can be severely impaired when activated by DCs previously treated with 2-DG [58]. In the currently study, we directly demonstrated defects in both

proliferation and inflammatory cytokine production in $\text{Glut1}^{\text{T-KO}}$ alloreactive T cells without simultaneously targeting non-T cells.

$\text{Glut1}^{\text{T-KO}}$ T cells previously demonstrated reduced viability compared to WT control after stimulation with plate-bound antibodies [27]. To determine whether apoptosis is involved in increased cell death of $\text{Glut1}^{\text{T-KO}}$ T cells, we assessed the expression of proteins involved in the regulation of apoptotic pathway, including Mdm2, Puma, Noxa, and Mcl-1. Proteins linked to the induction of apoptotic pathway were significantly upregulated as opposed to downregulation of the anti-apoptotic Mcl-1 in activated $\text{Glut1}^{\text{T-KO}}$ T cells compared to WT control (Figure 14A). Specifically, Puma, which is sensitive to rapid upregulation in response to glucose deprivation to promote apoptosis [99], was drastically induced in $\text{Glut1}^{\text{T-KO}}$ T cells, suggesting that glycolysis plays a critical role in regulating apoptosis in activated T cells. We also assessed Mdm2 expression due to its role in regulating cellular stress response and apoptosis. We demonstrated that Mdm2 is significantly increased expression in $\text{Glut1}^{\text{T-KO}}$ T cells (Figure 3A). We further evaluated whether alloreactive T cells are susceptible to apoptosis due to nutrient availability and cellular stress in the context of glycolysis. Annexin V and 7AAD staining confirmed that activated alloreactive $\text{Glut1}^{\text{T-KO}}$ T cells are prone to undergo apoptosis (Figure 3B). BH3-only Bcl-1 family members, including Bim, has been implicated in lymphocyte cell death during prolonged glucose deprivation [99]. We

showed that alloreactive Glut1^{T-KO} T cells upregulate Bim expression (Figure 14C), an indicator for ER stress and disruption of glucose metabolism [75; 99; 100]. Mcl-1, a prosurvival factor, is also linked to glycolysis and metabolic stress [74; 77; 101]. Regulated post-translationally, Mcl-1 is rapidly stabilized following TCR crosslinking [102; 103] and couples with Noxa to modulate the apoptosis threshold [77]. With a short half-life of 30 min, Mcl-1 has a rapid turnover rate and is highly sensitive to changes in global translation downstream of mTORC1 [104]. Indeed, Glut1^{T-KO} T cells are incapable of sustaining mTORC1 activation (Figure 13C) and Mcl-1 expression (Figure 14D) during alloantigen challenge. It is possible that Mcl-1 expression is regulated by mTORC1 in response to glucose utilization to regulate T cell survival. Overall, the above findings demonstrate increased apoptosis induction in activated Glut1^{T-KO} T cells compared to WT control. Interestingly, a previous study showed that viability was only slightly reduced in T cells following stimulation in the presence of 2-DG [105]. While these findings appear to be contradictory to the current study, this is potentially attributed to the difference in 2-DG concentration as a higher concentration was used in the current study. Importantly, the timing of 2-DG addition is different. Whereas 2-DG was added at the beginning of stimulation in the previous study, the current assays involved 2-DG addition 16 hours following stimulation, which preferentially affects already activated T cells that are highly sensitive to glycolysis usage.

Since allo-HSCT is the primary curative option for malignant leukemia and lymphomas, it is critical to assess the impact of glycolysis inhibition on GVL activity. Our results demonstrated for the first time that Glut1^{T-KO} T cells provide superior protection in recipients against tumor growth compared to TCDBM + tumor recipients (Figure 15C and 15H). Although GVHD was not completely eliminated with transfer of Glut1^{T-KO} T cells, both survival and body weight are significantly improved in comparison to WT T cell recipients (Figures 15A, 15B, 15F, and 15G). The reduced but detectable GVHD development (Figure 15B) in Glut1^{T-KO} T cell recipients may be contributed by metabolic processes other than glycolysis, including glutaminolysis and pentose phosphate pathway [29], hence simultaneous targeting of the above pathways is likely to further improve the abrogation of GVHD. However, the data support that Glut1^{T-KO} T cell retain the capacity to eliminate tumor development (Figures 15C and 15H). Previous studies suggest that expression of cytotoxic granules, such as granzyme B and perforin in CD8⁺ T cells, are not regulated by aerobic glycolysis [23], potentially mediating GVL effect in Glut1^{T-KO} T cells. Despite the earlier onset of apoptosis in glycolysis-inhibited alloreactive CD8⁺ T cells compared to CD4⁺ T cells (data not shown), ex vivo stimulated T cells were capable of controlling tumor development and improving survival outcome compared to TCDBM + tumor and untreated donor T cell recipients (Figure 17). Furthermore, Glut1^{T-KO} CD8⁺ T cells, which exhibited higher TNF α expression compared to control T cells (Figure 13H), suggesting a potential contribution

to tumor killing mediated by Glut1^{T-KO} CD8⁺ T cells. Glut1^{T-KO} T cells may also be able to facilitate GVL without meeting the threshold for GVHD induction, as the T cell dose to induce GVHD appears to be 10-fold higher than GVL in clinical studies [106; 107; 108; 109]. IFN- γ production (Figure 13G) and OXPHOS-dependent memory T cells can also contribute to GVL activity [40; 110; 111]. Collectively, we showed that T cells with impaired glycolysis retained the capacity to prevent tumor development in allogeneic recipients. Interestingly, studies by Uhl demonstrated that leukemia-derived lactic acid interferes with both glycolysis and OXPHOS in T cells, leading to reduced protection against tumor, which appears to be contradictory to the current finding [112]. However, Glut1^{T-KO} T cells demonstrate comparable basal OCR level to WT control, suggesting that the preservation of OXPHOS may be critical for GVL preservation in Glut1^{T-KO} T cell recipients. In regard to the metabolic flexibility of T cells, previous studies showed that glucose deprivation in activated T cells can be partially compensated by increased respiration [105]. In addition, a recent study demonstrated that CD8⁺ T cells can utilize inosine as an alternative carbon source when glucose utilization is restricted to mediate tumor-killing in xenograft models [113]. Hence it is possible that the metabolic plasticity of CD8⁺ T cells contributes to GVL preservation when glycolysis is impaired.

To evaluate the therapeutic potential in a clinically-relevant setting, we sought to assess selective inhibition of alloreactive T cells to remedy off-target effects on other cell

types that utilize glycolysis. In line with this approach, we and others previously examined ex vivo treatments to eliminate T cells activated by recipient antigens [114; 115; 116]. In the currently study, 2-DG strongly induced apoptosis in activated alloreactive T cells (Figure 16C). We further validated this approach using both murine and human models, where alloresponse was subdued upon alloantigen rechallenge while response against nonspecific stimulation remained intact (Figures 16D and 16E). The ex vivo assay using 2-DG also demonstrated the translational value of targeted glycolysis inhibition prior to transplantation (Figures 17A-17D). As expected, recipients of control T cells treated with media only demonstrated reduced survival with increased incubation time. In contrast, optimal 2-DG inhibition for 48 hours yielded significantly improved survival without losing GVL effect compared to recipients of untreated T cells or those treated with media control. Protection against both tumor and GVHD development through 2-DG inhibition for 48 hours was further evaluated using a second tumor model with the A20 cell line, highlighting the therapeutic potential of ex vivo glycolysis inhibition. Overall, we observed that the desired efficacy for acute GVHD suppression and GVL can be achieved through selective inhibition of alloreactive T cells ex vivo.

4.3. Improving T cell reconstitution using NT-I7

IL-7 is a homeostatic cytokine secreted by non-hematopoietic cells in bone marrow, thymus, and secondary lymphoid organs to maintain T cell viability [45]. Upon IL7 receptor engagement, JAK/STAT signaling pathway is activated to upregulate the antiapoptotic proteins including Bcl-2 and Mcl-1 [47]. Upon removal from the in vivo microenvironment in the absence of IL-7, T cells undergo apoptosis and atrophy [117]. Although IL-7 alone cannot induce T cell expansion, it is able to promote homeostatic proliferation of mature T cells in conjunction with self-peptide-MHC complexes or IL-15 [45]. Furthermore, IL-7 mediates the differentiation of common lymphoid progenitors to T cell and B cell progenitors, as well as supporting thymocyte development while suppressing lineage commitment to other cell types [118]. In addition to maintaining thymocyte survival and regulating the peripheral T cell pool, IL-7 has also been shown to regulate T cell metabolism. Resting T cells require IL-7 to maintain cell size in a glycolysis-dependent manner (Rathmell 2001). Moreover, reduced glucose metabolism in T cells lacking IL-7 signaling leads to impaired growth and proliferation rate upon stimulation with anti-CD3 and anti-CD28 antibodies [47]. Therefore, as an essential component in T cell homeostasis and growth, IL-7 is a promising candidate to promote T cell reconstitution following radiation-induced lymphopenia. Indeed, previous studies have shown that exogenous administration of IL-7 increases peripheral blood T cell recovery. However, the effect is offset by the short half-life (< 10 hours) in circulation. NT-I7 is a recombinant human IL-7 fused with hybrid Fc fragment, which has a

significantly longer half-life than endogenous and conventional recombinant IL-7, including CYT107, a glycosylated recombinant human IL-7 (63.3 hours vs. 9-35 hours) [51; 119]. Specifically, fusion of IL-7 to Fc fragments prolongs protein stability by binding to neonatal Fc receptors to initiate recycling mechanisms [120]. Moreover, the hybrid Fc fragment fused to IL-7 consists of human IgD and IgG4, which are non-immunogenic and cannot bind FcγR III or C1q to induce cytotoxicity mediated by antibodies or complement proteins. Given its increased stability in vivo, the kinetics and mechanisms of T cell reconstitution mediated by NT-I7 may be distinct from conventional forms of IL-7. Furthermore, mechanisms involved in the TBI setting have not been fully characterized. Although conventional IL-7 has been demonstrated to boost T cell counts in HIV- and radiotherapy-induced lymphopenia, there are few studies that directly addressed the role of IL-7 in modulating T cell generation following TBI, which affects T cells in lymphoid organs and peripheral tissues differently [121; 122]. Therefore, we sought to address the effect of a novel form of IL-7 with enhanced in vivo stability in T cell generation after TBI. We first measured the effect of NT-I7 on T cell reconstitution in the peripheral blood following 5 Gy TBI exposure. Two weekly treatment regimens were assessed, with the first dose starting at either 24 hr or 7 days (nadir) post-TBI. We showed that both regimens achieved similar effect on total T cell recovery kinetics, significantly reducing the window of T cell depletion compared to the vehicle group (Figure 18). Subset analyses revealed that both CD4 and CD8 populations

demonstrated remarkably enhanced recovery. Notably, CD8 T cells appeared to be more sensitive to NT-I7-mediated reconstitution than CD4 T cells. Although recovery via thymic-dependent versus homeostatic proliferation pathways cannot be distinguished in this model, the difference in NT-I7 responsiveness could be partially attributed to the intrinsic proliferation difference between naïve CD4 and CD8 T cells in response to homeostatic cues [45]. Indeed, this was reflected through the greater magnitude of CD8 T cell recovery following the nadir. Similar findings were observed in aged cohorts at both 38-41 weeks and 62 weeks of age, where NT-I7 induced a significant increase in both CD4 and CD8 T cell recovery (Figure 19). It is possible that T cell recovery with NT-I7 treatment is mediated through various mechanisms, including the regulation of stem and progenitor pool, thymocyte education, and peripheral expansion. As aging is associated with reduced lymphoid progenitor output, which is further exacerbated by radiation-induced HSC senescence, NT-I7 may be able to mitigate these effects upon TBI exposure in the aging population. Overall, we demonstrated that NT-I7 induced rapid expansion of total T cells in the peripheral blood, as well as the expansion of T cell subsets, including TN, TCM, and TEM. However, whether NT-I7 exerts similar effects on systemic T cell recovery remains unknown.

Having developed an in vivo imaging system to track systemic T cell reconstitution, we ventured to investigate the role of NT-I7 in regulating T cell

generation mechanisms after TBI. Following the generation of T-Luc chimeras (Figure 3), mice were subjected to TBI at 5 Gy. Systemic T cell recovery was assessed in vehicle- and NT-I7-treated mice via weekly imaging until 98 days after irradiation exposure. While T cell signal intensity in both groups reached the nadir on day 7, NT-I7 group underwent more rapid recovery compared to vehicle group, demonstrating significantly higher average radiance from day 21 to day 49 (Figure 21A). Furthermore, imaging analyses indicate enhanced signal intensity in both the thymic region and peripheral tissues in NT-I7-treated mice, bringing T cell level back to baseline much quicker than vehicle group. These findings also suggest that IL-7 boosts T cell regeneration through thymic-independent pathways. Previous studies showed concentrated IL-7 in organs where they are trapped near stromal cells via heparin sulfates [123]. As T cells recirculate over long distances through the lymphatic vasculature, the number of T cells within lymphoid organs can also reflect the level of systemic recovery [124]. Therefore, we further analyzed the spleen and bone marrow, a reservoir for memory T cells [125], to determine whether absolute cell counts are consistent with in vivo imaging results. Indeed, we showed that both lymphoid organ cellularity and total T cell counts per organ were significantly increased in NT-I7-treated mice (Figure 21). Notably, consistent with peripheral blood findings, CD8 T cells in both the spleen and bone marrow demonstrated a greater response to NT-I7 treatment (Figure 21C to 21H). In the bone marrow, CD8 TCM account for the primary population that contributed to the

significant difference between vehicle and NT-I7 groups (Figure 21H). As a major reservoir for CD8 TCM, NT-I7 can potentially mediate effective antigen-specific recall response upon pathogen challenge during the lymphopenic window, which requires further testing using viral challenge in vivo. However, future in vivo studies should be conducted to determine whether the rapid T cell recovery induced by NT-I7 is accompanied by an inflammatory response in the absence of pathogen challenge to ensure validate NT-I7 tolerance in the current treatment regimen. Collection of serum and organs such as skin, eyes, lung, GI tract further determine the presence of proinflammatory cytokines and tissue damage, respectively.

We further examined the effect of NT-I7 on thymic-dependent versus thymic-independent T cell generation pathways after TBI. We showed that NT-I7 led to a steep increase in systemic peripheral expansion early during recovery in contrast to slow and incremental changes in vehicle group (Figure 22C). Interestingly, NT-I7-mediated recovery gradually plateaued to levels comparable to vehicle group towards the end of the study. This could be the result of enhanced thymic output that generated new T cells to fill the niche in peripheral tissues (Figure 22B). The massive response mediated by peripheral expansion of mature T cells, peaking on day 35, represents a potential window of protection during severe lymphopenia. Memory T cells undergo rapid proliferation in response to homeostatic cytokines [45]. It is possible that virus-specific

memory T cells generated prior to TBI can undergo NT-I7-mediated expansion to mediate effective protection, which would require further validation in vivo. De novo T cell generation through the thymus is also significantly increased with NT-I7 treatment. The magnitude of response early during recovery is less pronounced compared to peripherally expanded T cells. However, thymic-dependent T cell generation is gradually increased and sustained at peak level until the end of the study, providing a consistent supply of de novo generated T cells to the periphery (Figure 22B). To assess the role of NT-I7 during thymocyte development, we further compared changes in thymocyte composition between vehicle and NT-I7 mice. We saw a significant increase in DN2 and DN3 frequencies in NT-I7-treated mice (Figure 23), which is consistent with previous findings as IL-7Ra in thymocytes is first detected on DN2 cells. Additionally, these findings also support the role of IL-7 in mediating the DN3 survival and proliferation during β -selection. Notably, absolute cell counts of all DN thymocytes are markedly increased in NT-I7 mice (Figures 23A to 23F), suggesting that there may be a greater number of bone marrow-derived early thymic progenitors seeding the thymus with NT-I7 treatment. Moreover, analyses of remaining thymocyte subsets revealed a selective increase in both the frequency and number of SP8 thymocytes, likely at the expense of SP4 thymocytes in NT-I7 animals. These results are consistent with the greater recovery of CD8 T cells in the peripheral blood, spleen, and bone marrow. Therefore, NT-I7 enforces CD8 cytolytic lineage commitment in the TBI setting, which

may be important in mediating protection against opportunistic infections during the lymphopenic window.

We demonstrated that NT-I7 induces rapid T cell recovery following radiation exposure partially owing to changes in the thymic-dependent pathway. Since early thymic progenitors are bone marrow-derived, it is unclear whether NT-I7 can also induce the reestablishment of other hematopoietic lineages at the HSC and progenitor level. We first sought to investigate the effect of NT-I7 on reconstitution of multiple hematopoietic lineages in the peripheral blood following TBI. We demonstrated that in addition to accelerating T cell recovery, NT-I7 treatment enhanced absolute numbers of total WBC, lymphocytes, neutrophils, and monocytes compared to vehicle group during TBI-induced lymphopenia (Figure 20). To determine whether changes in the recovery of T cells as well as other cell types in NT-I7-treated mice are associated with alterations at the stem cell and progenitor level, we examined the relative distribution of HSC, multipotent progenitors (MPP), hematopoietic progenitor 1 (HPC-1), and HPC-2 cells in the bone marrow. We showed that NT-I7 selectively increases the frequency and absolute numbers of HPC-1 (Figure 24). Colony formation assays and in vivo reconstitution assays suggest that HPC-1 is a heterogeneous population of lymphoid- and myeloid-restricted progenitors that no longer have the potential to differentiate into erythrocytes or megakaryocytes [87]. These findings are consistent with the decline in

platelets and red blood cells in the peripheral blood (Figure 20), as well as reduced potential of bone marrow cells to give rise to erythroid colonies (Figure 25) in NT-I7-treated animals. Furthermore, our data suggest that NT-I7 enhances the potential for bone marrow cells to differentiate into monocytes and granulocytes, which is also consistent with a corresponding increase in peripheral blood cell numbers. Intriguingly, HPC-1 can be further subdivided into two fractions by Flt3 expression: 1. Lymphoid-primed multipotent progenitors (LMPP) (Flt3⁺). 2. Flt3^{lo} HPC-1. Among the two HPC-1 fractions, LMPP can give rise to CLP, B cells, innate lymphoid cells. Although the number of LMPP was not directly measured in this study, the absolute number of bulk HPC-1 is approximately 28-fold higher in NT-I7 treated mice compare to vehicle group. Interestingly, LMPP can also differentiate into T cells independent of transition into CLP [126]. Moreover, LMPPs have been shown to differentiate into T cells more efficiently than CLPs [126], which may be a possible mechanism of NT-I7-mediated increase in T cell recovery. Additionally, previous studies demonstrated that similar to CLP, a subset of LMPP express IL-7R, which may mediate a direct response to NT-I7 treatment. Although IL-7 does not mediate early lymphoid priming in LMPP, it is required for maintaining cell numbers in the LMPP compartment [127]. IL-7 is known to target CLP and promote lymphoid lineage specification, facilitating differentiation into B cells, T cells, and innate lymphoid cells [88]. Therefore, it is also possible that enhanced T cell numbers was in part contributed by the effect of IL-7 on CLP. Interestingly, the increase

in HPC-1 population coincides with a decline in HSCs with NT-I7 treatment (Figure 24). One explanation is that NT-I7 promotes the differentiation from HSC into downstream progenitor populations through indirect mechanisms since HSCs lack the expression of functional IL-7R. We also examined the effect of NT-I7 on MPP, which are directly generated from HSCs and can give rise to LMPP, GMP, and MEP. Our data suggest that both frequency and absolute number of MPP are significantly increased in NT-I7-treated group (Figure 24), which may explain the corresponding increase in both lymphoid and myeloid population in the peripheral blood. However, as NT-I7 treatment induced a decline in platelets and red blood cells, it may be beneficial to include granulocyte-macrophage colony-stimulating factor (GM-CSF) as a combination therapy to prevent bleeding and anemia.

Having demonstrated the role of NT-I7 in mediating rapid T cell recovery through diverse pathways, we further explored whether NT-I7 treatment leads to functional recovery of T cells. In vitro stimulation assays revealed that NT-I7 treatment preserves the capacity of irradiated T cells to produce both cytotoxic mediators and inflammatory cytokines, including Gzmb, IFN- γ ⁺, and TNF- α (Figure 26). Notably, the frequency of Gzmb⁺ and IFN- γ ⁺ producers are significantly increased compared to T cells isolated from vehicle-treated mice. Moreover, proliferation assays in vitro demonstrated that NT-I7 preserves the proliferative capacity of T cells following TBI.

Taken together, we show that NT-I7 not only leads to rapid T cell recovery reflected by absolute cell counts, but also the functional recovery after TBI exposure.

5. Conclusions and implications

5.1 Overall conclusions

In the current study, we characterized the T cell recovery response to TBI in different settings: 1. Endogenous T cell recovery with TBI alone 2. Donor T cell recovery with TBI as a conditioning regimen in the bone marrow transplant model 3. The role of NT-I7 in mediating T cell recovery through diverse mechanisms. We utilized an in vivo imaging model to characterize systemic T cell recovery in response to radiation, which involves both the thymic-dependent and -independent pathways. We further revealed the unique metabolic and phenotypic profiles of radioresistant T cells that are actively involved in peripheral expansion. In particular, we showed that radioresistant T cells are highly dependent on OXPHOS metabolism during homeostatic proliferation. In contrast, recovery and expansion of donor alloreactive T cells in the bone marrow transplant setting preferentially utilize aerobic glycolysis, which provides metabolic intermediates to fulfill increased metabolic demand. We exploited the metabolic preference of donor alloreactive T cells to prevent GVHD and enhance the functional recovery of donor-derived non-alloreactive T cells that mediate protection from tumor development. Furthermore, we investigated the role of NT-I7 in mediating T cell recovery after TBI. As a recombinant human IL-7 with extended stability in vivo, NT-I7 is a promising candidate that integrates the metabolic requirements and T cell

generation pathways to restore T cell numbers and function. Our data suggest that NT-I7 regulates thymic-dependent and -independent pathways to promote T cell recovery post-TBI. NT-I7 also regulates lineage specification at the HSC and progenitor stage, facilitating the recovery of not only T cells, but also specific myeloid cell types. We further demonstrated that NT-I7 leads to the functional recovery of T cells following TBI.

5.2. Implications and future directions

5.2.1. Understanding the phenotypic, differentiation, and metabolic profiles of unique radioresistant T cell subsets during recovery following TBI

By studying systemic T cell recovery and characterizing the unique transcription profile of radioresistant T cell populations for the first time, we demonstrated direct outcomes and diverse pathways involved in T cell reconstitution in response to radiation. Specifically, we showed that peripheral blood T cell recovery and progenitor cells seeding the thymus are depleted in a TBI dose-dependent manner. Single-cell sequencing data further suggest that both naïve and memory radioresistant T cells undergo peripheral expansion, and significantly upregulate OXPHOS during the process. Approaches that enhance the utilization of OXPHOS, including reagents that modify mitochondrial fission and fusion, can be further tested for their role in enhancing

the proliferative capacity radioresistant T cells. Specifically, mice harboring T cell-specific Drp1 and Opa1 deletions, which are associated with enhanced and reduced OXPHOS utilization, respectively, can be assessed for the recovery of radioresistant T cells following exposure to varying doses of TBI.

We also showed that oxidative stress markers are also increased in radioresistant T cells, which can indicate increased ROS generation during T cell recovery. As oxidative stress which can reduce the metabolic fitness and T cell longevity in vivo, antioxidants that scavenge ROS can be assessed to determine the effect on regulating the survival and size of homeostatic expansion in the TBI setting. Furthermore, since proliferation of radioresistant T cells is a major mechanism of recovery during the lymphopenic period, in vivo functional studies will be able to further validate whether these populations can provide protection against pathogen challenge following TBI.

5.2.2. Reducing the recovery of alloreactive donor T cells while enhancing the functional recovery of non-alloreactive donor T cells through metabolic regulation

By using T cells genetically deficient in glycolysis utilization, we demonstrated that glycolysis is definitively required for alloreactive T cells to induce acute GVHD. We further established a role for glycolysis in promoting donor T cell pathogenicity through regulating proliferation, cell death, and proinflammatory cytokine production. One

potential limitation of 2-DG glycolysis inhibition in the clinical setting is its application as a preventative procedure but not as a curative treatment due to toxicity if administered systemically. However, reagents better tolerated for allogeneic BMT with low toxicity can be used as a curative treatment, including 3-(3-pyridinyl)-1-(4-pyridinyl)-2-propen-1-one, which has been assessed in a murine GVHD model [29]. Overall, the current study demonstrated that we can target glycolysis to selectively inhibit alloreactive donor T cells and prevent GVHD without compromising the functional recovery of donor T cells that mediate anti-tumor activity. Specifically, our findings demonstrated a proof of concept for the ex vivo treatment of donor T cells using glycolysis inhibitors to achieve desired clinical outcome following bone marrow transplantation. Although glycolysis inhibition significantly reduced GVHD in the current study, the treatment did not completely abolish disease development. In addition to glycolysis, pentose phosphate pathway and glutaminolysis are also metabolic processes that fuel the pathogenicity of alloreactive T cells. Future experiments should address the therapeutic potential of simultaneous inhibition of multiple metabolic pathways in addition to glycolysis to reduce the GVHD development. Although T cells demonstrate metabolic plasticity, GVL activity should be further assessed to determine whether the combination of metabolic inhibitors can lead to the preservation of anti-tumor effects.

5.2.3. NT-I7 integrates the requirement for thymic-dependent and -independent pathways, as well as metabolic demands for T cell growth and persistence, to induce rapid T cell recovery following radiation exposure.

As an essential component involved in T cell generation mechanisms in homeostatic conditions, the effect of IL-7 is also coupled to its metabolic regulation of glycolysis, which supports survival and prevents T cell atrophy. In the current study, we demonstrated that NT-I7, a recombinant human IL-7 with extended in vivo half-life, is a promising reagent that enhances T cell recovery following radiation exposure by regulating both thymic-dependent and -independent pathways. Our findings also revealed that NT-I7 ensures the functional recovery of T cells following TBI, indicating the potential to mount an effective immune response against opportunistic pathogens during lymphopenia. In the clinical setting, NT-I7 may be used to boost recall response mediated by radioresistant memory T cells generated during prior exposure to pathogens. Future studies should examine T cell-mediated pathogen clearance following total body irradiation. Effect of NT-I7 in mediating survival in infectious models can be assessed in both the acute and chronic setting. For example, a murine model of cytomegalovirus (CMV), a primary risk factor for bone marrow transplant-associated morbidity and mortality, can be used to determine T cell-mediated viral clearance. Specifically, the presence and activity of MCMV-specific CD8 T cells can be detected using MHC class I tetramers along with activation markers and inflammatory cytokines,

including CD44 and IFN- γ , respectively. In addition to T cell activation and survival outcomes, viral clearance through NT-I7-mediated T cell recovery can be assessed through MCMV DNA detection in various organs.

In addition to enhanced T cell reconstitution with NT-I7 administration, we further demonstrated the capacity of NT-I7 to enhance the recovery of specific myeloid lineages, potentially by modulating the frequency and absolute numbers of bone marrow-derived stem and progenitor cells. The enhanced recovery of neutrophils and monocytes induced by NT-I7 treatment may be capable of strengthening the first line of defense against infections. Further studies can also address whether NT-I7-mediated recovery of neutrophil and monocytes contribute to enhanced innate immunity through immunophenotyping and relevant infectious models.

We have also demonstrated the effect of NT-I7 on hematopoietic stem and progenitors, which affects subsequent differentiation capacity into distinct lymphoid and myeloid subsets. Specifically, we showed that NT-I7 enhances the absolute number of HPC-1 fraction within the bone marrow, which contains both LMPP and Flt3^{lo} cells. Further experiments should elucidate whether NT-I7 directly modulates the recovery of LMPP cells within the HPC-1 fraction through Flt3 expression. An increase in the LMPP fraction, which can give rise to both CLP and GMP, potentially contributes to enhanced innate and adaptive immunity upon pathogen challenge.

In conclusion, our studies demonstrated the therapeutic potentials of NT-I7-induced T cell reconstitution following total body irradiation to reduce the window of susceptibility to opportunistic pathogens. Future translational studies will further explore the efficacy of T cell-mediated immunity with NT-I7 administration in both murine and nonhuman primate models.

References

- [1] J.K. Waselenko, T.J. MacVittie, W.F. Blakely, N. Pesik, A.L. Wiley, W.E. Dickerson, H. Tsu, D.L. Confer, C.N. Coleman, T. Seed, P. Lowry, J.O. Armitage, and N. Dainiak, Medical management of the acute radiation syndrome: recommendations of the Strategic National Stockpile Radiation Working Group. *Annals of internal medicine* 140 (2004) 1037-51.
- [2] M. Hagby, A. Goldberg, S. Becker, D. Schwartz, and Y. Bar-Dayan, Health implications of radiological terrorism: Perspectives from Israel. *Journal of emergencies, trauma, and shock* 2 (2009) 117-23.
- [3] A. Ravichandran, J. Clegg, M.N. Adams, M. Hampson, A. Fielding, and L.J. Bray, 3D Breast Tumor Models for Radiobiology Applications. *Cancers* 13 (2021).
- [4] T.J. MacVittie, A.W. Bennett, V.C. M, A.M. Farese, A. Higgins, and K.G. Hankey, Immune cell reconstitution after exposure to potentially lethal doses of radiation in the nonhuman primate. *Health physics* 106 (2014) 84-96.
- [5] D. Schaeue, and W.H. McBride, T lymphocytes and normal tissue responses to radiation. *Frontiers in oncology* 2 (2012) 119.
- [6] J.L. Pugh, A.S. Sukhina, T.M. Seed, N.R. Manley, G.D. Sempowski, M.R. van den Brink, M.J. Smithey, and J. Nikolich-Zugich, Histone deacetylation critically determines T cell subset radiosensitivity. *Journal of immunology (Baltimore, Md. : 1950)* 193 (2014) 1451-8.
- [7] S. Xiao, I.D. Shterev, W. Zhang, L. Young, J.H. Shieh, M. Moore, M. van den Brink, G.D. Sempowski, and N.R. Manley, Sublethal Total Body Irradiation Causes Long-Term Deficits in Thymus Function by Reducing Lymphoid Progenitors. *Journal of immunology (Baltimore, Md. : 1950)* 199 (2017) 2701-2712.
- [8] K. Sudo, H. Ema, Y. Morita, and H. Nakauchi, Age-associated characteristics of murine hematopoietic stem cells. *The Journal of experimental medicine* 192 (2000) 1273-80.
- [9] J.L. Ferrara, J.E. Levine, P. Reddy, and E. Holler, Graft-versus-host disease. *Lancet (London, England)* 373 (2009) 1550-61.
- [10] M. Jagasia, M. Arora, M.E.D. Flowers, N.J. Chao, P.L. McCarthy, C.S. Cutler, A. Urbano-Ispizua, S.Z. Pavletic, M.D. Haagenson, M.-J. Zhang, J.H. Antin, B.J. Bolwell, C. Bredeson, J.-Y. Cahn, M. Cairo, R.P. Gale, V. Gupta, S.J. Lee, M.

- Litzow, D.J. Weisdorf, M.M. Horowitz, and T. Hahn, Risk factors for acute GVHD and survival after hematopoietic cell transplantation. *Blood* 119 (2012) 296-307.
- [11] A.D. Leiper, Late effects of total body irradiation. *Archives of disease in childhood* 72 (1995) 382-5.
- [12] W. Krenger, B.R. Blazar, and G.A. Holländer, Thymic T-cell development in allogeneic stem cell transplantation. *Blood* 117 (2011) 6768-76.
- [13] B.J. Chen, X. Cui, G.D. Sempowski, J. Domen, and N.J. Chao, Hematopoietic stem cell dose correlates with the speed of immune reconstitution after stem cell transplantation. *Blood* 103 (2004) 4344-52.
- [14] A.J. Barrett, Mechanisms of the graft-versus-leukemia reaction. *Stem cells* (Dayton, Ohio) 15 (1997) 248-58.
- [15] R. Zeiser, and B.R. Blazar, Acute Graft-versus-Host Disease - Biologic Process, Prevention, and Therapy. *The New England journal of medicine* 377 (2017) 2167-2179.
- [16] A. Bacigalupo, M.T. Van Lint, D. Occhini, F. Gualandi, T. Lamparelli, G. Sogno, E. Tedone, F. Frassoni, J. Tong, and A.M. Marmont, Increased risk of leukemia relapse with high-dose cyclosporine A after allogeneic marrow transplantation for acute leukemia. *Blood* 77 (1991) 1423-8.
- [17] F. Locatelli, M. Zecca, R. Rondelli, F. Bonetti, G. Dini, A. Prete, C. Messina, C. Uderzo, M. Ripaldi, F. Porta, G. Giorgiani, E. Giraldi, and A. Pession, Graft versus host disease prophylaxis with low-dose cyclosporine-A reduces the risk of relapse in children with acute leukemia given HLA-identical sibling bone marrow transplantation: results of a randomized trial. *Blood* 95 (2000) 1572-9.
- [18] C.H. Weaver, R.A. Clift, H.J. Deeg, R. Storb, F.R. Appelbaum, W. Bensinger, K. Doney, J.A. Hansen, P.O. Martin, J. Sanders, and et al., Effect of graft-versus-host disease prophylaxis on relapse in patients transplanted for acute myeloid leukemia. *Bone marrow transplantation* 14 (1994) 885-93.
- [19] M.A. Schroeder, and J.F. DiPersio, Mouse models of graft-versus-host disease: advances and limitations. *Disease models & mechanisms* 4 (2011) 318-33.
- [20] N.M. Chapman, M.R. Boothby, and H. Chi, Metabolic coordination of T cell quiescence and activation. *Nature Reviews Immunology* 20 (2020) 55-70.

- [21] E.L. Pearce, M.C. Poffenberger, C.H. Chang, and R.G. Jones, Fueling immunity: insights into metabolism and lymphocyte function. *Science (New York, N.Y.)* 342 (2013) 1242454.
- [22] C.-H. Chang, Jonathan D. Curtis, Leonard B. Maggi, Jr., B. Faubert, Alejandro V. Villarino, D. O'Sullivan, Stanley C.-C. Huang, Gerritje J.W. van der Windt, J. Blagih, J. Qiu, Jason D. Weber, Edward J. Pearce, Russell G. Jones, and Erika L. Pearce, Posttranscriptional Control of T Cell Effector Function by Aerobic Glycolysis. *Cell* 153 (2013) 1239-1251.
- [23] A.V. Menk, N.E. Scharping, R.S. Moreci, X. Zeng, C. Guy, S. Salvatore, H. Bae, J. Xie, H.A. Young, S.G. Wendell, and G.M. Delgoffe, Early TCR Signaling Induces Rapid Aerobic Glycolysis Enabling Distinct Acute T Cell Effector Functions. *Cell Reports* 22 (2018) 1509-1521.
- [24] L. Araujo, P. Khim, H. Mkhikian, C.L. Mortales, and M. Demetriou, Glycolysis and glutaminolysis cooperatively control T cell function by limiting metabolite supply to N-glycosylation. *eLife* 6 (2017).
- [25] W. Li, G. Qu, S.C. Choi, C. Cornaby, A. Titov, N. Kanda, X. Teng, H. Wang, and L. Morel, Targeting T Cell Activation and Lupus Autoimmune Phenotypes by Inhibiting Glucose Transporters. *Frontiers in immunology* 10 (2019) 833.
- [26] R.T. Liu, M. Zhang, C.L. Yang, P. Zhang, N. Zhang, T. Du, M.R. Ge, L.T. Yue, X.L. Li, H. Li, and R.S. Duan, Enhanced glycolysis contributes to the pathogenesis of experimental autoimmune neuritis. *Journal of neuroinflammation* 15 (2018) 51.
- [27] A.N. Macintyre, V.A. Gerriets, A.G. Nichols, R.D. Michalek, M.C. Rudolph, D. Deoliveira, S.M. Anderson, E.D. Abel, B.J. Chen, L.P. Hale, and J.C. Rathmell, The glucose transporter Glut1 is selectively essential for CD4 T cell activation and effector function. *Cell Metab* 20 (2014) 61-72.
- [28] S.E. Stimpson, J. Chen, B.N. Newby, R.B. Khattri, H. Chapman, T. Angelini, M. Merritt, D. Serreze, and C.J.b. Mathews, Human CD8+ T-cells Require Glycolysis to Elicit Effector Function. (2020).
- [29] H.D. Nguyen, S. Chatterjee, K.M.K. Haarberg, Y. Wu, D. Bastian, J. Heinrichs, J. Fu, A. Daenthansanmak, S. Schutt, S. Shrestha, C. Liu, H. Wang, H. Chi, S. Mehrotra, and X.-Z. Yu, Metabolic reprogramming of alloantigen-activated T cells after hematopoietic cell transplantation. *The Journal of Clinical Investigation* 126 (2016) 1337-1352.

- [30] C.A. Byersdorfer, V. Tkachev, A.W. Opipari, S. Goodell, J. Swanson, S. Sandquist, G.D. Glick, and J.L.M. Ferrara, Effector T cells require fatty acid metabolism during murine graft-versus-host disease. *Blood* 122 (2013) 3230-3237.
- [31] G.D. Glick, R. Rossignol, C.A. Lyssiotis, D. Wahl, C. Lesch, B. Sanchez, X. Liu, L.Y. Hao, C. Taylor, A. Hurd, J.L. Ferrara, V. Tkachev, C.A. Byersdorfer, L. Boros, and A.W. Opipari, Anaplerotic metabolism of alloreactive T cells provides a metabolic approach to treat graft-versus-host disease. *The Journal of pharmacology and experimental therapeutics* 351 (2014) 298-307.
- [32] G.D. Whitehill, S. Amarnath, P. Muranski, K. Keyvanfar, M. Battiwalla, A.J. Barrett, and D. Chinnassamy, Adenosine Selectively Depletes Alloreactive T Cells to Prevent GVHD While Conserving Immunity to Viruses and Leukemia. *Molecular therapy : the journal of the American Society of Gene Therapy* 24 (2016) 1655-64.
- [33] Y. Chalandon, S. Degermann, J. Villard, L. Arlettaz, L. Kaiser, S. Vischer, S. Walter, M.H. Heemskerk, R.A. van Lier, C. Helg, B. Chapuis, and E. Roosnek, Pretransplantation CMV-specific T cells protect recipients of T-cell-depleted grafts against CMV-related complications. *Blood* 107 (2006) 389-96.
- [34] M.A. Biernacki, V.S. Sheth, and M. Bleakley, T cell optimization for graft-versus-leukemia responses. *JCI insight* 5 (2020).
- [35] D.I. van der Lee, R.M. Reijmers, M.W. Honders, R.S. Hagedoorn, R.C. de Jong, M.G. Kester, D.M. van der Steen, A.H. de Ru, C. Kweekel, H.M. Bijen, I. Jedema, H. Veelken, P.A. van Veelen, M.H. Heemskerk, J.H.F. Falkenburg, and M. Griffioen, Mutated nucleophosmin 1 as immunotherapy target in acute myeloid leukemia. *J Clin Invest* 129 (2019) 774-785.
- [36] M. Sukumar, R.J. Kishton, and N.P. Restifo, Metabolic reprogramming of anti-tumor immunity. *Current opinion in immunology* 46 (2017) 14-22.
- [37] M. Peng, N. Yin, S. Chhangawala, K. Xu, C.S. Leslie, and M.O. Li, Aerobic glycolysis promotes T helper 1 cell differentiation through an epigenetic mechanism. *Science (New York, N.Y.)* 354 (2016) 481-484.
- [38] Z. Tothova, R. Kollipara, B.J. Huntly, B.H. Lee, D.H. Castrillon, D.E. Cullen, E.P. McDowell, S. Lazo-Kallanian, I.R. Williams, C. Sears, S.A. Armstrong, E. Passegué, R.A. DePinho, and D.G. Gilliland, FoxOs are critical mediators of hematopoietic stem cell resistance to physiologic oxidative stress. *Cell* 128 (2007) 325-39.

- [39] E.L. Pearce, M.C. Walsh, P.J. Cejas, G.M. Harms, H. Shen, L.S. Wang, R.G. Jones, and Y. Choi, Enhancing CD8 T-cell memory by modulating fatty acid metabolism. *Nature* 460 (2009) 103-7.
- [40] M. Sukumar, J. Liu, Y. Ji, M. Subramanian, J.G. Crompton, Z. Yu, R. Roychoudhuri, D.C. Palmer, P. Muranski, E.D. Karoly, R.P. Mohny, C.A. Klebanoff, A. Lal, T. Finkel, N.P. Restifo, and L. Gattinoni, Inhibiting glycolytic metabolism enhances CD8+ T cell memory and antitumor function. *J Clin Invest* 123 (2013) 4479-88.
- [41] L.C. Osborne, S. Dhanji, J.W. Snow, J.J. Priatel, M.C. Ma, M.J. Miners, H.S. Teh, M.A. Goldsmith, and N. Abraham, Impaired CD8 T cell memory and CD4 T cell primary responses in IL-7R alpha mutant mice. *The Journal of experimental medicine* 204 (2007) 619-31.
- [42] D. Chen, T.X. Tang, H. Deng, X.P. Yang, and Z.H. Tang, Interleukin-7 Biology and Its Effects on Immune Cells: Mediator of Generation, Differentiation, Survival, and Homeostasis. *Frontiers in immunology* 12 (2021) 747324.
- [43] C.L. Mackall, T.J. Fry, and R.E. Gress, Harnessing the biology of IL-7 for therapeutic application. *Nature reviews. Immunology* 11 (2011) 330-42.
- [44] C.D. Surh, and J. Sprent, Regulation of mature T cell homeostasis. *Seminars in immunology* 17 (2005) 183-91.
- [45] C.D. Surh, and J. Sprent, Homeostasis of naive and memory T cells. *Immunity* 29 (2008) 848-62.
- [46] D. Kamimura, and M.J. Bevan, Naive CD8+ T cells differentiate into protective memory-like cells after IL-2 anti IL-2 complex treatment in vivo. *The Journal of experimental medicine* 204 (2007) 1803-12.
- [47] S.R. Jacobs, R.D. Michalek, and J.C. Rathmell, IL-7 is essential for homeostatic control of T cell metabolism in vivo. *Journal of immunology (Baltimore, Md. : 1950)* 184 (2010) 3461-9.
- [48] G. Cui, M.M. Staron, S.M. Gray, P.C. Ho, R.A. Amezcua, J. Wu, and S.M. Kaech, IL-7-Induced Glycerol Transport and TAG Synthesis Promotes Memory CD8+ T Cell Longevity. *Cell* 161 (2015) 750-61.
- [49] S.G. Nanjappa, E.H. Kim, and M. Suresh, Immunotherapeutic effects of IL-7 during a chronic viral infection in mice. *Blood* 117 (2011) 5123-32.

- [50] C. Sportès, R.R. Babb, M.C. Krumlauf, F.T. Hakim, S.M. Steinberg, C.K. Chow, M.R. Brown, T.A. Fleisher, P. Noel, I. Maric, M. Stetler-Stevenson, J. Engel, R. Buffet, M. Morre, R.J. Amato, A. Pecora, C.L. Mackall, and R.E. Gress, Phase I study of recombinant human interleukin-7 administration in subjects with refractory malignancy. *Clinical cancer research : an official journal of the American Association for Cancer Research* 16 (2010) 727-35.
- [51] S.W. Lee, D. Choi, M. Heo, E.C. Shin, S.H. Park, S.J. Kim, Y.K. Oh, B.H. Lee, S.H. Yang, Y.C. Sung, and H. Lee, hIL-7-hyFc, A Long-Acting IL-7, Increased Absolute Lymphocyte Count in Healthy Subjects. *Clinical and translational science* 13 (2020) 1161-1169.
- [52] J.T. Sockolosky, and F.C. Szoka, The neonatal Fc receptor, FcRn, as a target for drug delivery and therapy. *Advanced drug delivery reviews* 91 (2015) 109-24.
- [53] A.W. Goldrath, C.J. Luckey, R. Park, C. Benoist, and D. Mathis, The molecular program induced in T cells undergoing homeostatic proliferation. *Proceedings of the National Academy of Sciences of the United States of America* 101 (2004) 16885-90.
- [54] E. Gatza, D.R. Wahl, A.W. Pipari, T.B. Sundberg, P. Reddy, C. Liu, G.D. Glick, and J.L. Ferrara, Manipulating the bioenergetics of alloreactive T cells causes their selective apoptosis and arrests graft-versus-host disease. *Science translational medicine* 3 (2011) 67ra8.
- [55] N.J. Maciver, S.R. Jacobs, H.L. Wieman, J.A. Wofford, J.L. Coloff, and J.C. Rathmell, Glucose metabolism in lymphocytes is a regulated process with significant effects on immune cell function and survival. *Journal of leukocyte biology* 84 (2008) 949-57.
- [56] B. Everts, E. Amiel, S.C. Huang, A.M. Smith, C.H. Chang, W.Y. Lam, V. Redmann, T.C. Freitas, J. Blagih, G.J. van der Windt, M.N. Artyomov, R.G. Jones, E.L. Pearce, and E.J. Pearce, TLR-driven early glycolytic reprogramming via the kinases TBK1- $IKK\epsilon$ supports the anabolic demands of dendritic cell activation. *Nature immunology* 15 (2014) 323-32.
- [57] B. Everts, E. Amiel, G.J. van der Windt, T.C. Freitas, R. Chott, K.E. Yarasheski, E.L. Pearce, and E.J. Pearce, Commitment to glycolysis sustains survival of NO-producing inflammatory dendritic cells. *Blood* 120 (2012) 1422-31.
- [58] C.M. Krawczyk, T. Holowka, J. Sun, J. Blagih, E. Amiel, R.J. DeBerardinis, J.R. Cross, E. Jung, C.B. Thompson, R.G. Jones, and E.J. Pearce, Toll-like receptor-induced

changes in glycolytic metabolism regulate dendritic cell activation. *Blood* 115 (2010) 4742-4749.

- [59] H. Fujiwara, Y. Maeda, K. Kobayashi, H. Nishimori, K. Matsuoka, N. Fujii, E. Kondo, T. Tanaka, L. Chen, M. Azuma, H. Yagita, and M. Tanimoto, Programmed death-1 pathway in host tissues ameliorates Th17/Th1-mediated experimental chronic graft-versus-host disease. *Journal of immunology* (Baltimore, Md. : 1950) 193 (2014) 2565-73.
- [60] A. Saha, K. Aoyama, P.A. Taylor, B.H. Koehn, R.G. Veenstra, A. Panoskaltsis-Mortari, D.H. Munn, W.J. Murphy, M. Azuma, H. Yagita, B.T. Fife, M.H. Sayegh, N. Najafian, G. Socie, R. Ahmed, G.J. Freeman, A.H. Sharpe, and B.R. Blazar, Host programmed death ligand 1 is dominant over programmed death ligand 2 expression in regulating graft-versus-host disease lethality. *Blood* 122 (2013) 3062-73.
- [61] S.R. Jacobs, C.E. Herman, N.J. Maciver, J.A. Wofford, H.L. Wieman, J.J. Hammen, and J.C. Rathmell, Glucose uptake is limiting in T cell activation and requires CD28-mediated Akt-dependent and independent pathways. *Journal of immunology* (Baltimore, Md. : 1950) 180 (2008) 4476-86.
- [62] R.D. Michalek, V.A. Gerriets, S.R. Jacobs, A.N. Macintyre, N.J. MacIver, E.F. Mason, S.A. Sullivan, A.G. Nichols, and J.C. Rathmell, Cutting edge: distinct glycolytic and lipid oxidative metabolic programs are essential for effector and regulatory CD4+ T cell subsets. *Journal of immunology* (Baltimore, Md. : 1950) 186 (2011) 3299-303.
- [63] C. Sportès, F.T. Hakim, S.A. Memon, H. Zhang, K.S. Chua, M.R. Brown, T.A. Fleisher, M.C. Krumlauf, R.R. Babb, C.K. Chow, T.J. Fry, J. Engels, R. Buffet, M. Morre, R.J. Amato, D.J. Venzon, R. Korngold, A. Pecora, R.E. Gress, and C.L. Mackall, Administration of rhIL-7 in humans increases in vivo TCR repertoire diversity by preferential expansion of naive T cell subsets. *The Journal of experimental medicine* 205 (2008) 1701-14.
- [64] T. Stuart, A. Butler, P. Hoffman, C. Hafemeister, E. Papalexi, W.M. Mauck, 3rd, Y. Hao, M. Stoeckius, P. Smibert, and R. Satija, Comprehensive Integration of Single-Cell Data. *Cell* 177 (2019) 1888-1902.e21.
- [65] X. Qiu, Q. Mao, Y. Tang, L. Wang, R. Chawla, H.A. Pliner, and C. Trapnell, Reversed graph embedding resolves complex single-cell trajectories. *Nature methods* 14 (2017) 979-982.

- [66] A. Caro-Maldonado, R. Wang, A.G. Nichols, M. Kuraoka, S. Milasta, L.D. Sun, A.L. Gavin, E.D. Abel, G. Kelsoe, D.R. Green, and J.C. Rathmell, Metabolic reprogramming is required for antibody production that is suppressed in anergic but exaggerated in chronically BAFF-exposed B cells. *Journal of immunology* (Baltimore, Md. : 1950) 192 (2014) 3626-36.
- [67] B.V. Kumar, T.J. Connors, and D.L. Farber, Human T Cell Development, Localization, and Function throughout Life. *Immunity* 48 (2018) 202-213.
- [68] J.J. Thome, B. Grinshpun, B.V. Kumar, M. Kubota, Y. Ohmura, H. Lerner, G.D. Sempowski, Y. Shen, and D.L. Farber, Longterm maintenance of human naive T cells through in situ homeostasis in lymphoid tissue sites. *Science immunology* 1 (2016).
- [69] J.J. Thome, N. Yudanin, Y. Ohmura, M. Kubota, B. Grinshpun, T. Sathaliyawala, T. Kato, H. Lerner, Y. Shen, and D.L. Farber, Spatial map of human T cell compartmentalization and maintenance over decades of life. *Cell* 159 (2014) 814-28.
- [70] S. Moertl, D. Buschmann, O. Azimzadeh, M. Schneider, R. Kell, K. Winkler, S. Tapio, S. Hornhardt, J. Merl-Pham, M.W. Pfaffl, and M.J. Atkinson, Radiation Exposure of Peripheral Mononuclear Blood Cells Alters the Composition and Function of Secreted Extracellular Vesicles. *International journal of molecular sciences* 21 (2020).
- [71] P.D. Issuree, C.P. Ng, and D.R. Littman, Heritable Gene Regulation in the CD4:CD8 T Cell Lineage Choice. *Frontiers in immunology* 8 (2017) 291.
- [72] R. Wang, Christopher P. Dillon, Lewis Z. Shi, S. Milasta, R. Carter, D. Finkelstein, Laura L. McCormick, P. Fitzgerald, H. Chi, J. Munger, and Douglas R. Green, The Transcription Factor Myc Controls Metabolic Reprogramming upon T Lymphocyte Activation. *Immunity* 35 (2011) 871-882.
- [73] H. Chi, Regulation and function of mTOR signalling in T cell fate decisions. *Nature Reviews Immunology* 12 (2012) 325-338.
- [74] Y. Zhao, B.J. Altman, J.L. Coloff, C.E. Herman, S.R. Jacobs, H.L. Wieman, J.A. Wofford, L.N. Dimascio, O. Ilkayeva, A. Kelekar, T. Reya, and J.C. Rathmell, Glycogen synthase kinase 3alpha and 3beta mediate a glucose-sensitive antiapoptotic signaling pathway to stabilize Mcl-1. *Molecular and cellular biology* 27 (2007) 4328-39.

- [75] B.J. Altman, and J.C. Rathmell, Metabolic stress in autophagy and cell death pathways. *Cold Spring Harbor perspectives in biology* 4 (2012) a008763.
- [76] F.M. Wensveen, K.P. van Gisbergen, I.A. Derks, C. Gerlach, T.N. Schumacher, R.A. van Lier, and E. Eldering, Apoptosis threshold set by Noxa and Mcl-1 after T cell activation regulates competitive selection of high-affinity clones. *Immunity* 32 (2010) 754-65.
- [77] F.M. Wensveen, N.L. Alves, I.A. Derks, K.A. Reedquist, and E. Eldering, Apoptosis induced by overall metabolic stress converges on the Bcl-2 family proteins Noxa and Mcl-1. *Apoptosis : an international journal on programmed cell death* 16 (2011) 708-21.
- [78] C. Granchi, and F. Minutolo, Anticancer agents that counteract tumor glycolysis. *ChemMedChem* 7 (2012) 1318-50.
- [79] T.J. Lampidis, M. Kurtoglu, J.C. Maher, H. Liu, A. Krishan, V. Sheft, S. Szymanski, I. Fokt, W.R. Rudnicki, K. Ginalski, B. Lesyng, and W. Priebe, Efficacy of 2-halogen substituted D-glucose analogs in blocking glycolysis and killing "hypoxic tumor cells". *Cancer chemotherapy and pharmacology* 58 (2006) 725-34.
- [80] B.K. Mohanti, G.K. Rath, N. Anantha, V. Kannan, B.S. Das, B.A. Chandramouli, A.K. Banerjee, S. Das, A. Jena, R. Ravichandran, U.P. Sahi, R. Kumar, N. Kapoor, V.K. Kalia, B.S. Dwarakanath, and V. Jain, Improving cancer radiotherapy with 2-deoxy-D-glucose: phase I/II clinical trials on human cerebral gliomas. *International journal of radiation oncology, biology, physics* 35 (1996) 103-11.
- [81] S.-C. Choi, A.A. Titov, G. Abboud, H.R. Seay, T.M. Brusko, D.C. Roopenian, S. Salek-Ardakani, and L. Morel, Inhibition of glucose metabolism selectively targets autoreactive follicular helper T cells. *Nature Communications* 9 (2018) 4369.
- [82] L.E. Raez, K. Papadopoulos, A.D. Ricart, E.G. Chiorean, R.S. Dipaola, M.N. Stein, C.M. Rocha Lima, J.J. Schlesselman, K. Tolba, V.K. Langmuir, S. Kroll, D.T. Jung, M. Kurtoglu, J. Rosenblatt, and T.J. Lampidis, A phase I dose-escalation trial of 2-deoxy-D-glucose alone or combined with docetaxel in patients with advanced solid tumors. *Cancer chemotherapy and pharmacology* 71 (2013) 523-30.
- [83] M. Stein, H. Lin, C. Jeyamohan, D. Dvorzinski, M. Gounder, K. Bray, S. Eddy, S. Goodin, E. White, and R.S. Dipaola, Targeting tumor metabolism with 2-deoxyglucose in patients with castrate-resistant prostate cancer and advanced malignancies. *The Prostate* 70 (2010) 1388-94.

- [84] Y. Yin, S.C. Choi, Z. Xu, D.J. Perry, H. Seay, B.P. Croker, E.S. Sobel, T.M. Brusko, and L. Morel, Normalization of CD4+ T cell metabolism reverses lupus. *Science translational medicine* 7 (2015) 274ra18.
- [85] M.K. Slifka, J.K. Whitmire, and R. Ahmed, Bone marrow contains virus-specific cytotoxic T lymphocytes. *Blood* 90 (1997) 2103-8.
- [86] Q. Yu, B. Erman, J.H. Park, L. Feigenbaum, and A. Singer, IL-7 receptor signals inhibit expression of transcription factors TCF-1, LEF-1, and RORgammat: impact on thymocyte development. *The Journal of experimental medicine* 200 (2004) 797-803.
- [87] H. Oguro, L. Ding, and S.J. Morrison, SLAM family markers resolve functionally distinct subpopulations of hematopoietic stem cells and multipotent progenitors. *Cell stem cell* 13 (2013) 102-16.
- [88] E. Velardi, J.J. Tsai, and M.R.M. van den Brink, T cell regeneration after immunological injury. *Nature reviews. Immunology* 21 (2021) 277-291.
- [89] M. Yamazaki, T. Yajima, M. Tanabe, K. Fukui, E. Okada, R. Okamoto, S. Oshima, T. Nakamura, T. Kanai, M. Uehira, T. Takeuchi, H. Ishikawa, T. Hibi, and M. Watanabe, Mucosal T cells expressing high levels of IL-7 receptor are potential targets for treatment of chronic colitis. *Journal of immunology (Baltimore, Md. : 1950)* 171 (2003) 1556-63.
- [90] I. den Braber, T. Mugwagwa, N. Vrisekoop, L. Westera, R. Mögling, A.B. de Boer, N. Willems, E.H. Schrijver, G. Spierenburg, K. Gaiser, E. Mul, S.A. Otto, A.F. Ruiter, M.T. Ackermans, F. Miedema, J.A. Borghans, R.J. de Boer, and K. Tesselaar, Maintenance of peripheral naive T cells is sustained by thymus output in mice but not humans. *Immunity* 36 (2012) 288-97.
- [91] O. Desouky, N. Ding, and G. Zhou, Targeted and non-targeted effects of ionizing radiation. *Journal of Radiation Research and Applied Sciences* 8 (2015) 247-254.
- [92] M.D. Buck, D. O'Sullivan, and E.L. Pearce, T cell metabolism drives immunity. *Journal of Experimental Medicine* 212 (2015) 1345-1360.
- [93] J.C. Assmann, D.E. Farthing, K. Saito, N. Maglakelidze, B. Oliver, K.A. Warrick, C. Sourbier, C.J. Ricketts, T.J. Meyer, S.Z. Pavletic, W.M. Linehan, M.C. Krishna, R.E. Gress, and N.P. Buxbaum, Glycolytic metabolism of pathogenic T cells enables early detection of GVHD by ¹³C-MRI. *Blood* 137 (2021) 126-137.

- [94] M. Stelljes, S. Hermann, J. Albring, G. Köhler, M. Löffler, C. Franzius, C. Poremba, V. Schlösser, S. Volkmann, C. Opitz, C. Bremer, T. Kucharzik, G. Silling, O. Schober, W.E. Berdel, M. Schäfers, and J. Kienast, Clinical molecular imaging in intestinal graft-versus-host disease: mapping of disease activity, prediction, and monitoring of treatment efficiency by positron emission tomography. *Blood* 111 (2008) 2909-2918.
- [95] K. Düvel, J.L. Yecies, S. Menon, P. Raman, A.I. Lipovsky, A.L. Souza, E. Triantafellow, Q. Ma, R. Gorski, S. Cleaver, M.G. Vander Heiden, J.P. MacKeigan, P.M. Finan, C.B. Clish, L.O. Murphy, and B.D. Manning, Activation of a metabolic gene regulatory network downstream of mTOR complex 1. *Molecular cell* 39 (2010) 171-83.
- [96] T. Porstmann, C.R. Santos, B. Griffiths, M. Cully, M. Wu, S. Leever, J.R. Griffiths, Y.-L. Chung, and A. Schulze, SREBP Activity Is Regulated by mTORC1 and Contributes to Akt-Dependent Cell Growth. *Cell Metabolism* 8 (2008) 224-236.
- [97] J.D. Powell, K.N. Pollizzi, E.B. Heikamp, and M.R. Horton, Regulation of immune responses by mTOR. *Annual review of immunology* 30 (2012) 39-68.
- [98] S. Herzig, and R.J. Shaw, AMPK: guardian of metabolism and mitochondrial homeostasis. *Nature reviews. Molecular cell biology* 19 (2018) 121-135.
- [99] J.L. Coloff, E.F. Mason, B.J. Altman, V.A. Gerriets, T. Liu, A.N. Nichols, Y. Zhao, J.A. Wofford, S.R. Jacobs, O. Ilkayeva, S.P. Garrison, G.P. Zambetti, and J.C. Rathmell, Akt requires glucose metabolism to suppress puma expression and prevent apoptosis of leukemic T cells. *The Journal of biological chemistry* 286 (2011) 5921-33.
- [100] Y. Zhao, J.L. Coloff, E.C. Ferguson, S.R. Jacobs, K. Cui, and J.C. Rathmell, Glucose metabolism attenuates p53 and Puma-dependent cell death upon growth factor deprivation. *The Journal of biological chemistry* 283 (2008) 36344-53.
- [101] L.A. Pradelli, M. Bénétiau, C. Chauvin, M.A. Jacquin, S. Marchetti, C. Muñoz-Pinedo, P. Auberger, M. Pende, and J.E. Ricci, Glycolysis inhibition sensitizes tumor cells to death receptors-induced apoptosis by AMP kinase activation leading to Mcl-1 block in translation. *Oncogene* 29 (2010) 1641-52.
- [102] U. Maurer, C. Charvet, A.S. Wagman, E. Dejardin, and D.R. Green, Glycogen synthase kinase-3 regulates mitochondrial outer membrane permeabilization and apoptosis by destabilization of MCL-1. *Molecular cell* 21 (2006) 749-60.

- [103] Q. Zhong, W. Gao, F. Du, and X. Wang, Mule/ARF-BP1, a BH3-Only E3 Ubiquitin Ligase, Catalyzes the Polyubiquitination of Mcl-1 and Regulates Apoptosis. *Cell* 121 (2005) 1085-1095.
- [104] K.W. Adams, and G.M. Cooper, Rapid turnover of mcl-1 couples translation to cell survival and apoptosis. *The Journal of biological chemistry* 282 (2007) 6192-200.
- [105] K. Renner, A.L. Geiselhöringer, M. Fante, C. Bruss, S. Färber, G. Schönhammer, K. Peter, K. Singer, R. Andreesen, P. Hoffmann, P. Oefner, W. Herr, and M. Kreutz, Metabolic plasticity of human T cells: Preserved cytokine production under glucose deprivation or mitochondrial restriction, but 2-deoxy-glucose affects effector functions. *European journal of immunology* 45 (2015) 2504-16.
- [106] F. Aversa, A. Tabilio, A. Velardi, I. Cunningham, A. Terenzi, F. Falzetti, L. Ruggeri, G. Barbabietola, C. Aristei, P. Latini, Y. Reisner, and M.F. Martelli, Treatment of high-risk acute leukemia with T-cell-depleted stem cells from related donors with one fully mismatched HLA haplotype. *The New England journal of medicine* 339 (1998) 1186-93.
- [107] A. Urbano-Ispizua, C. Rozman, P. Pimentel, C. Solano, J. de la Rubia, S. Brunet, J. Pérez-Oteiza, C. Ferrá, J. Zuazu, D. Caballero, A. Carvalhais, J.L. Díez, I. Espigado, C. Martínez, F. Campilho, M.A. Sanz, J. Sierra, J. García-Conde, and E. Montserrat, The number of donor CD3(+) cells is the most important factor for graft failure after allogeneic transplantation of CD34(+) selected cells from peripheral blood from HLA-identical siblings. *Blood* 97 (2001) 383-7.
- [108] A. Urbano-Ispizua, C. Rozman, P. Pimentel, C. Solano, J. de la Rubia, S. Brunet, J. Pérez-Oteyza, C. Ferrá, J. Zuazu, D. Caballero, J. Bargay, A. Carvalhais, J.L. Díez, I. Espigado, A. Alegre, M. Rovira, F. Campilho, J. Odriozola, M.A. Sanz, J. Sierra, J. García-Conde, and E. Montserrat, Risk factors for acute graft-versus-host disease in patients undergoing transplantation with CD34+ selected blood cells from HLA-identical siblings. *Blood* 100 (2002) 724-7.
- [109] P. Zhang, B.J. Chen, and N.J. Chao, Prevention of GVHD without losing GVL effect: windows of opportunity. *Immunologic research* 49 (2011) 49-55.
- [110] Michael D. Buck, D. O'Sullivan, Ramon I. Klein Geltink, Jonathan D. Curtis, C.-H. Chang, David E. Sanin, J. Qiu, O. Kretz, D. Braas, Gerritje J.W. van der Windt, Q. Chen, Stanley C.-C. Huang, Christina M. O'Neill, Brian T. Edelson, Edward J. Pearce, H. Sesaki, Tobias B. Huber, Angelika S. Rambold, and Erika L. Pearce,

Mitochondrial Dynamics Controls T Cell Fate through Metabolic Programming. *Cell* 166 (2016) 63-76.

- [111] G.J. van der Windt, and E.L. Pearce, Metabolic switching and fuel choice during T-cell differentiation and memory development. *Immunological reviews* 249 (2012) 27-42.
- [112] F.M. Uhl, S. Chen, D. O'Sullivan, J. Edwards-Hicks, G. Richter, E. Haring, G. Andrieux, S. Halbach, P. Apostolova, J. Büscher, S. Duquesne, W. Melchinger, B. Sauer, K. Shoumariyeh, A. Schmitt-Graeff, M. Kreutz, M. Lübbert, J. Duyster, T. Brummer, M. Boerries, T. Madl, B.R. Blazar, O. Groß, E.L. Pearce, and R. Zeiser, Metabolic reprogramming of donor T cells enhances graft-versus-leukemia effects in mice and humans. *Science translational medicine* 12 (2020).
- [113] T. Wang, J.N.R. Gnanaprakasam, X. Chen, S. Kang, X. Xu, H. Sun, L. Liu, H. Rodgers, E. Miller, T.A. Cassel, Q. Sun, S. Vicente-Munoz, M.O. Warmoes, P. Lin, Z.L. Piedra-Quintero, M. Guerau-de-Arellano, K.A. Cassady, S.G. Zheng, J. Yang, A.N. Lane, X. Song, T.W. Fan, and R. Wang, Inosine is an alternative carbon source for CD8(+)-T-cell function under glucose restriction. *Nat Metab* 2 (2020) 635-647.
- [114] M. Cavazzana-Calvo, J.L. Stephan, S. Sarnacki, S. Chevret, C. Fromont, C. de Coene, F. Le Deist, D. Guy-Grand, and A. Fischer, Attenuation of graft-versus-host disease and graft rejection by ex vivo immunotoxin elimination of alloreactive T cells in an H-2 haplotype disparate mouse combination. *Blood* 83 (1994) 288-98.
- [115] B.J. Chen, X. Cui, C. Liu, and N.J. Chao, Prevention of graft-versus-host disease while preserving graft-versus-leukemia effect after selective depletion of host-reactive T cells by photodynamic cell purging process. *Blood* 99 (2002) 3083-8.
- [116] E.C. Guinan, V.A. Boussiotis, D. Neuberg, L.L. Brennan, N. Hirano, L.M. Nadler, and J.G. Gribben, Transplantation of anergic histoincompatible bone marrow allografts. *The New England journal of medicine* 340 (1999) 1704-14.
- [117] J.C. Rathmell, E.A. Farkash, W. Gao, and C.B. Thompson, IL-7 enhances the survival and maintains the size of naive T cells. *Journal of immunology* (Baltimore, Md. : 1950) 167 (2001) 6869-76.
- [118] K. Akashi, M. Kondo, and I.L. Weissman, Role of interleukin-7 in T-cell development from hematopoietic stem cells. *Immunological reviews* 165 (1998) 13-28.

- [119] M.A. Perales, J.D. Goldberg, J. Yuan, G. Koehne, L. Lechner, E.B. Papadopoulos, J.W. Young, A.A. Jakubowski, B. Zaidi, H. Gallardo, C. Liu, T. Rasalan, J.D. Wolchok, T. Croughs, M. Morre, S.M. Devlin, and M.R. van den Brink, Recombinant human interleukin-7 (CYT107) promotes T-cell recovery after allogeneic stem cell transplantation. *Blood* 120 (2012) 4882-91.
- [120] J.Y. Lim, N.A. Kim, D.G. Lim, C.Y. Eun, D. Choi, and S.H. Jeong, Biophysical stability of hyFc fusion protein with regards to buffers and various excipients. *International journal of biological macromolecules* 86 (2016) 622-9.
- [121] H.K. Byun, S.Y. Chung, K.J. Kim, and J. Seong, Role of Interleukin-7 in the Development of and Recovery from Radiation-Induced Lymphopenia: A Post-hoc Analysis of a Prospective Cohort. *Cancer research and treatment* 53 (2021) 962-972.
- [122] Y. Lévy, I. Sereti, G. Tambussi, J.P. Routy, J.D. Lelièvre, J.F. Delfraissy, J.M. Molina, M. Fischl, C. Goujard, B. Rodriguez, C. Rouzioux, V. Avettand-Fenoël, T. Croughs, S. Beq, M. Morre, J.F. Poulin, R.P. Sekaly, R. Thiebaut, and M.M. Lederman, Effects of recombinant human interleukin 7 on T-cell recovery and thymic output in HIV-infected patients receiving antiretroviral therapy: results of a phase I/IIa randomized, placebo-controlled, multicenter study. *Clinical infectious diseases : an official publication of the Infectious Diseases Society of America* 55 (2012) 291-300.
- [123] S. Beq, S. Rozlan, D. Gautier, R. Parker, V. Mersseman, C. Schilte, B. Assouline, I. Rancé, P. Lavedan, M. Morre, and R. Cheynier, Injection of glycosylated recombinant simian IL-7 provokes rapid and massive T-cell homing in rhesus macaques. *Blood* 114 (2009) 816-825.
- [124] M.C. Hunter, A. Teijeira, and C. Halin, T Cell Trafficking through Lymphatic Vessels. *Frontiers in immunology* 7 (2016) 613.
- [125] I.B. Mazo, M. Honczarenko, H. Leung, L.L. Cavanagh, R. Bonasio, W. Weninger, K. Engelke, L. Xia, R.P. McEver, P.A. Koni, L.E. Silberstein, and U.H. von Andrian, Bone marrow is a major reservoir and site of recruitment for central memory CD8+ T cells. *Immunity* 22 (2005) 259-70.
- [126] M. Ghaedi, C.A. Steer, I. Martinez-Gonzalez, T.Y.F. Halim, N. Abraham, and F. Takei, Common-Lymphoid-Progenitor-Independent Pathways of Innate and T Lymphocyte Development. *Cell Rep* 15 (2016) 471-480.

[127] P. Tsapogas, S. Zandi, J. Åhsberg, J. Zetterblad, E. Welinder, J.I. Jönsson, R. Månsson, H. Qian, and M. Sigvardsson, IL-7 mediates Ebf-1-dependent lineage restriction in early lymphoid progenitors. *Blood* 118 (2011) 1283-90.

Biography

Yujing Zou received her Bachelor of Science degree with high distinction in May 2015 at University of Toronto, Canada, where she specialized in immunology. She matriculated into the Duke University (Durham, North Carolina) Department of Immunology in August 2015. She joined the Duke University Department of Pathology Graduate Program to complete her PhD dissertation in the Nelson Chao lab in 2017. Her research interests primarily focused on graft-versus-host-disease and immune reconstitution following radiation exposure. During her PhD training, Yujing received the core-specific voucher award in 2020 for the Functional Genomics Core to study T cell reconstitution. In 2021, she investigated the translational potential of a novel therapeutic agent to enhance T cell recovery in collaboration with scientists at NeoImmuneTech. Her work was selected for both oral and poster presentations at various local and national conferences. Her publications are listed below.

Zou Y, Huang Y, Jiao Y, Shi P, Nie X, Huang W, Xiong C, Choi M, Huang C, Macintyre A, Nichols A, MacIver N, Cardona D, Brennan T, Li Z, Chao N, Rathmell, J, Chen B. Targeting glycolysis in alloreactive T cells to prevent graft-versus-host disease while preserving graft-versus-leukemia effect. *Front Immunol* (2022). doi: 10.3389/fimmu.2022.751296

Zou Y, Chen B. T cell metabolism in graft-versus-host disease. *Blood Science* (2020) 1:16-21. doi:10.1097/BS9.0000000000000035

Huang W, Liu Y, Luz A, Berrong M, Meyer J, **Zou Y**, Swann E, Sundaramoorthy P, Kang Y, Jauhari S, Lento W, Chao N, Racioppi L. Calcium/Calmodulin dependent protein kinase kinase 2 regulates the expansion of tumor-induced myeloid-derived suppressor cells. *Front Immunol* (2021) 12:754083. doi:10.3389/fimmu.2021.754083

Zhang C, Lei L, Yang X, Zheng H, Su Y, Jiao A, Wang X, Liu H, **Zou Y**, Shi L, Zhou Xiao, Sun C, Zhang L, Hou Y, Xiao Z, Zhang B. Single-cell sequencing characterizes

intratumoral profile of immune cells in old mice. *J Immunother Cancer* (2021) 9(10): e002809. doi: 10.1136/jitc-2021-002809

Lei L, Zhang X, Yang X, Su Y, Liu H, Yang H, Wang J, **Zou Y**, Wang X, Jiao A, Zhang C, Zheng H, Zhang J, Zhang D, Shi L, Zhou X, Sun C, Zhang B. A genetic model reveals biological features of neonatal CD4 helper cells undergone homeostasis in mice. *Front Cell Dev Biol* (2020) 9:659744. doi:10.3389/fcell.2021.659744

Zhang P, Yang S, **Zou Y**, Yan X, Wu H, Zhou M, Sun Y, Zhang Y, Zhu H, Xu K, Wang Y, Sheng L, Mu Q, Sun Li, Ouyang G. NK cell predicts the severity of acute graft-versus-host disease in patients after allogeneic stem cell transplantation using antithymocyte globulin (ATG) in pretreatment scheme. *BMC Immunol.* (2019) 20:46. doi: 10.1186/s12865-019-0326-8